19th World Congress of Soil Science

Working Group 1.2
Architecture of soil structural diversity

Soil Solutions for a Changing World,

Brisbane, Australia

1 – 6 August 2010

Table of Contents

Table of Contents (Cont.)

A hydrological classification of UK soils based on soil morphological data

Allan Lilly[A]

[A]Macaulay Land Use Research Institute, Aberdeen, Scotland, United Kingdom, Email a.lilly@macaulay.ac.uk

Abstract
Hydrologists are often required to predict river flows, for example, when designing flood protection or river management schemes. Where historical records exist, flow indices can be calculated statistically but where there are none, or few records, other methods need to be used. The Hydrology of Soil types (HOST) classification makes use of the fact that the physical properties of soils, and soil structure in particular, have a major influence on catchment hydrology. While it is recognised that the soil hydraulic conductivity, soil water storage capacity and the pathways of water movement through the soil are the most important, these attributes are spatially and temporally variable making them costly and time consuming to measure. However, many of the morphological attributes recorded during soil survey describe key features of soil hydrology. Through the use of pedotransfer rules and functions, these attributes were used to develop a UK soil hydrological classification capable of predicting river flow levels of ungauged catchments (r^2 =0.79, s.e.e =0.089 in the case of *Base Flow Index*) and can be used in predictions of water quality, land suitability and environmental assessments.

Key Words
Soil morphology, hydrology, pedotransfer, hydropedology.

Introduction

Hydrologists are often required to predict river flows, for example, when designing flood protection or river management schemes. Where historical records exist, flow indices can be calculated statistically but where there are none, or few records, other methods need to be used. Various catchment scale models have been developed which are capable of predicting river flows. Some predict flows according to the topography within a catchment while others take cognisance of the fact that the nature and distribution on soils within a catchment can greatly influence both the flood response and the base flow characteristics of its streams and rivers. Processed-based models attempt to model the soil hydrological process in three dimensions and at numerous points over the catchment. These models generally require large amounts of soil data such as soil moisture retention characteristics and hydraulic conductivities which are inherently spatially and temporally variable. Another approach is to utilise the vast store of soil morphological data that often resides in soil survey archives throughout the world.

This has been achieved within the UK where 3 national soil survey organisations collaborated with hydrologists to produce a soil hydrological classification based on soil morphological data. The classification is called HOST (Hydrology of Soil types) and groups all UK soils into one of 29 response classes capable of predicting base and flood flows in UK rivers.

Methods

Using existing pedotransfer rules (PTRs) and functions that were derived for earlier land evaluation schemes, a set of soil profile attributes were derived that were subsequently used to develop the HOST classification. These properties were:

- Depth to a slowly permeable layer
- Depth to gleying
- Integrated air capacity (volume of pores that drain under the influence of gravity)
- An assessment of hydrogeology of the underlying substrate
- Presence or absence of peaty surface layers
- Notional depth to groundwater
- Spatial distribution of soil properties within catchments

Much of the initial work that lead to the development of the HOST classification came from the derivation of regression-based pedotransfer functions (PTFs) to predict soil structural properties responsible for water storage and flow such as water retention (e.g., Reeve *et al.* 1973; Hall *et al.* 1977; Hollis *et al.* 1977) and from the use of morphological attributes to estimate packing density, air capacity (pores >60 μm), and

Available Water Capacity (e.g., Hodgson 1997). This work, and that by others such as Thomasson (1975; 1978) and Avery (1980), also led to the development of the PTFs and PTRs used in UK land resource evaluation systems for Scotland (Bibby *et al.* 1982) and for England and Wales (MAFF 1988). The latter publication in particular set out the PTRs that underpins much of the HOST classification where texture-based class PTFs were developed to predict Available Water Capacity (θ_5 - θ_{1500}) for each soil texture class and modified according to soil structure (type, size, and grade) and consistence such that moderate and poor structures were deemed to have less available water. There are also complex PTRs largley based on soil structure assessments to determine if a soil horizon is slowly permeable (*Ksat* <10 cm/day), which influences a range of hydrological properties of the soil. First, the physical properties of the soil such as ped type, ped size, texture, consistence, and the presence of biopores are assessed. A slowly permeable horizon is recognized from the various combinations of these properties (Figure 1) and its presence within the profile is confirmed by evidence of gleying in either that horizon or the one immediately above. Gleying is strictly defined in terms of soil colour, and the presence of mottling or gleying on ped faces (Avery 1980). Soils with high value but low chroma (grey and pale colours) are classed as gleyed.

<table>
<tr><td rowspan="2">PED SHAPE</td><td colspan="4">PED SIZE</td></tr>
<tr><td>Fine</td><td>Medium</td><td>Coarse</td><td>Very coarse</td></tr>
<tr><td>Granular</td><td colspan="2" rowspan="2">permeable</td><td colspan="2" rowspan="2">slowly permeable if >18% clay and weakly developed structure</td></tr>
<tr><td>Subangular blocky</td></tr>
<tr><td>Angular blocky</td><td colspan="2">slowly permeable if >18% clay and weakly developed structure</td><td colspan="2" rowspan="2">slowly permeable if >18% clay</td></tr>
<tr><td>Prismatic</td><td colspan="2">slowly permeable if >18% clay and weakly developed structure</td></tr>
<tr><td>Platy</td><td colspan="4"></td></tr>
<tr><td>Massive</td><td colspan="4">slowly permeable if >18% clay or a silty loam, sandy silt loam or sandy loam texture and at least a firm consistence</td></tr>
</table>

Figure 1. Diagrammatic representation of the combinations of structure, texture and consistence which are characteristic of slowly permeable layers (*Ksat* <10 cm day^{-1}) in British soils (After MAFF 1988).

The rules and functions were applied to soil profile data held within the national soil databases in order to develop an attribute database of semi-quantitative soil properties from which the hydrological responses and flow pathways within UK soils could be predicted. Multiple regression analyses of these properties against two hydrological indices (Base Flow Index and Standard Percentage Runoff) were used to develop the soil hydrological classification through an iterative process that also involved conceptualising the dominant pathways of water movement through the soil and substrate (Figure 2).

Results

Through an iterative process of multiple linear regression of a hydrological index (Base Flow Index) against the proportion of these attributes within a catchment, a soil hydrological classification with 29 classes was developed for UK soils (Boorman *et al.* 1995). The resulting classification is capable of predicting river flow levels of ungauged catchments (r^2 =0.79, s.e.e =0.089 in the case of *Base Flow Index*) and can be used in predictions of water quality, land suitability and environmental assessments. More importantly, it has demonstrated the value of the soil morphological and observational data collected as part of normal soil survey activities for predicting hydrological responses. Table 1 shows the HOST framework and the values for the Standard percentage Runoff for a particular HOST class.

Conclusions

The development of the HOST classification has demonstrated the value of soil morphological data such as soil texture, structure and colour in predicting hydrological response and is also an example of how hydrology and pedology can be brought together to form a true hydropedological classification. HOST is now embedded in many hydrological software packages designed for applied hydrologists who are largely unaware of the extent of the soils component. As well as being useful to hydrologists, HOST has been used in modeling nitrate leaching, apportioning flow in biogeochemical models and predicting the potential for groundwater contamination by microbes.

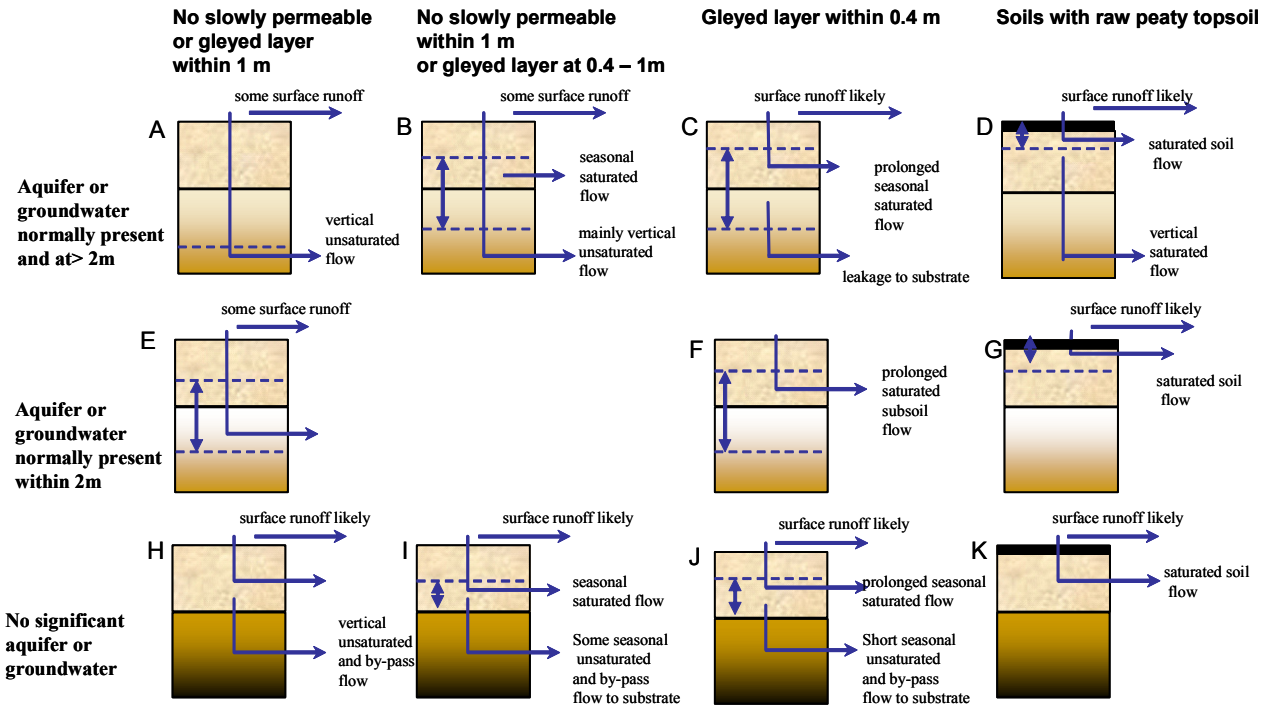

Figure 2. HOST conceptual response models used to classify soil cover (structural) units.

Table 1. The HOST framework with HOST class (black) and Standard Percentage Runoff index (brackets) for all UK soils.

Substrate hydrogeology	groundwater or aquifer	Mineral soils			Peat soils	
		No SPL or gleying	SPL within 100 cm or gleyed within 40- 100cm	Gleyed within 40cm		
Weakly consolidated microporous, by-pass flow uncommon	Normally present and at > 2m	1 (2)	13 (2)	14 (25.3)	15 (48.4)	
		2 (2)				
Weakly consolidated macroporous, by-pass flow uncommon		3 (14.5)				
Strongly consolidated, non - slightly porous, by-pass common		4 (2)				
Unconsolidated, macroporous, by-pass flow uncommon		5 (14.5)				
Unconsolidated, microporous, by-pass flow common		6 (33.8)				
Unconsolidated, macroporous by-pass flow uncommon	Normally present and at<2m	7 (44.3)		IAC<12.5	IAC>12.5	drained	undrained
Unconsolidated, microporous, by-pass common		8 (44.3)		9 (25.3)	10 (25.3)	11 (2)	12 (60)
Slowly permeable	No significant aquifer or groundwater	16 (29.2)	IAC>7.5 18 (47.2)	IAC<7.5 21 (47.2)	24 (39.7)	26 (58.7)	
Impermeable (hard)		17 (29.2)	19 (60)	22 (60)		27 (60)	
Impermeable (soft)			20 (60)	23 (60)	25 (49.6)		
Eroded peat						28 (60)	
Raw peat						29 (60)	

References

Avery BW (1980) 'Soil classification for England and Wales (Higher Categories). Soil Survey Technical Monograph no.14. Soil Survey of England and Wales'. (Lawes Agricultural Trust: Harpenden).

Bibby JS, Douglas HA, Thomasson AJ, Robertson JS (1982) 'Land capability classification for agriculture. Soil Survey of Scotland Monograph'. (The Macaulay Institute for Soil Research: Aberdeen).

Boorman DB, Hollis JM, Lilly A (1995) 'Hydrology of Soil Types: A Hydrologically-Based Classification of the Soils of the United kingdom. Institute of Hydrology Report No. 126'. (Institute of Hydrology: Wallingford).

Hall DGM, Reeve MJ, Thomasson AJ, Wright VF (1977) 'Water retention, porosity and density of field soils. Soil Survey Technical Monograph no.9. Soil Survey of England and Wales'. (Lawes Agricultural Trust: Harpenden).

Hollis JM, Jones RJA, Palmer RC (1977) The effects of organic matter and particle size on the water retention properties of some soils in the west Midlands of England. *Geoderma* **17,** 225-238.

Hodgson JM (1997) 'Soil Survey Field Handbook: Describing and Sampling Soil Profiles. 3rd Edition. Soil survey Technical Monograph No. 5'. (Soil Survey and Land Research Centre: Silsoe, England).

MAFF (Ministry of Agriculture Fisheries and Food) (1988) Agricultural land classification of England and Wales.

Reeve MJ, Smith PD, Thomasson AJ (1973) The effect of density on water retention properties of field soils. *Journal of Soil Science* **24,** 355-367.

Thomasson AJ (1975) 'Soils and Field Drainage. Soil Survey Technical Monograph No.7. Soil Survey of England and Wales'. (Lawes Agricultural Trust: Harpenden).

Thomasson AJ (1978) Towards an objective classification of soil structure. *Journal of Soil Science* **29,** 38-46.

A method to increase vertical resolution of soil moisture measurements by TDR Trime FM3 tube sensor probe

Olga S. Ermolaeva[A] and **Anatoly M. Zeiliguer[B]**

[A]Geo- and Hydroinformation Center, Moscow State University of Environmental Engineering Prjanishnikova Street, 19, Moscow 127550, Russia, Email o_ermolaeva@yahoo.com
[B]Geo- and Hydroinformation Center, Moscow State University of Environmental Engineering Prjanishnikova Street, 19, Moscow 127550, Russia, Email azeiliguer@mail.ru

Abstract
A special method of overlapping measurements was proposed to increase the vertical resolution of a TDR tube soil moisture sensor-probe Trime FM3. An inversion algorithm has been developed to derive soil moisture profiles along single TDR sensor-probe, which is based on the hypothesis of linear contribution of soil moisture content of layers enclosed in a cylindrical soil volume. This model was tested during experimentation on an artificial soil monolith assembled from 18 homogeneous horizontal discrete macro layers of 5 cm of height fabricated from dark-chestnut soil and artificially moistened to different values. For the first step, a series of overlapping measurements was produced using a TDR device, with step size of 1cm. Measured values were then compared to calculations based on the proposed model using moisture values of discrete macro layers as input parameters. At this stage the best agreement between measured moisture values and proposed model was achieved with a height of the soil cylinder of about 15-16 cm. For the second step, moisture values of discrete macro layers were calculated by the proposed model from values of overlapping measurements. At this stage the best agreement was gained with a height value of the soil cylinder of 16cm, when comparing moisture values of discrete macro layers of the artificial monolith derived from overlapping measurements and determined by the conventional direct gravimetric method.

Key Words
Soil moisture, TDR, overlapping measurement.

Introduction

An accurate measurement of the moisture of a soil profile is essential in many areas of environmental and agricultural research. However, the design of standard probes does not allow using these devices for monitoring vertical soil moisture distribution with adequate resolution. Nowadays, time domain reflectometry (TDR) is a widely used technique for measuring volumetric soil moisture. Recently, TDR tube probe sensor - Trime FM3 was produced by IMKO to respond to this demand. The research carried out by the producer has shown that the geometrical body of measurement by a probe represents a cylinder with height about 15-16 cm and the basis in the form of an ellipse with the greatest radius around 40 cm. In this case, it is quite uncertain whether direct use of the results of soil moisture monitoring by this probe can be used for flow modelling in soil. Trime FM3 tube probe sensor was successfully used on an experimental site in Saratov region of Russia in the work of INTAS 2000-436, NATO Travel Grant ESP.NR.CLG 982355, FP6 Water Reuse 516731 and FP6 DESIRE 037046 projects to monitor moisture distribution in soil profiles during field experimentation on irrigated and not irrigated areas. For this study a special method of overlapping measurement was developed with the aim of increasing vertical resolution of soil moisture measurements.

Methods

Soil water content measurements

Standard methods of soil moisture measurement such as oven-drying are very time-consuming and destructive, neutron scattering or gamma attenuation measurements make use of potentially hazardous radioactive sources. The determination of moisture content with time-domain reflectometry (TDR) technology is based on measurements of travel-time of an electromagnetic pulse on a transmission-line of known length Top *et al.* (1980). A review of TDR techniques for the measurement of permittivity and bulk electrical conductivity along with description of probe design and probe construction are given in Robinson *et al.* (2003). However, standard measurement TDR-techniques gives only mean or point results.

Experimentation on soil water content with borehole TDR in soil monolith
At the first stage of experiment, a measurement with TDR Trime-FM3 (Figure 1) was carried out. Experimental data was obtained for a constructed soil profile with horizontal dimensions of 70x70 cm and height of 90 cm with soil layers with different moisture contents. The soil monolith was assembled from 18 homogeneous horizontal layers. The soil material of the monolith was selected from the top of upper horizons of dark-chestnut soil of Saratov region (Russia). The sides of this monolith as well as boundaries between layers with different moistures have been protected by impermeable film to prevent evaporation as well as transfer of moisture inside the monolith. To avoid formation of significant air cavities inside of a monolith, the soil material was exposed to preliminary processing (a removal of roots and crushing of large blocks), then the soil was placed in a monolith, which was made level-by-level (1 cm) by compressing to obtain homogeneous soil body of layers and planned values (gravimetric moisture in a range from 0.08-0.30 g/g, density from 1.1 up to 1.38 g/cm^3).

Figure 1. TDR Trime-FM3 probe for borehole moisture measurements. Picture from the site of the IMKO Company.

The plastic tube (1 m height) was vertically installed in the center of the monolith using borehole and pathway to measure the soil water content using the Trime-FM3 tube sensor probe. After completing the developing of soil monolith, a series of overlapping measurements of soil moisture were done from the bottom of the monolith up to its surface with steps of 1 cm. The repetition of overlapping measurements was carried out several times during three days and showed an absence of any soil moisture changes in the fabricated soil monolith. After the end of the measurements the fabricated soil monolith was disassembled. Soil samples from each layer were taken out to determine values of density and soil moisture by gravimetric methods. Obtained values of soil moisture and bulk density of were quite uniform inside each layer and were similar to the planed values.

Modelling of measurement of water content in soil using TDR Trime FM3.
A simple mathematical model has been chosen to describe the performance of the TDR during the measurement of soil moisture. This model simulates the contributions of horizontal micro layers inside a soil cylinder to the overall measured value and is based on the hypothesis of linearity of the moisture content of these layers and is expressed by following expression

$$\theta(h_2, h_1) = \frac{1}{h_2 - h_1} \int_{h_1}^{h_2} \theta(h)\, dh \qquad (1)$$

where $\theta(h_1,h_2)$ - volumetric soil water content measured by the TDR probe device placed between depth h_1 and h_2 representing upper and bottom positions of this device in the soil profile, $\theta(h)$ - is the vertical distribution of soil water content, dh - is the height of soil micro layers.
We assume that the smallest height of distinct macro layers is 1 cm (simplification). In this case integration of Eq.1 by height of micro layers into discrete macro layers gives an expression of overall measured value as the linear sum of soil water contribution of each macro layer as follows:

$$\theta(h_2, h_1) = \frac{1}{h_2 - h_1} \sum_{h_1}^{h_2} \theta_i \qquad (2)$$

where dh_i - height of discrete macro layer, N - number of discrete macro layers in the soil cylinder.
The determination of the vertical distribution of soil water content θ(h) is the key component to be achieved by reconstruction of the soil water content from overlapping measurements. This can be represented by the following matrix equation

$$\{\theta(h)\}[P] = \{\theta(h_1, h_2)\} \quad (3)$$

where {θ(h)} is a one-dimensional matrix of soil water content of 1 cm height macro layers, [P] is two-dimension vector of position of the soil probe device in the soil profile, $\theta(h_1,h_2)$ is one-dimension matrix of values measured with the soil probe device in the "sampled" soil cylinder. In order to reconstruct measurement data at different positions of the sensor-probe Trime FM3 for the soil water content profile, input data of soil water content of soil profile is needed as well as parameters describing the position of the sensor-probe in the soil profile.

The model expressed by Equation.2 provides a tool to calculate a curve describing outputs of model $\{\theta(h_1,h_2)\}$ with a set of input parameters related to the position of TDR probe device in the soil monolith [P] and water content of discrete macro layers of monolith {θ(h)} during the scanning procedure. Experimental values of volumetric water content of soil layers were received as a result of disassembly of monolith. This information is based on the soil water profile of the artificial monolith as well as a series of values measured by profile sensor-probe Trime FM3 and reconstructed data of these measurements based on Equation 2; shown in Figure 2. In contrast to the abrupt changes of this artificial soil water content example (related to the chosen spatial discretization step), natural soil profiles show smooth trends in the water content.

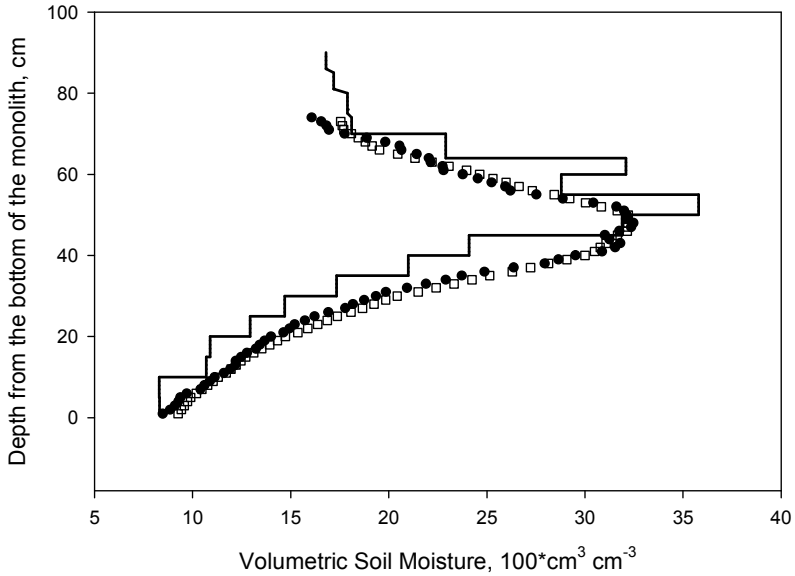

Figure 2. Results of comparison the measured soil moisture averaged from four measurements with different horizontal directions of the TDR-probe, and the results calculated by the additive model.

Results of inverse problem resolving

The aim of the calculation based on Eq.2 is to determine a unknown distribution of {θ(h)} with input data of overlapping measurements $\{\theta(h_1,h_2)\}$ obtained with profile sensor-probe Trime FM3 at different positions [P]. For this purpose a new simple inversion algorithm has been developed to derive soil moisture profiles from a series of measurements. The inversion algorithm starts calculation from one side of soil profile at either top or bottom. First layer height about 15cm is considered to be known. Using this parameter for soil distribution in this layer and following consecutive measurement the soil water content of engaged layers can be calculated without any optimization of parameters. Calculations have been carried out for various combinations of size of active and inactive zones of a probe at a scanning step of 1 cm. As a result of comparison of derived curves with measured data, it has been shown, that the best reproduction (coefficient of pair correlation 0,994) corresponds to sizes of an active zone in a range of 15-16 cm. Results of deriving the soil moisture profile of artificial soil monolith from overlapping measurements by sensor-probe Trime FM3 with a step of 1 cm for an active zone equal to 15 cm are shown in Figure 3. One can see that for the artificial soil monolith there is a good approximation of the given soil moisture profile.

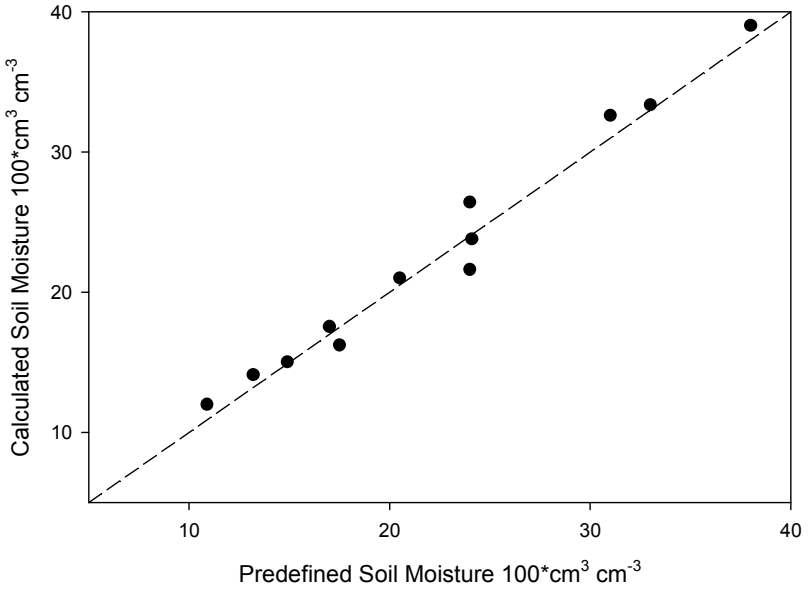

Figure 3. Comparison between the created soil moisture distribution of the artificial soil monolith and soil moisture derived from overlapping measurements with sensor-probe Trime FM3.

Conclusion

A new simple inversion technique is presented that derives a soil moisture profile with higher resolution from overlapping TDR measurements with the Trime-FM3 sensor probe device. The algorithm is based on a resolution matrix equation. The algorithm leads to a reliable soil moisture profile which is derived from overlapping standard transformations provided by the TDR device. The presented inversion technique is also suitable for the simultaneous reconstruction of data on the soil water profile during infiltration or subsequent water redistribution. Using laboratory tests - artificial soil monolith with specially formed soil moisture profile - it is shown that TDR overlapping data is suitable for reconstruction of soil moisture profiles.

References

Topp GC, Davis JL, Annan AP (1980) Electromagnetic determination of soil water content: Measurements in coaxial transmission lines, *Water Recourses. Research* **16**, 574-582.

Topp GC, Yanuka M, Zebchuk WD, Zegelin SJ (1988) Determination of electrical conductivity using time domain reflectometry: Soil and water experiments in coaxial lines, *Water Recourses. Research* **24**, 945-952.

Acid sulfate soil depositional environments of the Barron River delta, North Queensland

Jeremy Manders

Queensland Department of Environment and Resource Management, Indooroopilly, Qld, Australia.
Jeremy.manders@derm.qld.gov.au

Abstract
An acid sulfate soil map for the Cairns area was completed by Department of Environment and Resource Management (DERM) in 2009 (Manders *et al.* 2009). Investigation of field morphological properties and laboratory data from sites examined during the Cairns ASS mapping reveals that sites within geomorphologically similar areas can be extrapolated to spatially predict the upper limit of ASS deposition. This paper discusses the ASS depositional environments encountered on the Barron River delta within geomorphologically similar areas reflect these depositional environments.

Introduction
Coastal Acid Sulfate Soils (ASS) are soils or sediments containing iron sulfides, primarily in the form of pyrite (FeS_2). They commonly form in coastal environments where a supply of iron, sulfate, and organic matter are available to bacteria in an anaerobic environment. ASS have been forming for many thousands of years and can be encountered in at least 23,000 km^2 of the Queensland coast, both at the surface and buried beneath newer soils (National Working Party on Acid Sulfate Soils 2000). ASS are relatively benign in their natural (wet or buried) environment but can be hazardous when disturbed, having the potential to cause widespread environmental damage via the release of acid and metals from the soil.

The Barron River delta is located just north of Cairns on the northeast wet tropical coast of Queensland and experiences hot and humid summers and mild dry winters. Sugar cane is the main land use for the delta and was first planted in 1879, with substantial industry expansion occurring in the 1960s. Other land uses include urban areas (located on the beach ridges), residential canal developments (low-lying areas behind the beach ridges), and sand mining (upper riverine reaches). The delta's position in the landscape has provided an ideal environment for the aforementioned ASS formation factors to interact throughout the Holocene.

Acid sulfate soil depositional environments
Acid sulfate soils are deposited in large areas under coastal plains because the rapid rate of sea level rise during the Holocene exceeded the rates of coastal deposition and thus valleys and low lying coastal areas were drowned. Once sea level stabilises (termed still stand), new estuaries are formed and coastal deposition processes are able to commence filling the newly created subaqueous space (Dalrymple *et al.* 1992). Marine sands are deposited as tidal deltas behind the barrier by incoming tides. In the upper reaches (dominated by river energy), fluvial sediments are deposited as bay head or fluvial deltas. The area of neutral energy (central basin) between the two is generally filled with finer sediment such as clays and silts. With time and a sufficient sediment supply, estuaries eventually fill with sediment and mature (Roy 1984). Once the central basins (or lagoons) are filled, river processes begin to build alluvium out over the top of the marine sediments during flood events.

Coastline evolution and ASS deposition
The Barron River delta is a wave dominated delta stretching from Earl Hill in the north to Ellie point in the south and Kamerunga at the headwaters of the delta in the west (OzCoast 2009) (Figure 1). Wave energy, in combination with tidal currents, causes sediment to move along shore (northwards drift) and onshore into the mouth of the estuary where a barrier such as a spit or submerged sand bar forms. The entrances of wave-dominated deltas are relatively narrow due to constriction by the formation of the sandbar, and due to the relatively high river influence they are rarely closed off from the sea. However migration of river channels is commonplace during delta development because the gradient and the capacity of the river to flow gradually decreases towards its exit point. The Barron River is no exception and has several prior channels, including Moon River, Yorkeys Creek, Thomatis Creek, Ritchers Creek, Barr Creek and Redden Creek. Moon River and Barr Creek are currently only connected to the Barron River through overland flow (Figure 1). All of these prior channels dissect the large beach ridge barrier and are flanked by low-lying areas colonised by mangroves.

The beach ridge barriers prevent much of the wave energy from entering the estuary (Dalrymple *et al.* 1992). The barriers occur from Mt Whitfield located south of the Barron River, northwards to Yorkeys Knob. The supply of sand via northward drift to the beaches north of Yorkeys Knob has been disrupted by the protruding headlands (which include Yorkeys Point, Earl Hill, and Taylor Point) limiting the supply and formation of large beach ridge barriers north of the Barron River delta. The progradation of the Barron River delta has occurred by the extension of beach ridge barrier deposits over prodelta deposits. The beach ridge barrier deposits consist of a series of sand ridges with the intervening depressions colonised by either melaleucas or mangroves.

Identification of ASS horizons is based upon field morphological properties, pH results and laboratory analyses of sulfur content that exceed the texture-based action criteria (sands 0.03% S, loams 0.06% S and clays 1.00% S; Ahern *et al.* 1998). The elevation (metres AHD) of the sites mapped (calculated from airborne laser profiling of Light Detection and Ranging (LiDAR) ground point extraction) minus the depth to the ASS layer (where the action criteria is exceeded) gives the relative upper limit (m) AHD of ASS and a comparison between sites.

Beach ridges are high energy environments, and as such are not conducive to ASS formation and generally have an average concentration of 0.2% S in loam to coarse sands above prodelta muds. The sites sampled (Table 1) within the beach barrier recorded an average ASS upper limit of -1.0m AHD.

Table 1. Beach Ridge Barrier Sites

	Sites (m) AHD					Average	Median	Standard Deviation
Elevation	4.80	2.25	1.94	4.25	3.69	3.4	3.69	1.25
Depth to ASS	5.05	3.45	3.45	5.00	4.80	4.4	4.8	0.83
Upper Limit of ASS	-0.25	-1.2	-1.5	-0.75	-1.1	-1.0	-1.1	0.48

The back barrier low-lying mangrove colonised swales situated directly behind the beach ridges have a high tidal exchange and are ASS at or near the surface. The sites sampled (Table 2) have an average upper limit of ASS at 0.9m AHD. ASS will not normally form above the 0.5m AHD (based upon mapping in South East Queensland) level due to the oxidation during the wetting and drying cycle between tides. The occurrence of ASS within mangrove areas (>1.0m AHD elevations) can be variable at the surface. The back barrier low-lying mangrove areas with low energy environments combined with the high tidal exchange promotes the formation ASS at higher than normal upper limits.

Table 2. Mangrove Swales

	Sites (m) AHD			Average	Median	Standard Deviation
Elevation	0.9	1.05	1.0	1.0	1.0	0.08
Depth to ASS	0.0	0.2	0.0	0.1	0.0	0.12
Upper Limit of ASS	0.9	0.85	1.0	0.9	0.9	0.08

Where no hydrological modification or vegetation clearing has occurred mangrove communities have colonised most of the supratidal and extratidal areas up to the 1.7m AHD. This has resulted in the presence of only small areas of saltmarsh communities with in the mapping area. A number of factors contributing to the poor development of saltmarsh areas include the presence of the steep coastal plain, the coarse sedimentary composition of the coastal deposits and the area's high rainfall. Some hydrological modification of the delta has occurred with a series of bund walls and floodgates constructed to keep tidal inundation and storm surges out of low-lying land while allowing for flood water to escape. The areas protected by bund walls have been cleared of mangroves in the elevation range 1.0 - 1.7m AHD. These areas are used to grow sugarcane but often they have undergone oxidation and have become acidic in the surface layers.

The central basin of the delta is dominated by fine clays, however sands tend to dominate where the river channels have migrated across the delta. Approximately 50 sites were sampled in the central basin with the elevation of the sample sites varying from 1.7m to 4.4m AHD. The average elevation of the sites was 2.63m AHD, the average depth to ASS was 2.79m AHD, and the average upper limit of ASS was -0.16m AHD.

The upper reaches of the delta are dominated by river energy with riverine (non-marine) sands deposited over ASS clays and sands. The land surface varies from 4m to 7m AHD in height, with major floods removing and redepositing surface material. The site with the upper limit of ASS at -2.1m (Table 3) is

located on the southern bank of the Barron river. The site consists of alluvial clay loam to 1.4m over riverine coarse sands to 7.0m, ASS sands occur from 7.0m to the depth of sampling at 12.0m. The site with the upper limit of ASS at -1.0m (Table 3) is located 1.5km south of the Barron River and the start of freshwater valley. The site consists of alluvial clay loam to 2.2m, over riverine coarse sands to 6.7m, over ASS clays and sands to 15.5m. Below 15.5m is non ASS riverine material to at least 16.8m. Both of the above sites have undergone a reworking of the ASS deposition by a riverine environment. The site with the upper limit of ASS at 0.2m (Table 3) is located 1.2km south of the Barron River and east of Freshwater Creek. The site consists of predominately mottled clays and fine sands (non-riverine) material to 7.6m AHD over ASS clays to 13.2m AHD. A non-marine pre-Holocene surface was encountered at 13.2m. This site has had no reworking by migrating river channels. The areas that have undergone a reworking of the ASS deposition by a riverine environment are likely to have the upper limit below 0.0m AHD.

Table 3. Upper Reaches Riverine over ASS

	Sites (m) AHD							Average	Median	Standard Deviation
Elevation	6.40	6.70	4.00	5.70	5.30	7.60	4.90	5.9	5.70	1.21
Depth to ASS	6.20	7.10	4.70	6.70	6.80	9.20	7.00	6.8	6.80	1.33
Upper Limit of ASS	0.20	-0.40	-0.70	-1.00	-1.50	-1.60	-2.10	-0.9	-1.00	0.79

Freshwater Creek exits from a valley located to the south of the Barron River delta. The river-dominated environment restricts the likelihood of ASS deposition up the valley to approximately 2.7km from the Barron River. At the margin of the marine influence alternating layers of marine and riverine deposition can be found. Examination of the area above the marine influence found that in a river-dominated environment if ASS was not found before the -1.0m upper height then it was unlikely to found at depth. The migrating river channels and interaction of the riverine environment cause the deposition of ASS in this area to be highly variable.

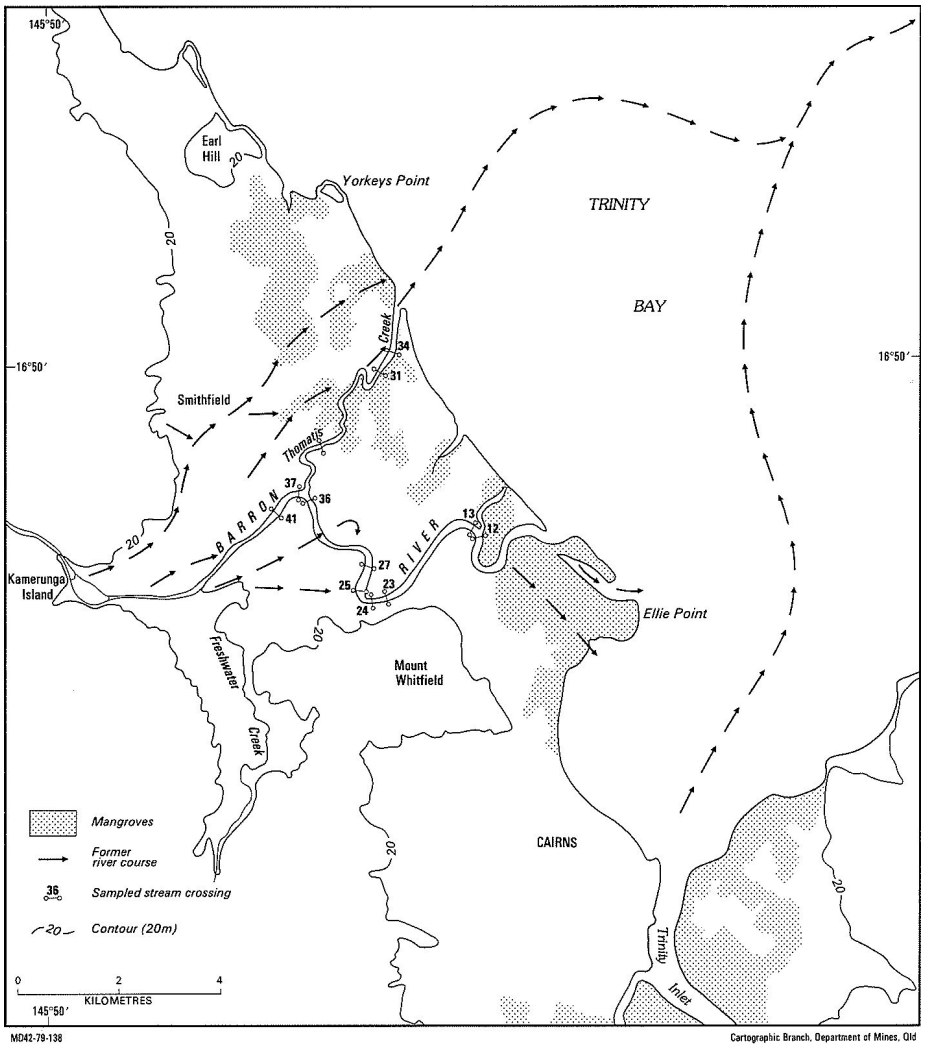

Figure 1. Locations of former river courses. Jones (1985)

References

Ahern CR, Ahern MR, Powell B (1998) 'Guidelines for Sampling and Analysis of Lowland Acid Sulfate Soils (ASS) in Queensland'. (Department of Natural Resources, Indooroopilly, Queensland, Australia).

Beach Protection Authority (1984) 'Mulgrave Shire northern beaches : a detailed study of coastline behaviour in north Queensland'. (Beach Protection Authority, Queensland, Brisbane).

Dalrymple RW, Zaitlin BA, Boyd R (1992). Estuarine Facies Models: Conceptual basis and stratigraphic implications. *Journal of Sedimentary Petrology* **62**(6), 1130-1146.

Jones MR (1985). 'Quaternary geology and coastline evolution of Trinity Bay, north Queensland'. (Geological Survey of Queensland Publication 386).

Manders JA, O'Brien LE, Morrison DW (2009) 'Acid Sulfate Soils of Cairns, North Queensland'. (Department of Environment and Resource Management, Indooroopilly, Queensland, Australia).

National Working Party on Acid Sulfate Soils (2000) 'National Strategy for the Management of Coastal Acid Sulfate Soils'. (New South Wales Agriculture: Wollongbar).

OzCoast Australian Online Coastal Information www.ozcoast.org.au

Roy PS (1984) New South Wales estuaries: their origin and evolution. In 'Coastal Geomorphology in Australia'. (Ed BG Thom) pp. 99–121. (Academic Press, Australia).

Applying hydropedological principles to analyse soil moisture variability at a field scale

N. Baggaley[A,C], T. Mayr[B] and P. Bellamy[B]

[A]Macaulay Land Use Research Institute, Craigiebuckler, Aberdeen AB15 8QH, UK.
[B]Cranfield University, Cranfield, Bedfordshire MK43 0AL, UK.
[C]Corresponding author. Email n.baggaley@macaulay.ac.uk

Abstract
The aim of this study was to investigate soil moisture variations and how soil and terrain data can be used in combination to explain the spatial variation in soil moisture contents. Field monitoring of surface soil moisture content on eight occasions in three different fields in Bedfordshire (UK) was undertaken. The results from regression models show that up to 80% of the variation in surface soil moisture can be explained using information derived1:10,000 soil series maps and terrain variables. An index of Short-wave radiation on a sloping surface (SWRSS), calculated by SRAD, and a topographic wetness index combined explained a maximum of 44% of the variation. The additional variation explained by adding 1:10 000 soil series information to terrain variables was up to 50% and adding 1:25 000 soil series information increased the variation explained by up to 29%. These results show that the terrain effect on soil moisture is modified by soils. They also indicate that there is temporal stability to soil moisture patterns which highlights this modification. The interactions in the variation explained by soil and landscape indices at different scales show that pedological knowledge is key to understanding hydrological processes at a landscape scale.

Key Words
Hydropedology, digital terrain model, Theta probe.

Introduction

The literature points to soil properties being a major driver in the spatial distribution of soil moisture at a small-catchment scale. It also suggests that detailed soil mapping is the key to representing distributed soil moisture patterns (Lin *et al.* 2006). However, detailed scale soil mapping is only available for very small areas. In this study where detailed soil mapping is available, there is the opportunity to compare its ability to predict soil moisture contents with that of lower resolution soil mapping combined with terrain variables, the aim being to quantify the difference in the predictive power of the different data sets (Baggaley *et al.* 2009). The objectives of this research are to identify key soil, terrain and meteorological properties that influence the spatial distribution of soil moisture throughout the growing season and assess the temporal stability of the soil moisture patterns.

Methods

Field methods

Field monitoring of surface soil moisture content on eight occasions in three different fields in Bedfordshire (UK) was undertaken between April and July in 2004 and 2005. Between 100 and 120 points were sampled on an approximately 30 m paced grid in each survey using a Delta-T ML2x Theta Probe.

Soil and terrain variables

The 10 m Ordnance Survey Land-Form PROFILE^{TM} elevation data was used to calculate two wetness indices (Quasi-Dynamic Wetness Index (QDWI) and Steady State Wetness index (SSWI)) and a solar radiation index (Short-wave radiation on a sloping surface (SWRSS)). These were chosen as surrogates to represent both lateral (wetness indices) and vertical (radiation index) movement of soil moisture. Soils data was available at1:25 000, scale in the form of the Biggleswade Sheet TL14 (Wright 1987) for all three field sites and at 1:10 000 scale for Stone Hill and Church Meadow (Burton 2003 unpublished).

Analysis methods

Two analyses were undertaken:

- An ANOVA of the soil moisture in each of the field sites with respect to the different mapping scales. The significant effects were then investigated using Fisher least significant difference (Fisher LSD).
- Two regression analyses. First, on the soil moisture contents with respect to the three terrain variables

(SSWI, QDWI and SWRSS) and second on the soil moisture contents with respect to SSWI and SWRSS combined with the two different mapping scales.

Results and discussion

ANOVA with respect to soil mapping scales

At Stone Hill in 2004, the variance in soil moisture explained by the eight soil series that were identified at the 1:10 000 scale decreases from 55 to 29% between April and July as the soils dry out. This compares to 19 to 15% of the variation being explained by 1:25 000 scale soils data. The patterns in soil moisture, however, appear to display temporal stability (Figure 1). Fisher LSD shows the soil series at 1:10 000 at Stone Hill generally fall into three groups based on the measured soil moisture content. These are slowly permeable clay rich soil soils, freely draining loamy soils and freely draining sandy soils, in order of decreasing soil moisture content.

In Church Meadow in 2005, the variance explained by the eight soil series mapped at 1:10 000 scale decreases from 76 to 61% between June and July. This compares to 38 to 33% of the variation being explained by 1:25 000 scale soils data. The average moisture is driven by the patterns in rainfall, however, as in Stone Hill, the patterns appear to be temporally stable (Figure 1). Investigating the soil series effect using Fisher LSD highlights three groups of soil series based on the measured soil moisture content. These are slowly permeable clay rich soils, freely draining loamy soils and freely draining sandy soils, in order of decreasing soil moisture content.

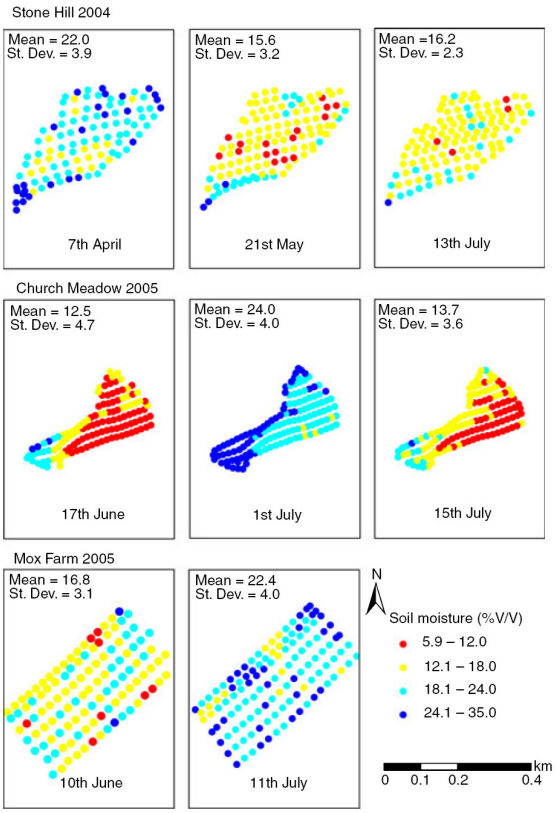

Figure 1. Surface soil moisture measurements (top 100 mm) at Stone Hill, Church Meadow and Mox Farm. Taken using Delta-T ML2x Theta Probe.

Combining terrain and soils

In Stone Hill the variance explained by terrain variables was at a maximum on 21 May. Here, the SSWI explains 35% and the SWRSS 31% and when combined they explain 44% of the variation in soil moisture content. Adding 1:10 000 scale soil data to the regression models developed for the terrain variables explained an additional 14–21% of the variance. When soil data at 1:25 000 are used, the additional variation explained varies from not being significant on 7 April and 21 May to 8% on 13 July. The variation explained by soils at 1:25 000 scale and terrain indices was always less than the variation explained by soils alone at 1:10 000 scale (Table 1).

In Church Meadow the maximum variation explained by the combination of SSWI and SWRSS was 31% on 17 June, decreasing to 22% on 15 July. Adding 1:10 000 scale, soil data to the regression models developed for the terrain variables explained 42–50% more variation. When soil data at 1:25 000 are used, the additional variation explained varies from 26% on 15 July to 29% on 1 July (Table 1). At Mox Farm terrain explained a maximum of 7% of the variation in the soil moisture in the field and together with the soils data at 1:25,000 scale the variation explained was 20% (Table 1).

Table 1. Regression models explaining the largest proportion of variation in surface soil moisture for each of the eight sampling dates in Stone Hill, Church Meadow and Mox Farm.

Field	Date	Regression Model	Non significant variables	% Variance in Soil moisture explained
Stone Hill	7 April 2004	SSWI + SWRSS		38
		1:10,000 soil + SWRSS	SSWI	59
		SSWI + SWRSS	1:25,000 soil	38
	21 May 2004	SSWI + SWRSS		44
		1:10,000 soil + SSWI + SWRSS		58
		SSWI + SWRSS	1:25,000 soil	44
	13 July 2004	SSWI	SWRSS	12
		1:10,000 soil	SSWI + SWRSS	32
		1:25,000 soil + SSWI	SWRSS	20
Church Meadow	17 June 2005	SSWI + SWRSS		31
		1:10,000 soil + SWRSS	SSWI	80
		1:25,000 soil + SSWI + SWRSS		57
	1 July 2005	SSWI + SWRSS		24
		1:10,000 soil + SWRSS	SSWI	74
		1:25,000 soil + SSWI + SWRSS		53
	15 July 2005	SSWI + SWRSS		22
		1:10,000 soil + SWRSS	SSWI	64
		1:25,000 soil + SSWI + SWRSS		48
Mox Farm	10 June 2005	SSWI	SWRSS	3
		1:25,000 soil + SSWI	SWRSS	7
	11 July 2005	SWRSS	SSWI	7
		1:25,000 soil + SSWI + SWRSS		20

Model (i) SSWI + SWRSS + 1:10 000 soil data (ii) SSWI + SWRSS + 1:25 000 scale soil data. Only the variables significant in the regression models are shown.

Conclusion

This paper highlights the modification of landscape-driven hydrological processes by pedology. The temporal variations in mean soil water content are driven by rainfall events in the days preceding sampling but the patterns of soil moisture observed appear to show temporal stability. To understand these patterns we need to examine the spatial distribution of soil moisture with respect to topography together with the modifying effect of subsurface soil properties. In addition, when modelling hydrological processes in soils it is important to consider what the impact that soils may have on modifying the terrain effect on soil moisture and consequently water movement. The patterns observed will differ in areas with increased terrain variation and increased variation in soil permeability characteristics which result from differing underlying parent material. This work could be developed and by applying soil moisture retention curves to high spatial resolution soil moisture data and examining the spatial variability of pressure head with respect to terrain. This would give further valuable insight into the nature of water movement within fields.

References

Baggaley NJ, Mayr T, Bellamy P (2009) Identification of key soil and terrain properties that influence the spatial variability of soil moisture throughout the growing season. *Soil Use and Management* **25,** 262–273.

Lin HS, Kogelmann W, Walker C, Bruns MA (2006) Soil moisture patterns in a forested catchment: a hydropedological perspective. *Geoderma* **131**, 345–368.

Wright PS (1987) 'Soils in Bedfordshire I: sheet TL14 (Biggleswade). Soil survey record no. 112 and 1:25,000 map'. (Soil Survey of England and Wales Publishing: Harpenden).

Architecture of soil structural diversity: from the micro to the landscape scale

Hans-Jörg Vogel

Helmholtz Center for Environmental Research - UFZ, Leipzig/Halle, Germany, Email hans-joerg.vogel@ufz.de

Irrespective the spatial scale, soils or terrestrial systems in general exhibit some sort of structure or heterogeneity. On one hand, this is a well known feature, on the other hand it is often neglected - or at least not considered adequately - in our daily scientific efforts for an improved understanding of processes from the pore space within soil to the heterogeneous pattern of soil properties within landscapes.
Another antagonism is that nearly all processes in soil depend on zones of gradients in terms of some state variables and hence they depend on heterogeneity and structural diversity, whereas the analyses of these processes are notoriously complicated by this heterogeneity. In any case, structural diversity and the related interfaces and gradient zones is an essential part of the very nature of soil and the processes therein

We address two critical questions which we feel are at the core for an improved system oriented understanding**:**
i) How is structural diversity generated and preserved? Here the answers are lying in the field of pedology but also in the field of soil mechanics and soil biology addressing important agents for structure formation in soil. ii) How to cope with structural diversity when modeling actual processes of flow, transport and biogeochemical interactions in soil? This addresses soil hydrology but also soil biology and biogeochemistry. The concept of hydropedology is intended to provide new insight related to these questions by the coupling of disciplines of hydrology and pedology.

In this contribution we discuss different avenues how structural diversity can be directly included in modeling soil processes. The impact of structural diversity is often lumped into ad-hoc model parameters which cannot be measured independently but need to be fitted to some experimental observations. In contrast, a direct link between structure and function will improve our understanding of soil processes and will increase the predictive power of the related models. This concept is exemplified for different processes at different scales:

1) Biogeochemical interactions in soil, including sorption and the turnover of soil organic matter, happen at the scale of pore-solid interfaces. The structure of the pore space is crucial for what a particle 'sees' when moving through soil. Experiments based on homogenized samples merely tell us what may happen potentially but not what is really going on. We present an approach to quantify and to model the complex pore geometry thereby linking directly-measured structural properties to the expected biogeochemical interactions in soil. The required instruments for non-invasive structure analysis become more and more available (e.g. X-ray microtomography). The observed structure can inform processes of structure formation which closes the loop between pedology and functions.

2) At the scale of soil profiles preferential flow is still an open problem for the prediction of soil water dynamics and solute transport. In groundwater, stochastic continuum theory has already demonstrated the possibility of translating structural aspects into process-relevant model parameters. However, within the unsaturated zone the highly transient conditions lead to hydraulic non-equilibrium that triggers preferential flow in a non-linear way.
Existing multi-domain models are based on conceptual 'effective' parameters that typically need to be calibrated to experimental observations and cannot be measured independently. We discuss an approach which considers the state space of water content and water potential as a probability space so that water content, water potential and hydraulic conductivity are no more tightly coupled by constitutive relations. Based on numerical simulations using well defined heterogeneities we demonstrate that the trajectories within this state space can be derived from structural properties in the form of variance, correlation length and topology of the local hydraulic properties.

3) At the scale of hillslopes and catchments surface runoff and interflow are large scale preferential flow events which are triggered by the hydraulic structure of individual soils (i.e. vertical profile of water capacity and hydraulic conductivities) and their spatial distribution pattern within the catchment. This structural

diversity determines the onset of fast lateral flows in response to external forcing by climatic conditions. It can be mapped by direct field measurements, geophysical exploration and remote sensing data. However such data are hard to get and, hence, are typically not available. As an attractive alternative, we discuss the approach of pedometrics to use more readily available data related to geology, relief, vegetation, and land management together with our understanding of soil genesis to set up a soil-landscape model providing a probabilistic spatial pattern of relevant soil attributes. This, again, would close the loop between pedology and actual hydrological processes.

Characterization of soil structure and water infiltration spatial variability using electrical resistivity tomography at decimetre scale. A study of two contrasted soil tillage modalities

Didier Michot[A], Vincent Hallaire[A], Simon Besnard[A], Gaétane Chirié[A], Yannick Besnard[A] and Gilles Dutin[A]

[A]UMR 1069 Sol-AgroHydrosystèmes-Spatialisation (SAS), Agrocampus-Ouest / INRA, 65 rue de St Brieuc - CS 84215, 35042 Rennes Cedex, France.

Abstract
Simplification of tillage practices is often considered as a solution for reducing time constraints and costs, and also for limiting soil erosion. Simplified tillage practices adopted over several years progressively induce modifications of soil physical properties in the top soil layer at decimetric scale. The general aim of this study was to test the capacity of electrical resistivity tomography to characterize the spatial variability of soil structure, bulk density and water flow in a loamy Cambisol with two modalities of tillage (conventional tillage, no tillage). For each tillage treatment, the experiment combined: 1) a description of the soil structure profile, 2) measurements of bulk density and soil hydraulic conductivities; 3) 2D electrical resistivity tomographies measured before and after an irrigation to characterize the spatial variability of soil water fluxes. These geophysical data are correlated to the spatial variability of soil structure and hydrodynamics properties.

Key Words
Electrical resistivity tomography, bulk density, hydraulic conductivity, structure, tillage.

Introduction

Agricultural soil structure evolves in space and time with tillage practices, climate and crop growth. Simplified tillage practices were adopted by farmers for several reasons: i) reduce their production costs, ii) increase the organic matter content in the top soil layer; iii) increase the soil structural stability to limit soil erosion. These new practices induced changes in soil structure and soil physics properties in the cultivated horizon at decimetric scale. The description of soil structure spatial variability is usually based on soil profile observations, soil properties measurement as bulk density and porosity. Moreover, water infiltration depends on soil structure. Tools actually available to study soil structure or water flow in soil are limited by their point-to-point measurement. They are also generally destructive. The geophysical methods are non invasive. They disturb neither the structure nor the water dynamics of the soil. Recent papers showed the relevance of electrical resistivity prospecting to detect some structural heterogeneity of the tilled soil (Seger *et al.* 2009; Besson *et al.* 2004) or to detect soils cracks that form during shrinking and swelling phenomena (Samouëlian *et al.* 2004). Besson *et al.* (2004) linked soil electrical resistivity changes with bulk density variations. Moreover, Michot *et al.* (2003) have shown that water infiltration could be monitored in space and time using electrical resistivity tomographies. The aim of this work was to test the efficiency of 2D electrical resistivity tomography (ERT) to characterize the spatial variability of soil structure, bulk density and water infiltration of a loamy Cambisol according to two different tillage modalities (conventional tillage, no tillage).

Methods

The experiment was conducted on the experiment site of Kerguéhennec (Morbihan, France). The soil was a pebbly loamy Cambisol developed on a micaschist. Two plots were studied : i) a plot with a conventional tillage until 25 cm depth realized 18 month before; ii) a plot with zero tillage for 8 years. The experimental setup is presented in Figure 1. It is composed of a row of 64 electrodes lined up at the soil surface with a spacing of 10 cm. The measurements were realised by a multielectrodes system. The electrodes were connected to 4 multinodes linked to a Syscal R1 resistivimeter (Iris Instruments) and numerous measurements were performed rapidly thanks to a pre-recorded sequence of quadripoles with a dipole-dipole array. ERT were measured before and after irrigation by sprinkling. Simultaneously, hydric potential profiles, soil water electrical conductivity, soil temperature and irrigation inputs were measured. Each measured resistivity section was inverted with RES2DINV software (Loke and Barker 1996). Water infiltration was monitored by electrical resistivity changes, *i.e.* soil electrical resistivity decreases when the soil water content increases, and vice versa. After ERT measurements, soil structure was described along a 6m long soil profile.

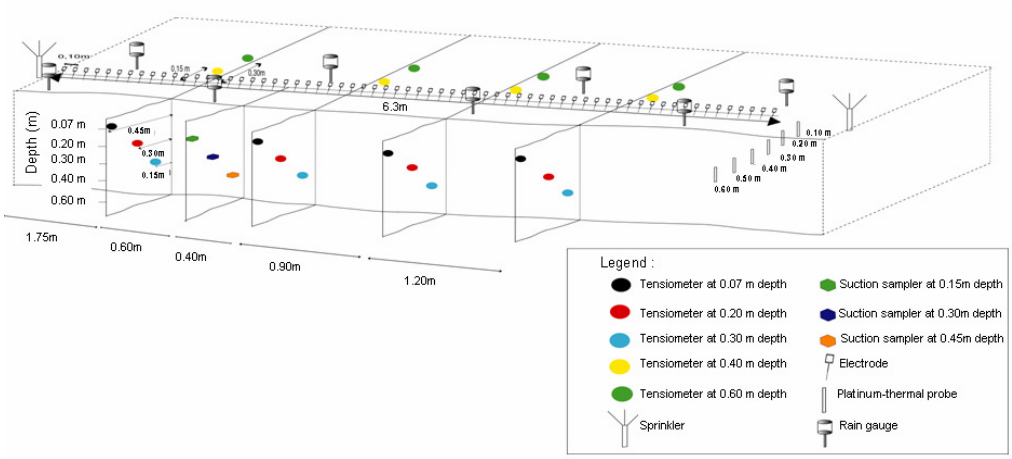

Figure 1. Experimental setup of water flow monitoring by 2D electrical resistivity tomography.

Structural and hydrodynamic properties were also characterized with bulk density and hydraulic conductivity measurements to be compared with electrical resistivity results. Hydraulic conductivity K(h) was measured using infiltrometer « decagons » (Soils Physics Instruments Decagon Devices, Washington, USA) at 3 water potentials at - 0.05, - 0.2 and - 0.6 kPa.

Results

First results indicate that conventional tillage modality induced higher spatial variability of top soil soil structure, soil bulk density (Figure 2) and hydraulic conductivity at -0.05 kPa and -0.20kPa hydric potentials (Figure 3), than the no tillage modality. From soil surface to 5 cm depth, hydraulic conductivities values were significantly higher for the conventional tillage treatment than for the no tillage treatment. Globally, the no tillage modality showed a general phenomenon of settling of the top soil layer with higher bulk density and lower hydraulic conductivity at water potentials of -0.20 hPa (Figures 2 and 3) by comparison with conventional tillage.

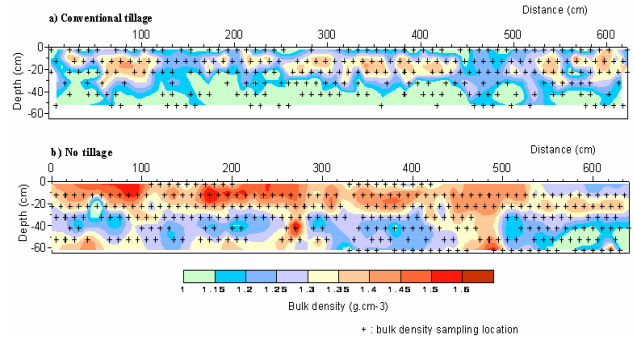

Figure 2. Maps of soil bulk density for the two tillage treatments: a) for conventional tillage treatment; b) for no tillage treatment.

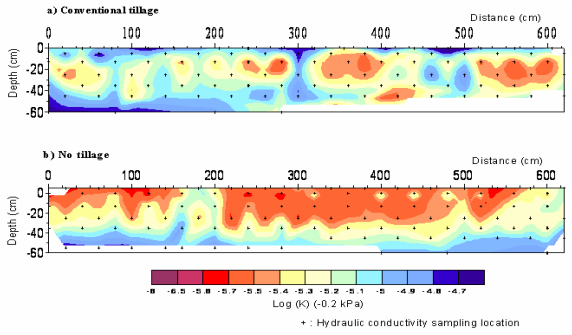

Figure 3. Maps of hydraulic conductivity at -0.20 kPa hydric potential: a) for the conventional tillage treatment; b) for the no tillage treatment.

Electrical resistivity changes (Figure 4) are clearly linked to water infiltration according to hydric potential gradients in the whole profiles for both modalities. But, for the no tillage modality, we observed some lower decrease of electrical resistivity in the top soil layer. These data will be compared to the spatial variability of soil structure and hydrodynamics properties.

Conclusion

Cultivated soil profiles present spatial heterogeneities of physic and structural properties which explain water flow variability at soil profile scale. Electrical resistivity tomographies could be a help to characterize the spatial variability of soil structure and water infiltration without disturbing the soil. The results of the individual applied methods complement each other. The geophysical data will be confronted to the spatial variability of soil structure and hydrodynamics properties measured with conventional methods.

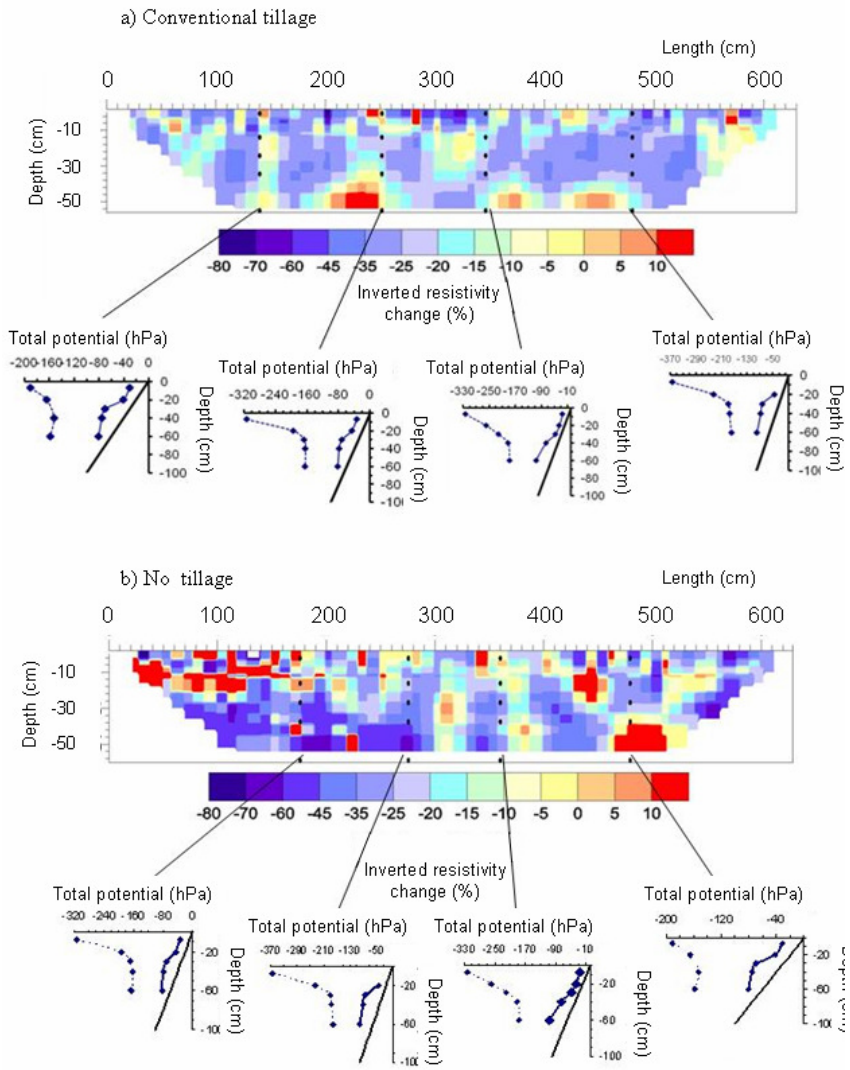

Figure 4. Soil section of relative resistivity changes measured over time during the soil wetting phase after irrigation: a) for conventional tillage treatment; b) for no tillage treatment.

References

Besson A, Cousin I, Samouëlian A, Boizard H, Richard G (2004) Structural heterogeneity of the soil tilled layer as characterized by 2D electrical resistivity surveying. *Soil & Tillage Research* **79**, 239-249.

Loke MH, Barker RD (1996) Rapid least-squares inversion of apparent resistivity pseudosections by a quasi-Newton method. *Geophysical Prospecting* **44,** 131–152.

Michot D, Benderitter Y, Dorigny A, Nicoullaud B, King D, Tabbagh A (2003) Spatial and temporal monitoring of soil water content with an irrigated corn crop cover using electrical resistivity tomography. *Water Resour. Res.* **39**, 1138-1158.

Samouëlian A, Richard G, Cousin I, Guérin R, Bruand A, Tabbagh A (2004) Three-dimensional crack monitoring by electrical resistivity measurement. *European Journal of Soil Science* **55**, 751–762.

Ségera M, Cousin I, Frison A, Boizard H, Richard G (2009). Characterisation of the structural heterogeneity of the soil tilled layer by using in situ 2D and 3D electrical resistivity measurements. *Soil & Tillage Research* **103**, 387-398.

Characterization of the hydraulic property of the plow sole under double-cropped paddy fields in southern Japan

Keiko Nakano[A], Hideo Kubotera[B] and Yoshitaka Hara[A]

[A] Lowland Crop Rotation Research Team(Kyushu Region),National Agricultural Research Center for Kyushu Okinawa Region,496 Izumi, Chikugo, Fukuoka 833-0041, Japan, Email nakak@affrc.go.jp
[B] Sustainable Soil Management Research Team, National Agricultural Research Center for Kyushu Okinawa Region 2421 Suya, Koshi, Kumamoto 861-1192, Japan

Abstract
The saturated hydraulic conductivity of plow soles in paddy fields appears to increase when the fields are used for double-cropping, due to the creation of macropores during the upland growing season. Since these macropores cannot act as a route for water and solute transport in the unsaturated state, the degree of hydraulic conductivity of the plow sole, excluding macropores, is the key to ensure successful cultivation of upland crops. However, such hydraulic conductivity has been rarely determined for paddy fields. Near-saturated hydraulic conductivities were measured by using a tension disk infiltrometer with supply pressure heads (h) ranging from 0 to –12 cm. The hydraulic conductivities at $h = 0$ cm in double-cropped fields were greater than those in single-cropped rice fields, due to the presence of macropores. In fine-textured soil areas found near the lower reaches of rivers, hydraulic conductivities at $h < 0$ cm in double-cropped fields were greater than those in single-cropped rice fields, suggesting that the cropping system employed affects the hydraulic property while unsaturated during the upland growing season. In coarse-textured soil areas found near the middle reaches of rivers, the near-saturated hydraulic conductivities in double-cropped fields were no different with those in single-cropped rice fields.

Key Words
Soil structure, unsaturated hydraulic conductivity, drainage, ponding water.

Introduction
The hydraulic properties of near-saturated soil are very important for water and solute transport processes. In southern Japan, the double cropping is employed on many rice paddy fields. One of the essential functions of paddy fields is to pond water; this function is usually a result of the very low hydraulic conductivity of the plow sole and/or due to puddling of the topsoil. When using paddy fields for upland planting, the saturated hydraulic conductivity of the plow sole tends to increase due to the creation of macropores caused by root penetration, resulting in the soil drying out down to the plow sole (Yoshida *et al*. 1997). This high-saturated hydraulic conductivity has the effect of preventing injury by excess moisture in winter wheat in southern Japan, which experiences high rainfall during the growing season. Repeated and regular planting of upland crops tends to create fields suitable for double cropping, which need to have the opposing functions of both ponding and draining water. However, a lack of concern about the unsaturated state of paddy fields had led to no numerical evidence having been collected. The tension disk infiltrometer is an effective tool for studying the hydraulic properties under near-saturated conditions in the field (Perroux and White 1988; Ankeny *et al*. 1988; Angulo-Jaramillo *et al*. 2000). The objective of this study was to determine the differences in the near-saturated hydraulic conductivity of the plow sole between double-cropped fields and single-cropped rice fields.

Methods
Study areas and fields
The study region encompassed adjoining plains known as the Chikugo Plain, the Saga Plain, and the Shiroishi Plain in northern Kyushu, Japan. Many farmers in this region engage in double-cropping. Fields are usually planted with rice or soybean from June to October, followed by winter wheat from November to May. On the basis of soil maps of Japan, 11 areas were selected for the study area. Gray Lowland soil was distributed widely in the study region, enabling the selection of multiple study areas. Although the distribution of the other soil groups (Andosol and Brown Lowland soil) was rare, only a study area was selected for each group. Gray Lowland soil and Brown Lowland soil correspond to Hydragric Stagnic Anthrosols in the World Reference Base for Soil Resources. Two or three double-cropped fields or single-cropped rice fields were selected from each study area (Table 1).

1 – 6 August 2010, Brisbane, Australia. Published on DVD.

Table 1. Summary of selected study fields.

Cropping system	Area name	Soil group on Japanese soil maps
Double cropping (paddy rice/soybean – wheat)	Shiroishi	Gray Lowland soil
	Kawazoe	Gray Lowland soil
	Yanagawa	Gray Lowland soil
	Oki	Gray Lowland soil
	Takeo	Gray Lowland soil
	Nabeshima	Gray Lowland soil
	tanushimaru	Gray Lowland soil
	Yasutake	Brown Lowland soil
	Amagi	Andosol
	Yanagawa	Gray Lowland soil
Single cropping (paddy rice)	Oki	Gray Lowland soil
	Kinryu	Gray Lowland soil
	Yasutake	Brown Lowland soil

Measurements

Infiltration measurements using a tension disk infiltrometer were conducted at three supply pressure heads, h, of –12, –3, and 0 cm, applied successively at the same position from low to high pressure to give a dry to wet sequence. If no water infiltrated at h= –12 cm for 10 min, the minimum h were increased by 1 cm until water infiltration occurred. Measurement was performed at 2–3 spots in each field. The instrument was set on the plow sole, which was judged according to soil hardness and root distribution. Steady-state infiltration rates were measured, and the hydraulic conductivity was calculated by using the method described by Ankeny *et al*. (1991). Measurements were carried out in June 2007 and May 2008. Particle size distribution was measured by bulk soil sampling of the plow sole.

Results and discussion

Study area classification according to soil texture

Soils in Shiroishi, Kawazoe, Yanagawa and Oki had a fine texture due to their clay content exceeding 30 %. In Amagi, although the clay content exceeded 30 %, the sand content was also above 40 %, giving the soil a coarse texture. The sand content was above 40% in Takeo, Nabeshima, Kinryu, Tanushimaru and Yasutake; moreover, the coarse sand content was above 10 % in these areas, except in Takeo. As shown in Figure1, fine-textured soils were located around the lower reaches of rivers, while coarse-textured soils were found in the middle reaches. Soil texture in the study region was likely to depend on the location. We have therefore classified the study areas into two groups: the lower reaches and the middle reaches; we have discussed the characteristics of near saturated hydraulic conductivity accordingly.

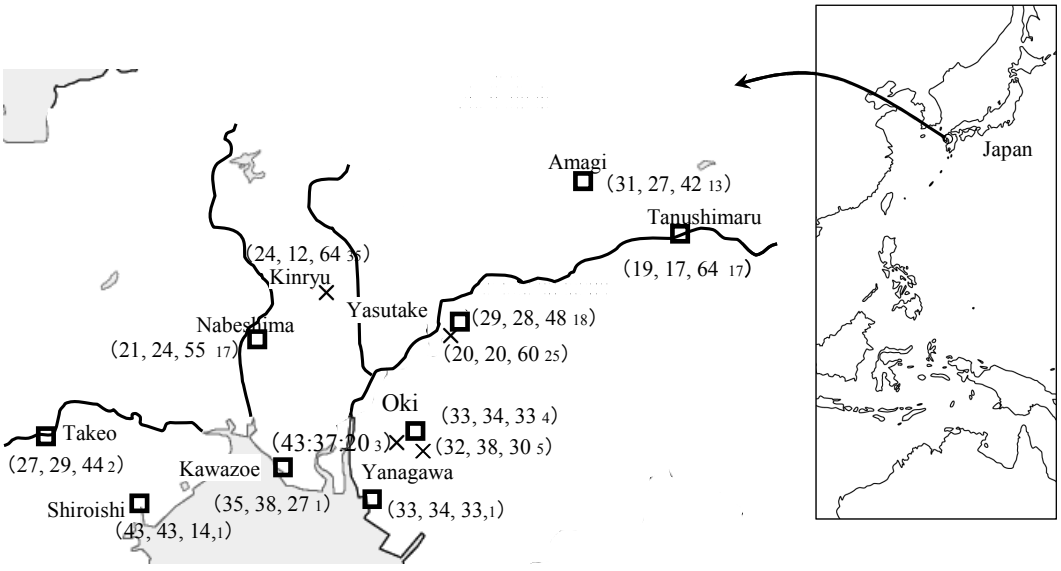

Figure 1. Spatial distribution of the study areas and their soil textures (clay, silt, sand coarse sand %) . Areas labelled with □ were under double-cropping, and areas labelled with × were under single rice-cropping.

The hydraulic conductivities of the plow sole at h = 0 cm

The average hydraulic conductivity in each area is shown in Figure 2. These values at h = 0 cm in double-cropped fields were in the order of 10^{-3} cm s^{-1}; overall, it was greater than the corresponding value in single-cropped rice fields. This high hydraulic conductivity is likely to be attributable to macropores because of a steep decrease with increased supply tension.

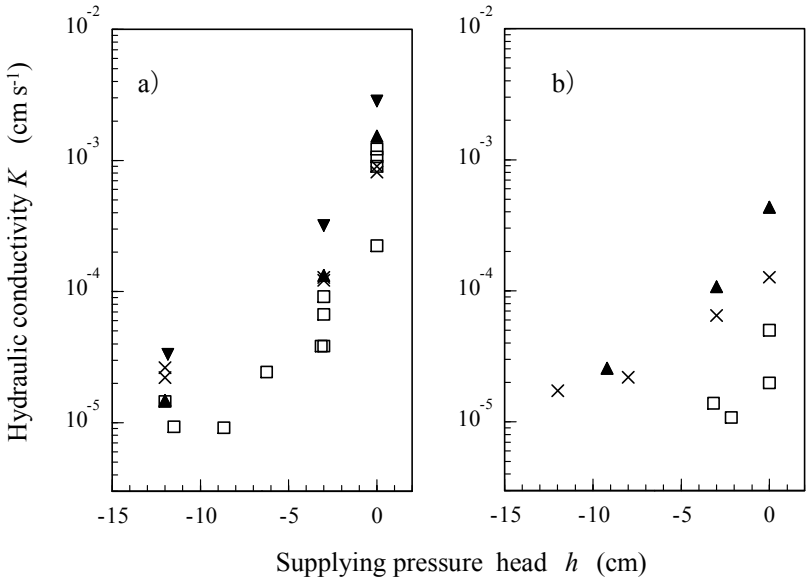

Figure 2. Near-saturated hydraulic conductivity in the plow sole of a) double-cropped fields and b) single-cropped rice fields.
×Gray Lowland soil around the middle reaches of rivers; □Gray Lowland soil around the lower reaches of rivers; ▼Andsol; ▲Brown Lowland soil

The hydraulic conductivities of the plow sole under supplying pressure head, especially h = –12 cm

Hydraulic conductivities of the plow sole at h = –12 cm in single-cropped rice fields in lower reaches (Oki and Yanagawa) were markedly lower than those in double-cropped fields (Oki, Yanagawa, Shiroishi and Kawazoe), as shown in Figure 2. They were in fact below the measurement limit of the tension disk infiltrometer. In fields with fine-textured soil, the effect of macropores on the permeability of the plow sole under the single rice cropping system was lower than under the double-cropping system. In the middle reaches, there was no difference in the hydraulic conductivity of the plow sole at h = –12 cm between the double-cropped fields (Kinryu, Tanushimaru, Takeo and Yasutake) and the single-cropped fields (Nabeshima and Yasutake). The value was in the order of 10^{-5} cm s^{-1}. These results indicated that the cropping system in coarse-textured soil fields would not significantly affect the hydraulic conductivity under h < 0 cm, i.e. the permeability of the plow sole during upland cropping.

Management according to cropping system, based on the near-saturated hydraulic conductivity of the plow sole

In double-cropped fields, fertilizers may promptly flow out from the root zone following heavy rain during upland growing season owing to the presence of macropores in the plow sole. For ponding water on the field during rice planting, double-cropped fields need to be managed to limit infiltration, irrespective of the permeability of the plow sole, akin to that caused by puddling of the topsoil or a high water table due to water filling the ditches in the surrounding of the fields.

Conclusion

The near-saturated hydraulic conductivity of the plow sole in single-cropped rice fields and double-cropped fields was determined by using a tension disk infiltrometer. Macropores significantly affected the saturated hydraulic conductivity of the plow sole in double-cropped field. In areas around the lower reaches of rivers, the effect of macropores was seen up to h = –12 cm. The choice of the cropping system and its continuous use are likely to lead to the development of a specific structure of the plow sole and affect water and solute transport during upland growing season, especially in fine-textured soil.

References

Angulo-Jaramillo R, Vandervaere JP, Roulier S, Thony JL, Gaudet JP, Vauclin M (2000) Field measurement of soil surface hydraulic properties by dis and ring infiltrometers: A review and recent developments. *Soil and Tillage Research* **55**, 1-29.

Ankeny MD, Kaspar TC, Horton R (1988) Design for an automated tension infiltrometer. *Soil Science Society of America Journal* **52**, 893-896.

Ankeny MD, Ahmaed M, Kaspar TC, Horton R (1991) Simple field method for determining unsaturated hydraulic conductivity. *Soil Science Society of American Journal* **55**, 467-470.

Perroux KM, White I (1988) Design for disc permeameters. *Soil Science Society of America Journal* **52**, 1205-1215.

Yoshida S, Itoh K, Adachi K (1997) Improvement of drainage in clayey rotational filed by introducing winter crops after conversion from paddy. *Soil Physical Conditions and Plant Growth, Japan* **76**, 3-12 (in Japanese with English Abstract).

Compilation of a 3D soil physical database for the unsaturated zone

Zsófia Bakacsi, **László Pásztor** and József Szabó

Research Institute for Soil Science and Agricultural Chemistry of the Hungarian Academy of Sciences, Hungary, Email pasztor@rissac.hu

Abstract
The most commonly used basis for the estimation of soil hydraulic parameters is the particle-size distribution (PSD) data or class pedotransfers. In this paper we outline an attempt for compilation of an integrated and harmonized stratified soil physical database for a model area, using different origin data sources. Due to their appropriate spatial and thematic resolution and data processing status, the Digital Kreybig Soil Information System (DKSIS) and Hungarian Agrogeological Database were chosen as pedological and agrogeological data sources of the database, which were able to describe the soil physical properties in the unsaturated zone. The resulted database characterizes the distinguished soil and sediment layers –have at least 10 cm thickness- for a 690 km^2 model area, describing their thickness and texture classes to the depth of the permanent groundwater level, in every single square kilometer cell of the model area. The compiled database is indispensable in coupled (deterministic - stochastic) model simulation based analysis of regional water management problems like drought, flood and inland inundation.

Key Words
Spatial soil information system, stratified soil physical data, unsaturated zone, data harmonization.

Introduction

Describing the water movement in the unsaturated zone, numerous soil hydraulic data as input parameters are required concerning the water retention curve and the hydraulic conductivity function as the main hydraulic properties. Because of the direct measurement of the hydraulic parameters is difficult and time-consuming, the estimation of them can be an alternative. The most commonly used basis of the estimation is the particle-size distribution (PSD) data or class pedotransfers (e.g. Rajkai *et. al* 1996; Tietje and Hennings 1996; Hwang and Powers 2003). Based on the Unsaturated Soil Hydraulic Database of Hungary (HUNSODA) Nemes (2002) defined the main hydraulic parameters for each texture class both in the FAO and USDA classification system.

The aim of our work was to compile the first version of a stratified soil physical database, describing the soil physical properties and stratification of the formations to the depth of the permanent groundwater level. Usually, the strength of a pedological dataset is the detailed description of the surface and subsurface horizons of the soil; however the depth of the soil profiles is limited and does not explore the whole unsaturated zone. Close to the surface an agrogeological dataset is less sensitive for the fine stratification than the pedological one, but the depth of the boreholes is used to be enough for the description of the whole unsaturated zone.

Since the existing pedo- and agrogeological databases are not able to serve separately the 3D model requirements, their integration was necessary. Using different origin data sources for harmonized database construction is common, especially in those cases when the accessible individual datasets cannot fulfill the requirements, e.g. in a transboundary soil database (Dobos *et al.* 2008). Large amount of soil information in different spatial and thematic resolution is available in Hungary, in different data processing status. The existing Hungarian Soil Monitoring network points (1200 sites) have had detailed profile description and measured particle size distribution data since 1992, but its spatial resolution is not adequate in the target area. For less than half of the territory of Hungary 1:10, 000 scale soil maps and site descriptions would be available, but the described areas are fragmented and just at the beginning of GIS processing.

Materials and Methods

Processing of pedological data

The Digital Kreybig Soil Information System (DKSIS) compiled in the Institute for Soil Science and Agricultural Chemistry of the Hungarian Academy of Sciences, based on the first national soil mapping program (1933-44, and after war, till 1951) in Hungary. The survey sheets are 1:25,000 scale mounted

topographic maps (area about: 25 000 ha), which indicate field observations and contain the original location of the reference sites (Pásztor *et al.* 2010). Even though some of the laboratory methods have been changed, the field, -and laboratory data of the Kreybig archive represent valuable information on soil physical/chemical properties (e.g. texture, pH-value, exchangeable acidity, carbonate- and salt content) and can take into account as „baseline values" comparing with the present-day condition (e.g. acidification, salinization). Lack of measured PSD data, the field estimation of the textural classes, air dry soil moisture content and the so-called "capillary rise of water" defined the texture classes (Kreybig 1937). In the latter method, a 100 cm high (20-25 mm caliber), open-end glass-cylinder was filled up with ground soil sample and stand in water. The capillary rise is recorded in consecutive 5 h, 10 h, 20 h and 100 h intervals. In Kreybig-survey time the "capillary method" has been widely used and accepted, but because of its debated reproducibility, has become unaccepted. The so-called "air dry soil moisture content" in the explanatory booklets, practically means hygroscopic moisture content (hygroscopicity, *hy*), mainly according to Kuron (Mados 1938). The capillary rise and especially the *hy* values could be take into consideration in fine texture class definition (Filep and Ferencz 1999), but regarding the Kreybig database, the verification reliability of legacy data relation to the texture classes was not proved to our satisfaction.

From the 1940s till nowadays, the so-called plasticity index according to Arany (K_A) has been an accepted "low-cost" method for texture class definition (Ballenegger 1962) in the Hungarian practice. Determination of K_A in laboratory is similar to the saturation percentage (SP %), but requires another consistency status and its values are approx. 10 percent lower than the SP values (Búzás 1993). At the time of Kreybig survey the laboratory routine had not extended for the K_A determination, but in 2009 a unique explanatory booklet from 1944 with measured KA data was emerged (num. 5264/3 from Alpár region). The legacy K_A values could serve as a link between Kreybig laboratory data and the applied texture class definition in the practice today. The relation of K_A values and the applied texture classes with hygroscopicity and capillary rise values are shown in Table 1.

Table 1. Hungarian conventional texture classes for practical purposes, their relation to hygroscopicity, 5 hours capillary rise values and plasticity index according to Arany (based on Ballenegger 1962; Stefanovits *et al.* 1999).

texture classes	hy (%)	capillary (mm)	KA
coarse sand	< 0,5	-	< 25
sand	0,5-1,0	> 300	25-30
sandy loam	1,0-2,0	250-300	31-37
loam	2,0-3,5	150-250	38-42
clayey loam	3,5-5,0	75-150	43-50
clay	5,0-6,0	40-75	51-60
heavy clay	> 6,0	< 40	61-80

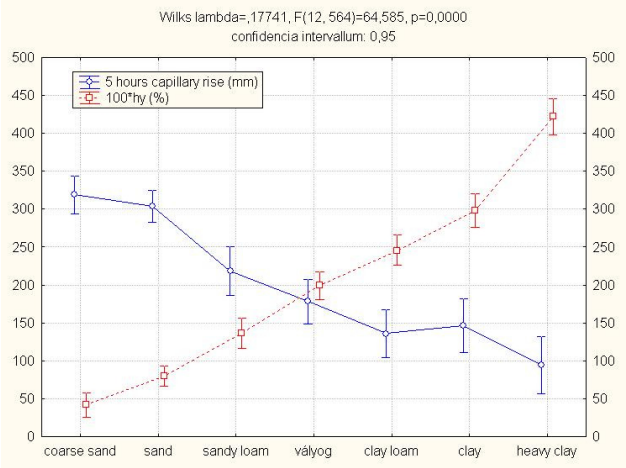

Figure 1. 5 hour capillary water rise (mm) and hygroscopicity values (multiplied by 100) according to the Hungarian conventional texture classes as categorical factor, based on 290 data origin from the Alpár (num. 5264/3) map sheet.

At the 5264/3 sheet, for 290 samples the measured capillary water uptake and hygroscopicity has good empirical relation with the textural classes of the sample according to their plasticity index. In each texture class the standard deviations of capillary rise values are higher than the hygroscopicity ones. The capillary rise seems to be less reliable at the clay-heavy clay classes, but we should take into consideration the weakness of the plasticity index (Ballenegger 1962) in this measuring range (Figure 1).
The 690 km^2 large Szentes model area is situated on the southeastern part of the Great Hungarian Plain, developed on alluvial sediments of Tisza River and tributaries. In the DKSIS 649 soil mapping units cover the model area, 582 of them are agricultural land and 67 of them with other land use (forest, settlement, waterlogged area). 484 sites of soil profiles as point features were joined to the polygons, using "one representative point to one polygon" method, and characteristically each profile has two or three horizons (with approx. 1200 samples). There was not soil description for the non-agricultural lands; these polygons

were affiliated to their largest neighbor.
During the data processing the inconsistent field vs. capillary or *hy* data pairs was excluded. Sand, sandy loam, loam, clay loam and clay classes were defined according to the Hungarian practice.

Processing of agrogeological data
The agrogeological dataset belongs to the Hungarian Geological Institute and derives from 10 m depth boreholes drilled in the period of 1964-1985. In the model area the exposed 152 boreholes are along an equidistant grid, drilled 3.5 km from each other. According to the agrogeological method all the different geological formations were sampled, at least in each 1.0 m. Based on the description and particle size distribution data, 110 similarly stratified patches were delineated on 1:100 000 scaled maps. 134 boreholes (with approx. 2000 samples) have complete stratification description and PSD analysis. The geological practice for describing the sediments differs from the pedological nomenclature; therefore we turned back to the detailed PSD data and re-defined their particle-size classes according to the USDA triangle (Soil Survey Staff 1975). The used particle-size intervals in the Hungarian geological practice slightly differ from the pedological requirements. They measure the clay fraction (< 0.002 mm), but define the silt/sand size limit at 0.06 mm, while it is 0.05 mm in the pedological practice. Numerous interpolation methods are used for estimation of missing particle-size classes (e.g. Buchan 1989; Rousseva 1997; Nemes *et al.* 1999). In our "first approximation" considering the silt/sand limitation differences (0.06 mm in place of 0.05 mm) loglinear interpolation method was used. Significant gravel-sediments (over 2 mm grain size) were not exposed in the unsaturated zone, so it was not necessary to re-calculate the grain size distribution only for the earth fraction before arranging data in textural triangle. We defined texture classes based on the clay-silt-sand triangle, and divided the agrogeological samples into 12 classes according to the USDA classification. Most of the samples were fine-grained silt sediments.

Results
Both in the DKSIS and agrogeological maps, the spatial extension of the polygons varied, in the large patches numerous islands-like polygons can be found with the same attributes. The place of the profiles and boreholes as point features was joined to the polygons, using "one to one" method, and after spatial joining, the polygons got "deepness", as third dimension from the attribute table of the point data (Figure 2). For the calculation of the km*km grid content, the vector maps was converted into raster format. The structured (depth and texture) data follow each other not equidistantly; the resulted data layers preserve the stratification characteristic of the profiles and boreholes.

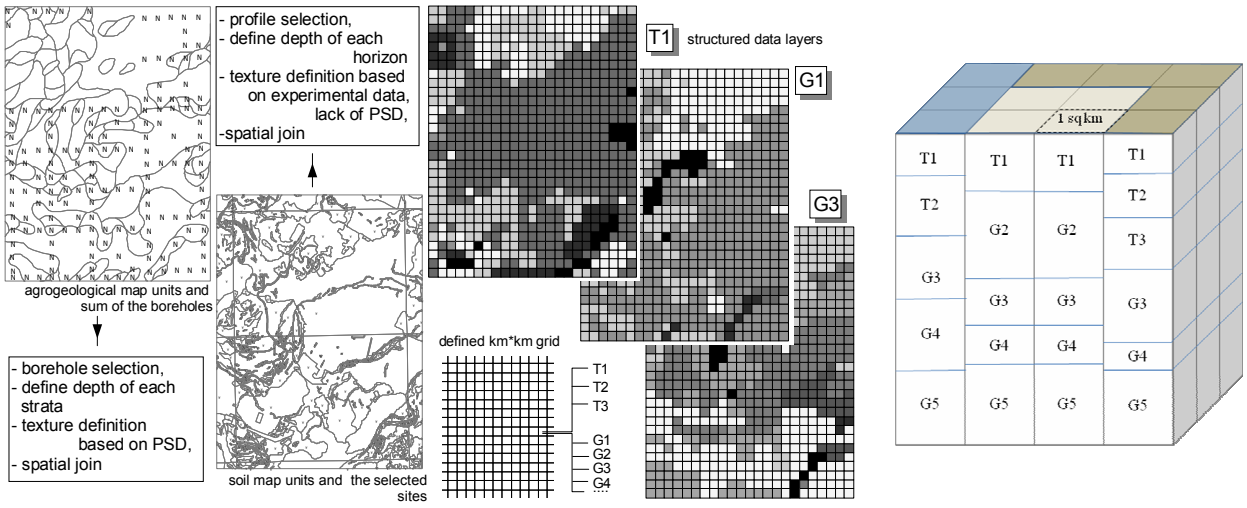

Figure 1. Summarizing the main stages of database compilation. The colored grids illustrate the spatial distribution of the different textures in the selected layers (left), and a conceptional cube (right) to demonstrate the spatial structure and resulted stratification of the database down to the fifth agrogeological depth interval.

Because of the same texture name according to the Hungarian "practical" nomenclature and the USDA triangle does not cover necessarily the same hydrological character, for further studies and hydrological characterization the database reserve the origin of the layers and the data from the DKSIS were coded as "T", the others, noted their agrogeological origin, as "G". The repetitions were excluded regarding the same depth

interval originating from the DKSIS and agrogeological data and the layers with less than 10 cm thickness, too. Describing the structural diversity of the pilot area, 9 kinds of layer-combinations fitted to requirements T1T2T3G3G4 (184 case num.); T1G2G3G4G5 (170); T1T2T3G2G3 (137); T1T2G2G3G4 (137); T1T2G3G4G5 (44); T1T2G2G3G5 (7); T1T2T3G4G5 (6); T1T2T3G3G5 (4); T1T2G4G5G5 (1).

Conclusion

The compiled stratified soil physical database for the unsaturated zone can be the base of soil hydraulic parameter estimation, which can serve as input data for soil hydrological modeling. The database structure reflects both the fine stratification of the soil layers near to the surface, and the sedimentation of the parent material and deeper structures, frequently down to 10 m. Its adaptation and spatial extension for larger area makes possible the more realistic description of vadose zone, accommodating to the hydraulic model requirements, solving regional water management problems.

Acknowledgements

The present work was partly founded by the WateRisk Project (TECH_08-A4/2-2008-0169) and the Hungarian National Research Foundation (OTKA, Grant No. NK73183). The authors are grateful to the staff of RISSAC GIS Lab: Judit Matus, Zita Krammer, Annamária Laborczi and Szilvia Vass-Meyndt.

References

Ballenegger R (1962) Talaj- és tápanyagvizsgálati módszerek (in Hungarian). Mezőgazdasági Kiadó, Budapest

Buchan GD (1989) Applicability of the simple lognormal model to particle-size distribution in soils. *Soil Science* **147,** 155-161.

Búzás I (1993) Talaj- és agrokémiai vizsgálati módszerkönyv 1 (in Hungarian). INDA 4231 Kiadó, Budapest.

Dobos E, Bialkó T, Michéli E (2008) Határon átnyúló talajtani adatbázisok készítése digitalis talajtérképezési eszközök segítségével (in Hungarian). *Talajvédelem* special issue, 577-584.

Filep Gy, Ferencz G (1999) Javaslat a magyarországi talajok szemcseösszetétel szerinti osztályozásának pontosítására (in Hungarian). *Agrokémia és Talajtan* **48,** 305-320.

Hwang SI, Powers SE (2003) Using Particle-Size Distribution Models to Estimate Soil Hydraulic Properties. *Soil Sci. Soc. Am. J.* **67,** 1103-1112.

Jamagne M, King D, Le Bas C, Daroussin J, Burill A, Vossen P (1994) Creation and use of a European Soil Geographic Database. In '15th International Congress of Soil Science, Transactions, Commission V, Symposia', Acapulco, Mexico, Vol. 6a, pp. 728-742.

Kreybig L (1937) The survey, analytical and mapping method of the Hungarian Royal Institute of Geology (in Hungarian and German). M. Kir. Földtani Intézet Évkönyve, 31, 147–244.

Mados L (1938) A higroszkópos nedvesség, mint a talaj kötöttségi állapotának jellemzője (in Hungarian). Mezőgazdasági Kutatások, XI. évf. Budapest, pp. 217-229.

Nemes A, Wösten JHM, Lilly A, Oude Voshaar JH (1999) Evaluation of different procedures to interpolate particle-size distributions to achieve compatibility within soil databases. *Geoderma* **90,** 187-202.

Nemes A (2002) Unsaturated Soil Hydraulic Database of Hungary: HUNSODA. *Agrokémia és Talajtan* **51,** 17-26.

Pásztor L, Szabó J, Bakacsi Zs (2010) Digital processing and upgrading of legacy data collected during the 1:25 000 scale Kreybig soil survey. *Acta Geodaetica et Geophysica Hungarica* **45**, 127-136.

Rajkai K, Kabos S, van Genuchten MTh, Jansson P (1996) Estimation of water-retention characteristics from the bulk density and particle-size distribution of Swedish soils. *Soil Science* **161,** 832-845.

Rousseva SS (1997) Data transformations between soil texture schemes. *European Journal of Soil Science* **48,** 142-147.

Soil Survey Staff (1975) Soil taxonomy: A basic system of soil classification for making and interpreting soil surveys. USDA/SCS Agricultural Handbook No. 436, U.S. Government Printing Office, Washington, D.C., USA.

van Genuchten MTh (1980) A closed-form equation for predicting the hydraulic conductivity of unsaturated soils. *Soil Sci. Soc. Am. J.* **44,** 892-898.

Deposit structure, water mineralization and groundwater recharge of a rubber-tree-planted watershed in Northeast Thailand

Jean-Pierre Montoroi[A], Olivier Grünberger[B], Onjamala Elarimisa[C], Jean-Luc Michelot[C], and Wanpen Wiriyakitnateekul[D]

[A]Institut of Research for Development, UMR Bioemco, Bondy, France, Email jean-pierre.montoroi@ird.fr
[B]Institut of Research for Development, UMR Lisah, Montpellier, France, Email olivier.grunberger@ird.fr
[C]University of Paris-Sud, UMR Ides, Orsay, France, Email elarimisa@yahoo.fr, jean-luc.michelot@u-psud.fr
[D]Land Development Department, Bangkok, Thailand, Email wwanphen@gmail.com

Abstract
In Northeast Thailand rubber-tree cropping is widespread according to economy market and in spite of climate constraints. A study was undertaken in farmer's plantation to characterize the pedological and geological deposits within a 2 km^2 watershed, to monitor groundwater fluctuations within shallow and deep aquifers and to assess water mineralization and water chemistry composition. The soil profile comprises a more or less thick clayey layer above the bedrock (sandstone-siltstone), the top depth of which is less than one meter at slope summit and increases along the slope until few meters. The sandy layer is a temporary aquifer where a shallow perched groundwater is flowing laterally towards lowlands owing to the underlying and low impermeable clay layer. The sandstone-siltstone bedrock is a fractured and permanent aquifer which is most often at the same elevation in uplands than in lowlands and is recharged from the upland summit. The deep groundwater mineralization is saline-contaminated whereas the shallow groundwater origin is meteoric. The study leads to the conclusion that variability in deposit structure and groundwater functioning should be taken into account in management of rubber-tree plantations.

Key Words
Tropical soil, Sandstone, Water chemistry, Watershed, Rubber-tree, Thailand.

Introduction

The landscapes of North Eastern Thailand (NT) are dominated by undulating hills with elevation ranging from 170 m (lowlands) to 240 m (uplands). The lowlands are managed for rain-fed and flooded paddy rice fields which are nowadays severely affected by salinity. *Dipterocarpus* forest natively occupied the uplands but was massively cleared over the last mid-century. Forest area decreases from 70,400 km^2 in 1961 to 21,370 km^2 in 1993, namely from 41% to 13% of the NT area (Wannakomol 2005). Intensive wood-cutting propelled on the farming of cash crops including cassava, sugar cane, kenaf and maize. It is arguing that the ancient and widespread land use change leads to a comprehensive change of hydrology balance in NT including a groundwater rise up due to a deep aquifer recharge increase, an evapotranspiration inefficiency of seasonal crops and an extension of saline seepage on lower slopes and valley floors (Ilstedt 2007). Lowland salinity features are visually displayed in dry season as discrete patches of various sizes (from some m^2 to some ten m^2) and shapes which cover soil surface with white efflorescences, mainly halite. Salinity contamination comes from the artesian rise up of the regional groundwater which is enriched with dissolved salts by flowing through the Cretaceous Maha Sarakham evaporite deposits embedded within siliclastic formations (El Tabakh *et al.* 1998, Williamson *et al.* 1989, Imaizumi *et al.* 2001). An area of 28,400 km^2, namely 17% of the NT region, is salt-affected from slightly to severely stages (Arunin 1992). Last cultivated cash crop in NT is rubber-tree (*Hevea brasiliensis*), which is intensively developing (from 30,965 ha in 1990 to 94,450 ha in 2003) and economically following the increasing demand for manufactured rubber devices as tyres. The recent land use change, which is expected to last over several decades, is likely to modify aquifer recharge leading to a water infiltration decrease, as deep rooted trees contribute more efficiently than shallow rooted crops towards evapotranspiration, a groundwater fall and a slightly decrease of lowland salinization. However, NT is not as suitable for rubber-tree cropping as other Thai regions. Climate is highly variable in time and space, constraining the plant growth and the latex production. The objective of the study is (i) to evaluate the relationships between aquifer recharge and water mineralization at a small watershed scale, which is partly five-year rubber-tree planted, by deposit surveying, groundwater monitoring and conceptual modelling; (ii) to assess the rubber-tree cropping sustainability on a long-term basis.

Methods

Experimental site

Located nearby Ban Non Tun village (16°20'N; 102°44'30"E), the 2 km^2 studied watershed is about 20 km southwest of the city of Khon Kaen in the district of Phra Yun. The Tropical Savannah climate is influenced by Asian monsoon and marked by distinct rainy season (from May to October) with a mean annual rainfall of 1,212 mm and 107 rainy days per year in average (Wada 1994) and dry season (from November to April). Soils are classified along a toposequence as Typic Haplustult (upland summit), Arenic Paleustalfs (from upper to lower slope) and Typic Paleustult (toe slope). Clay and silt contents increase with depth ranging from 3% to 28% for clay fraction and from 5.6 to 14.3% for silt fraction. Sandy layer displays iron oxide features which attest iron mobility under reduced conditions. Clayey layer underlines a highly fractured bedrock which is described as sandstone and siltstone. Quartz, smectite and kaolinite are the predominant constituents in the clay fraction with some illite and trace amounts of feldspar and goethite. Quartz is the major component in the silt fraction with small amount of feldspar and trace of goethite. Formation of poorly crystalline kaolinite along the slope may formed by pedogenesis under an intermediate to poorly drainage whereas a dense clay layer at 50-70 cm depth produced a waterlogging in rainy season (Wiriyakitnateekul 2009).

Field surveying and water sampling

A field survey was performed using outcrop observations, manual auger soundings until bedrock along transects (90 samples) and an electromagnetic conductivimeter (EM38 from Geonics^{TM}) (Figure 1). Soil of each sounding was sampled every 10 cm within one meter and every 20 cm depth below. Soil samples were analysed in field for manual particle size distribution. Depth and thickness of sandy, clayey and bedrock were assessed and mass soil water content was measured at laboratory by gravimetric method.

A piezometer network was installed in lowlands and along two transects to localize the shallow (< 3 m in depth) and deep (from 10 m to 32 m in depth) aquifers by manual and mechanical drilling, to ascertain the magnitude of groundwater fluctuations by monitoring in time and to determine the chemical types of underground waters by laboratory analyses. Piezometers were base-screened from one meter (shallow ones) and two meters (deep ones) to avoid aquifer mixture. Surface waters stored in small ponds and aquifer waters were sampled at late dry season (March) and at rainy season (September) for chemical and isotopic analyses.

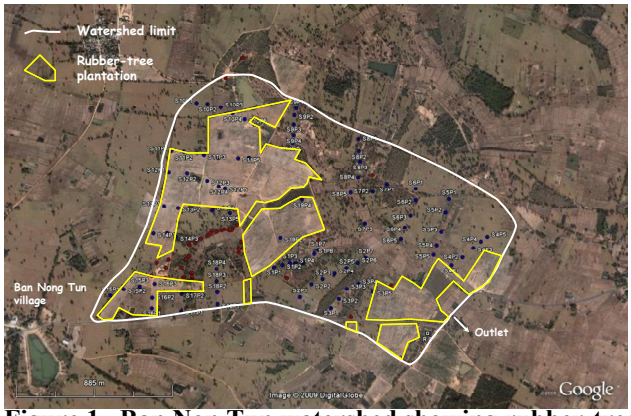

Figure 1. Ban Non Tun watershed showing rubber-tree plantation area and soil sampling location

Results

Characterization of soil and deposit features

The thickness of the sandy and clayey layers is highly variable showing a regular increase towards down slope and lowlands. The spatial distribution of the bedrock (sandstone-siltstone) top elevation is closely related to the watershed topography (Figure 2). These results are confirmed by EM38 measurements. The general distribution of the clayey layer is a key point to control groundwater recharge. The distribution of the soil mass water content is spatially clay content-related.

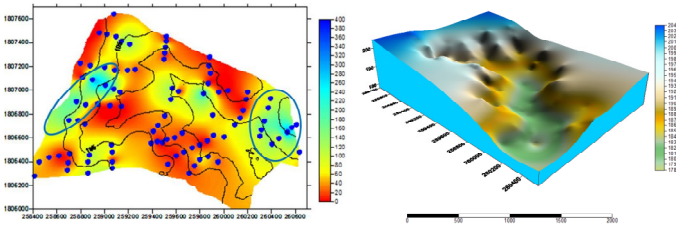

Figure 2. Spatial distribution of clayey layer thickness (in cm) and bedrock top elevation (in m)

Groundwater monitoring

Figure 3 shows a slightly trend to a groundwater recharge of the deep aquifer where groundwater level elevation is ranging from 177 m to 179 m. Only the piezometer located at slope summit (PB1K) quickly reacts at any heavy rainy event indicating that a preferential vertical recharge by direct infiltration occurs through the sandy later and the fractured bedrock (lack of clayey layer at this location). All the shallow piezometers react when rain is falling.

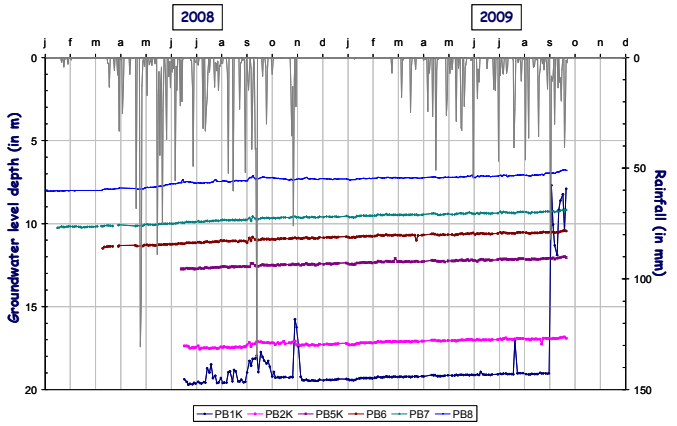

Figure 3. Time evolution of deep groundwater and daily rainfall amount

Mineralization and stable isotope features of groundwaters

Three groundwater types are distinguished taking in account the electrical conductivity parameter, the chemical composition and the groundwater elevation assessed at the screening piezometer base. The shallow groundwater of the sandy layer aquifer is weakly mineralized and Na-HCO_3 type whereas the deep groundwater of the sandstone-siltstone aquifer is highly mineralized (up to 6.5 dS/m) and Na-Cl type assuming a saline contamination. An intermediate type which is related to the shallow groundwater of the sandy layer aquifer located in paddy fields has an average mineralization and type (Figure 4).

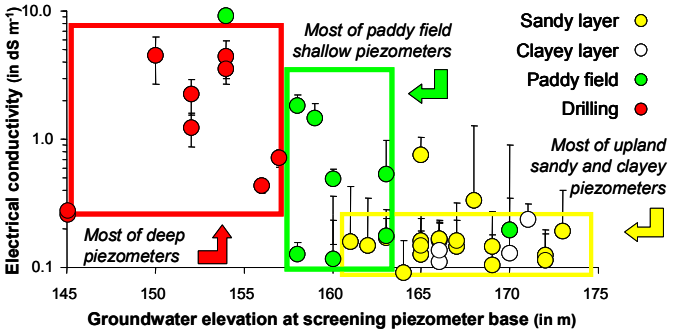

Figure 4. Mineralization patterns of shallow and deep groundwaters

Deep groundwaters are not evaporated assuming that they are meteoric in origin. A slight evaporated pattern is observed for some shallow groundwaters. Pond surface waters contributing to groundwater recharge are slightly evaporated according to isotope values (Figure 5).

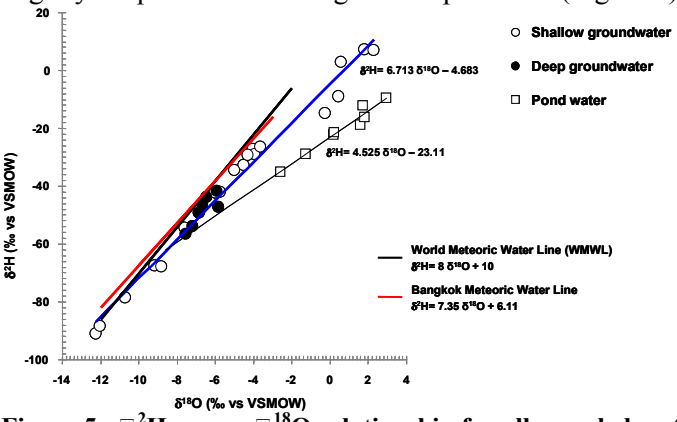

Figure 5. □^{2}H versus □^{18}O relationship for all sampled waters within Ban Non Tun watershed

Conceptual modelling

Figure 6 summarizes the recharge pathways and the chemical features of groundwaters using a synthetic scheme. The evolution with time (dry and wet seasons) is assumed for groundwater movement .

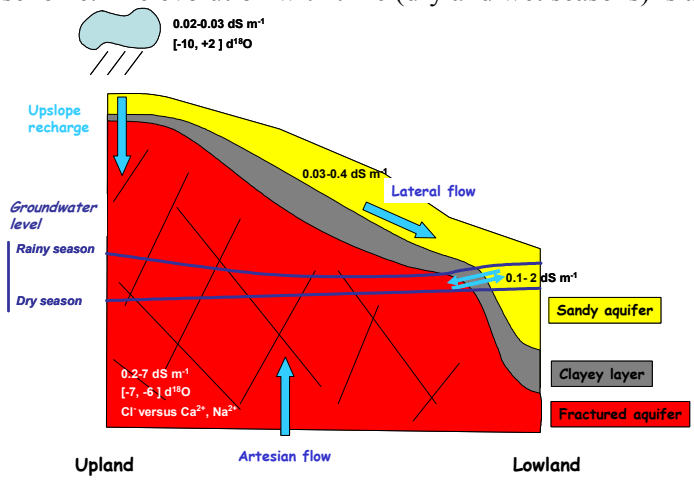

Figure 6. Conceptal model of groundwater pathways within deposit toposequence. Chemical and isotopic data ranges of groundwaters sampled at late dry season are included.

Conclusion

The field study performed at a small watershed scale leads shows (i) the presence of an impermeable clayey layer which has a double role as controlling the recharge distribution of the upland groundwater and protecting the shallow groundwater flowing within the sandy top layer; (ii) a high downwards recharge and a weak upwards recharge for both sandy layer and sandstone-siltstone aquifers; (iii) a deep deposit origin of groundwater mineralization with a slightly contamination of the shallow sandy aquifer and a strongly contamination of the deep sandstone-siltstone aquifer by saline and artesian flow uprising.

The present study site has lower annual precipitation rate and rainy day amount than the suitable values for rubber-tree cropping (1,250 mm and 120-150 rainy days) inferring a severe climate constraint. Moreover root system growth might be interfered according to the tree position along the slope. Soil layer thickness, clay layer barrier and waterlogging duration are determinant factors leading to increase the biomass variability within rubber-tree plantations. Soil and water resources need to be properly managed by smallholders and rubber production would be improved using inter-rank cropping and water harvesting.

References

Arunin S (1992) Strategies for utilizing salt-affected lands in Thailand, In 'Proceedings of the International Symposium on Strategies for Utilizing Salt Affected Lands, February 17-19, 1992', pp. 26-37 (Department of Land Development, Ministry of Agriculture and Cooperatives, Bangkok, Thailand).

El Tabakh M, Utha-Aroon C, Schreiber BC (1998) Sedimentology of the Cretaceous Maha Sarakham evaporites in the Khorat plateau of northeastern Thailand. *Sedimentary Geology* **123**, 31-62.

Ilstedt U, Malmer A, Verbeeten E, Murdiyarso D (2007) The effect of afforestation on water infiltration in the tropics: A systematic review and meta-analysis. *Forest Ecology and Management* **251**, 45-51.

Imaizumi M, Sukchan S, Wichaidit P, Srisuk K, Kaneko F (2001) Hydrological and geochemical behaviour of saline groundwater in Phra Yun, Northeast Thailand. *JIRCAS working report* **30**, 7-14.

Wada H, Wichaidit P, Pramojanee P (1994) Salt-affected area in Northeast Thailand. Nature, properties and management. Technical paper 15, (Agric. Dev. Res. Center in NE Thailand-Japan Int. Coop. Agency).

Wannakomol A (2005) Soil and groundwater salinization problems in the Khorat plateau, NE Thailand - Integrated study of remote sensing, geophysical and field data. Doctorate Thesis, (Berlin, Germany).

Williamson DR, Peck AJ, Turner JV, Arunin S (1989) Groundwater hydrology and salinity in a valley in Northeast Thailand. In 'Groundwater Contamination', IAHS Publication, **185**, 147-154.

Wiriyakitnateekul W, Hammecker C, Anusontpornperm S, Boonrod S (2009) Clay mineralogy of soils derived from sandstone along a toposequence in Northeast Thailand. In 'Proceedings of 14th International Clay Conference' (Castellaneta Marina, Italy).

Effect of soil management on pore geometry and the implications for fungal invasion and interactions

Alexandra Kravchenko[A], Ruth Falconer[B], Dmitri Grinev[C] and Wilfred Otten[D]

[A]Department of Crop and Soil Sciences, Michigan State University, East Lansing, MI, USA, Email kravche1@msu.edu
[B]SIMBIOS Centre, University of Abertay Dundee, Dundee, UK, Email R.Falconer@abertay.ac.uk
[C]SIMBIOS Centre, University of Abertay Dundee, Dundee, UK, Email D.Grinev@abertay.ac.uk
[D]SIMBIOS Centre, University of Abertay Dundee, Dundee, UK, Email w.otten@abertay.ac.uk

Abstract
Despite the importance of fungi in soil functioning they have received comparatively little attention and our understanding of fungal interactions and communities is lacking. This study aims to combine a physiologically based model of fungal growth and interactions with digitized images of undisturbed soil samples from contrasting management practices to determine the effect of physical structure on fungal growth and colonization. We quantified pore geometries of the undisturbed soil samples from long-term agricultural and native vegetation land uses, modelled invasion of a single fungal species and of two different fungal species within the soil samples; and evaluated the role of soil structure on fungal invasion and species interactions; in particular, we identified those characteristics of the pore volume that promote or exclude fungal invasion.

Key Words
Fungal growth model, 3D pore space, X-ray microtomography, land use.

Introduction
Fungi are a major player in soil functioning. They contribute to soil structure formation and shaping of plant communities through their role in nutrient cycling, pathogenesis and symbiosis. Surprisingly, fungi have received comparatively little attention; and theoretical approaches which have emerged over the years and improved considerably our understanding of above ground plant communities are still lacking below ground. A theoretical framework is needed, such that links soil physics, fungal biology, mathematical biology and statistics in order to understand fungal community dynamics and diversity in undisturbed soils. Such a framework is essential if we are to understand how environmental change or soil manipulation impacts biodiversity. Different land use and management practices significantly affect soil environmental characteristics crucial for fungal communities by contributing different quantities and qualities of biomass inputs, generating different levels of soil disturbance, influencing soil temperature and moisture regimes, and affecting structure and geometry of soil pore space. Differences in pore structures generated by long-term differences in land use and management are reflected in notable changes in soil physical and hydraulic properties, including soil porosity, hydraulic conductivity and water retention (Brye and Pirani 2005). Changes in numbers, shapes, and distributions of soil macropores have been often observed (e.g., Pachepsky *et al.* 1996; Giménez *et al.* 1997; Udawatta *et al.* 2008). However, specific implications of these differences in pore structure and geometries for ability of pathogenic as well as non-pathogenic fungi to colonize soil body have not been address yet. Recent advances in computed tomography and microscopy facilitate detailed examination of the inner pore structures of undisturbed soil samples as well as visualization of fungal mycelia. Such tools together with modelling generate a new level of understanding of the mechanisms governing fungal behaviour at microscopic scales, and for the first time allow us to examine species interactions in a 3D environment. The goal of this study is to assess how physical structure of the environment affects fungal growth and spread through the space? We hypothesize that analyses and comparisons of the pore structures and their colonization by fungi in soils of the same origin but subjected to long-term contrasting management, e.g., conventional agriculture with or without intensive tillage versus native vegetation, will provide insights for understanding functioning of soil fungal communities.

The specific objectives are (i) to quantify pore geometries of the undisturbed soil samples from long-term agricultural and native vegetation land uses based on the analysis of 3D images; (ii) to model invasion of a single fungal species and of two different fungal species within the soil samples; and (iii) to evaluate the role of soil structure on fungal invasion and species interactions; in particular to identify those characteristics of the pore volume that promote or exclude fungal invasion.

Methods

Sample collection

Soil samples were collected from Long Term Ecological Research (LTER) experiment located in Southwest Michigan, USA (42 ^{o} 24' N, 85^{o} 24' W) established in 1988. Soils are classified as well-drained, Typic Hapludalfs either fine-loamy, mixed mesic (Kalamazoo series) or coarse-loamy, mixed, mesic (Oshtemo series). The three of the LTER treatments used in this study are (i) conventionally tilled (chisel ploughed) (CT) and (ii) no-till (NT) corn-soybean-wheat rotation with conventional chemical inputs, and (iii) native succession vegetation established on the experimental plots abandoned from agricultural use in 1989 (NS). For each treatment we collected ~15 undisturbed soil samples from depth 2-7 cm in plastic cylinders 5 cm in diameter and 5 cm length.

X-ray scanning and image analyses

The 3D pore space of each of the soil samples has been visualised with an X-TEK HMX micro-tomography system at SIMBIOS (http://simbios.abertay.ac.uk/). The computed tomography data sets were reconstructed in 3D using filtered back-projection algorithm in 32-bit floating point format to enhance contrast between the phases in soil. From the centre of each soil sample image we selected a cube ~2x2x2 cm in size. Cube data were reconstructed at 110 micron resolution to lead to soil image data sets 180x180x180 pixels in size. Each voxel was classified either as a pore or a solid based on its gray-scale value using manual thresholding approach in ImageJ (http://rsbweb.nih.gov/ij/). After pore/solid thresholding, pore characteristics, including total porosity, pore connectivity and pore-size distribution were determined for each cube using an in-house developed SCAMP plugin for ImageJ.

Fungal growth modelling

Analyses of soil heterogeneity effects on fungal growth and interactions were built upon a modelling approach developed by Falconer *et al.* (2005). The approach explores fungal traits that allow for effective colonisation of heterogeneous environments. It describes the physiological processes of vegetative growth and development of fungal colonies in a 3D soil environment. The model formulation represents the pore space as a set of voxels and models an individual mycelial network growing in the pore space as comprising three fractions: immobilized insulated biomass, non-insulated biomass and mobilized biomass. The relative proportions of these components are dynamic and are determined by four physiological processes: uptake, inter-conversion rates between mobile and immobile biomass, redistribution of mobile biomass and growth. The model incorporates biomass recycling and production of extracellular enzymes and antibiotics through which interactions between fungal species are regulated.

Three inoculums placement densities were explored, i.e., 1, 5, and 20 inoculums were introduced in randomly selected pore voxels within the soil domain. Such range of inoculation densities allowed us to cover a variety of possibilities in terms of fungal colonization of the pore space. While 20 inoculums can be regarded as a representation of a scenario for a spread of a commonly present species after a dormancy period and encompasses almost the entire pore space, a single inoculum scenario may represent a pathogen spread from a single source and is likely to be influenced by the shape and connectivity patterns of the largest connected pores.

At each iteration step we recorded the percent of the total pore space that has been occupied by the fungus. Change in the percent of pores as a function of the model iteration step (time) was then fitted with a mathematical equation:

$$\%pore=\%final(1-\exp(-(iter/a)^{b})) \quad (1)$$

where *%pore* is the percent occupied pore space, *iter* is the iteration number, *%final* is the plateau amount of pore space that has been accessed at the end of the simulation, and *a* and *b* are the parameters defining the shape of the curve. Equation (1) was fitted to the observed data from each model run of every sample using PROC NLIN procedure in SAS (SAS Inc. 2008). Statistical data analyses were performed using PROC MIXED in SAS (SAS Inc. 2008).

Results

Assessment of pore geometry characteristics

Porosity of NT was significantly lower than porosity of both CT and NS treatments. It was also much less variable, ranging only from 3 to 8%, as compared from 7 to 29 % for CT and 10 to 32% for NS. Analysis of the sizes of the largest connected pores indicated that the largest pores in CT and NS occupied much bigger

proportion of the total pore space than in NT (Table 1). On average the largest connected pore volume occupied 79 and 88% of pore space in CT and NS treatments, respectively, while it only occupied 46% of the pore space in NT. The second connected pore volume occupied around 11% of the pore space in NT, while became negligible (2-3%) in CT and NS treatments. Examples of the largest and the second largest connected pore volumes for samples from NS and NT treatments are shown in Figure 1.

Table 1. Percent of pore space occupied by five largest connected pores. Standard errors are shown in parentheses.

Treatments	Connected pore volume class				
	1	2	3	4	5
CT	79.2(9.2)a	2.8(1.4)a	1.8(1.0)ab	0.6(0.3)a	0.4(0.2)a
NS	88.5(6.7)a	1.5(0.9)a	0.5(0.4)a	0.4(0.3)a	0.3(0.2)a
NT	46.5(8.1)b	11.6(3.0)b	4.5(1.4)b	1.8(0.4)b	1.3(0.3)b

* means within the same column followed by the same letters are not significantly different from each other ($p<0.05$).

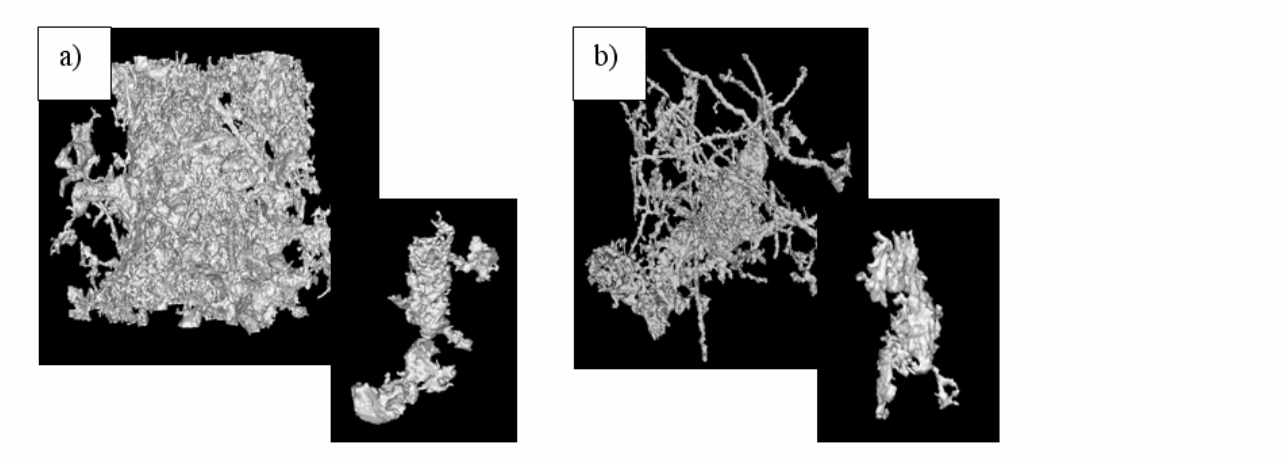

Figure 1. Examples of the largest and second largest connected pore volumes in a sample from NS (a) and NT(b) treatments.

Assessment of fungal growth

Percent of pore space occupied at the end of simulation with 5 starting inoculums in NT was only 53% while it was > 80% in NS and CT treatments (Table 2). With 20 inoculums the percentages of occupied pore space increased only slightly in CT and NS, and greatly increased in NT (to 65%). In CT and NS either with 5 or 20 inoculum points at least some seeds were placed within the largest connected pore volume which constituted on average 80-85% of the entire pore space and then were able to eventually colonize it. In NT, with 5 inoculum points the likelihood of initial seed placement to occur in more than 1-2 largest connected pore volumes is relatively low, thus only the largest and the second largest pores (combined ~58% of the pore space) were typically colonized.

Percent of pore space filled data fitted with Eq. (1) are shown on Figure 2a. There was no treatment or method differences in terms of parameter *a* at either 5 inoculum or 20 inoculum simulations (Table 2). For parameter *b* in 5 inoculum simulations, NT was lower than that of NS, but not significantly different from CT. This reflected a tendency for more S-shaped curve from NS, where possibly initial fungal spread was slow when the inoculum seeds ended up in tortuous components of the connected pore volumes. In all treatments pore space was occupied at a much slower rate with 1 and 5 inoculums points as compared to 20 inoculum points (Figure 2b).

Table 2. Parameters of Eq. (1) characterizing fungal colonization in 5 and 20 starting inoculum seeds simulations. Standard errors are shown in parentheses.

	%final		Parameter *a*		Parameter *b*	
Treatments	5	20	5	20	5	20
CT	81.5(5.5)a	83.8(5.2)a	14.1(1.4)a	6.6(0.6)a	1.9(0.2)ab	1.6(0.2)a
NS	86.5(4.3)a	88.2(4.5)a	12.4(1.2)a	7.0(0.5)a	2.1(0.2)b	1.6(0.2)a
NT	52.6(5.3)b	65.7(4.7)b	11.7(1.4)a	5.8(0.5)a	1.7(0.2)a	1.4(0.2)a

* means within the same column followed by the same letters are not significantly different from each other ($p<0.05$)

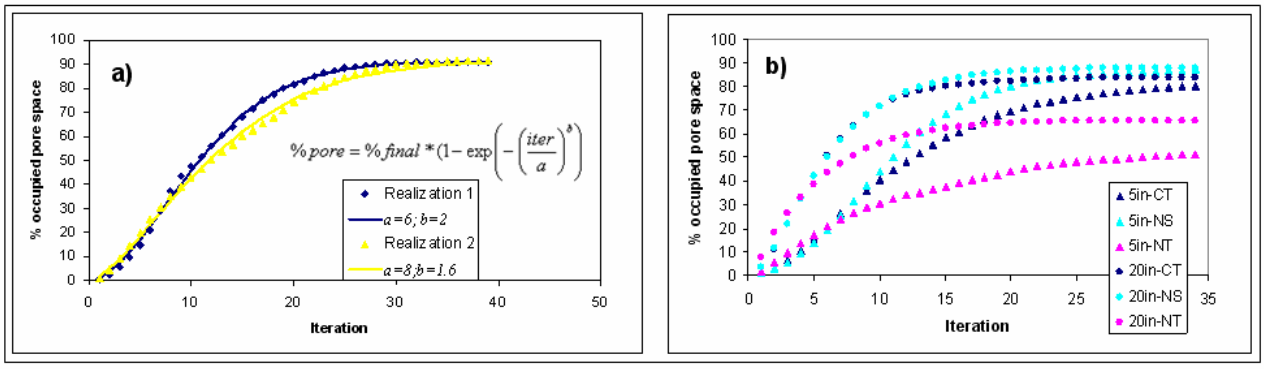

Figure 2. Example of percent of pore space occupied by fungus in a course of growth simulation fitted with mathematical function (Eq. (1)) (a) and an average % pore space occupied in simulations with 5 and 20 inoculums.

Modelling of two species interactions is currently in progress. An example of the model outcomes for two species interaction within a 3D soil pore space is shown on Figure 3. Preliminary results clearly indicate that two fungal species occupy different volumes of the soil and that the pore space heterogeneity will be a key factor in their interaction.

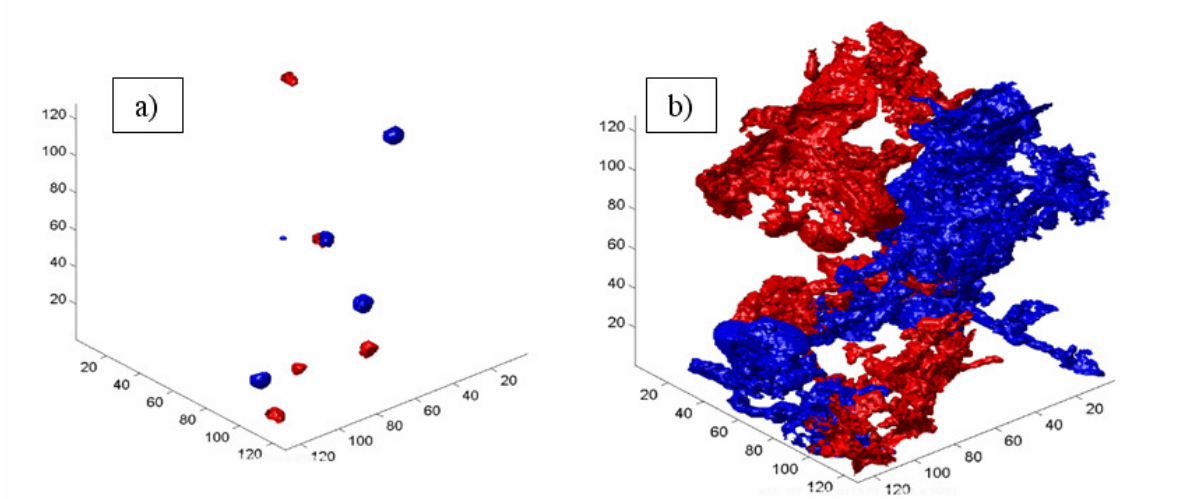

Figure 3. Example of colonization of the 3D soil pore space by two fungal species at the initial stage (a), at and final iteration (b) steps. X-, y-, and z- axes represent dimensions of the sample in voxel units (one voxel is equal to 100 μm). Two fungal species are shown in red and blue, respectively.

Conclusions

No-till had substantially lower porosity (pores >100 μm) and connectivity of pores >100 μm than CT and NS soils. These characteristics significantly reduced possibility of fungal pathogen invasions from a single inoculum, while still enabled almost complete colonization of pore space in case of multiple (20) inoculums.

References

Brye KR, Pirani AL, (2005) Native soil quality and the effects of tillage in the grand prairie region of eastern Arkansas. *Am. Midl. Nat.* **154,** 28-41.

Falconer RE, Bown JL, White NA, Crawford JW (2005) Biomass Recycling and the origin of phenotype in fungal mycelia. *Proc. Roy. Soc B. Lond.* **272,** 1727-1734.

Giménez D, Allmaras RR, Nater EA, Huggins DR (1997) Fractal dimensions for volume and surface of interaggregate pores - scale effects. *Geoderma* **77,** 19-38.

Pachepsky YA, Yakovchenko V, Rabenhorst MC, Pooley C, Sikora LJ (1996) Fractal parameters of pore surfaces as derived from micromorphological data: effect of long-term management practices. *Geoderma* **74,** 305-319.

Udawatta RP, Anderson SH, Gantzer CJ, Garrett HE (2008). Influence of prairie restoration on CT-measured soil pore characteristics. *J. Environ. Qual.* **37,** 219–228.

Elucidating soil structural associations of organic material with nano-scale secondary ion mass spectrometry (NanoSIMS)

Ingrid Kögel-Knabner[A], Katja Heister[A], Carsten W. Mueller[A] and François Hillion[B]

[A]Lehrstuhl für Bodenkunde, Technische Universität München, Freising-Weihenstephan, Germany, Email koegel@wzw.tum.de
[B]Cameca, 29 Quai des Gresillons, 92622 Gennevilliers Cedex, France.

Abstract
The specific features of the nano-scale secondary ion mass spectrometry (nanoSIMS) technology with the simultaneous analysis of up to seven ions species with high sensitivity and resolution enables us to perform multi-element and isotope measurements at the submicron-scale. In order to demonstrate the power of this technique, we performed an incubation experiment with primary soil particles of the fine silt and clay fraction and soil aggregates (< 6.3 µm) from an Albic Luvisol and a Haplic Chernozem, respectively, with a ^{13}C and ^{15}N labelled amino acid mixture as tracer. Before and at selected time intervals after addition of the tracer, samples were derived and prepared for nanoSIMS investigation. For this purpose, different sample pre-treatments for single soil particles and soil aggregates were developed. Primary soil particles high in carbon showed an enrichment of ^{13}C and ^{15}N after label addition which decreases over time. In soil aggregates, nanoSIMS analyses revealed that the labelled amino acids were transported most likely by diffusion through the pores of the aggregate from the outside to its interior. From these first results, it can be concluded that the nanoSIMS technology will allow a major step forward in the understanding of biogeochemical processes and properties of soil.

Key Words
^{13}C, ^{15}N, aggregate, label, stable isotope, submicron-scale.

Introduction

Soils consist of a complex mixture of solid, liquid and gaseous components. Major inorganic solid components are quartz, clay minerals, oxides and hydroxides of Fe, Mn and Al and carbonates. Soil organic matter (SOM) represents a complex mixture of partially recalcitrant substances composed of humified and non-humified materials derived from plant litter, faunal and microbial biomass, like e.g. polysaccharides, lignin, aliphatic biopolymers, tannins, lipids, proteins and amino sugars. Accordingly, soils are structurally heterogeneous across a wide range of spatial and temporal scales (Herrmann *et al.* 2007b; Totsche *et al.* 2010). During soil formation, primary soil particles are rearranged and glued together to microaggregates which are bound together to macroaggregates. Subsequently, a hierarchic aggregate system of increasing structural and functional complexity is formed (Totsche *et al.* 2010). Microorganisms inhabit the thus developed microhabitats and change them according to their own needs (Herrmann *et al.* 2007a, b). In order to unravel the heterogeneous composition of these submicron sized organo-mineral associations, the simultaneous analysis of the spatial distribution of C, N and other elements at the nano-scale will allow a major step forward in the understanding of soil formation with significant implications for our concepts of the soil C and N cycle, soil structural stability and the sorptive properties. (Totsche *et al.* 2010).

The specific features of the novel nano-scale secondary ion mass spectrometry (nanoSIMS) technology, which allows the simultaneous analysis of up to seven ion species with high sensitivity and resolution, make it an unprecedented tool for the analysis of biogeochemical processes and properties of soils (Herrmann *et al.* 2007a, b). In the nanoSIMS, a beam of primary ions (Cs^+ or O^-) releases secondary ions from the sample. These secondary ions are collected and filtered by a magnetic mass analyser. With Cs^+ as primary ions, negatively charged ions, like *e.g.* $^{12}C^-$, $^{13}C^-$, $^{12}C^{14}N^-$, $^{12}C^{15}N^-$ and $^{28}Si^-$, are collected with a lateral resolution of 50 nm; by using O^- as primary ions beam, positively charged ions, like *e.g.* K^+ and Na^+, are detected with a lateral resolution of 150 nm. The mass resolution is so high that a differentiation between the mass of $^{13}C^{14}N$ (27.016 amu) and the mass of $^{12}C^{15}N$ (27.009 amu) is possible (*c.f.* Lechene *et al.* 2006). Consequently, the nanoSIMS enables us to explore the elemental and isotopic composition of soils at the submicron-scale.

Until now, the nanoSIMS technique has been applied mainly in the field of cosmochemistry, material science, biology, geology and mineralogy. We demonstrate the feasibility of this technique for soil science. After incubation of soil particle size fractions and soil aggregates with a ^{13}C and ^{15}N labelled amino acids

mixture, we traced the label at different time intervals on the single particles and in the aggregates. With this technique, we were able to show the isotopic enrichment of ^{13}C and ^{15}N on particle surfaces and the diffusion of the label among aggregate pores.

Methods

In this study, primary soil particles and soil aggregates were investigated with nanoSIMS with respect to the spatial distribution of freshly introduced organic matter (OM). The fine silt and clay soil particle size fraction (< 6.3 µm) of an Ah horizon from an Albic Luvisol from Bavaria (Southern Germany) was pre-incubated for 500 days at 20°C. Intact soil aggregates were taken from a Haplic Chernozem (Ap horizon, < 6.3 mm) from South of Kazan (Russia). Both soil materials were incubated with an amino acid mixture (approx. 99 atom% ^{13}C and ^{15}N) as readily bioavailable OM input and isotopic tracer. Samples were taken before, directly after the addition of the labelled amino acids and after 1, 2 and 6 days.

Sample preparation was carried out directly after sampling. The primary particles were deposited as a suspension on pieces of a silicon wafer and then dried in a desiccator. The soil aggregates were embedded in epoxy resin by stepwise combined drying and saturation of the soil aggregates with resin/acetone mixtures of different ratios. Then, the resin blocks were cut to obtain a transect through the aggregate and the obtained surface was polished with diamond paste. The samples were investigated with an optical microscope and a scanning electron microscope (SEM). The spatial distribution of the OM and the fate of ^{13}C and ^{15}N, which is expected to be influenced by diffusion, sorption and microbial activity, were studied with nanoSIMS. The presented nanoSIMS data were obtained at the nanoSIMS 50 unit of the Institut Curie in Paris, France.

Results

In the primary particle samples, particles were analysed by selection of "regions of interest" (ROI) and measurement of the elemental and isotopic composition of these sample areas. Figure 1 shows several particles high in carbon derived after 6 days of incubation. Ten different ROIs were selected and are marked with a red line. From these measurements, the isotopic ratios of these particles were calculated (Figure 2).

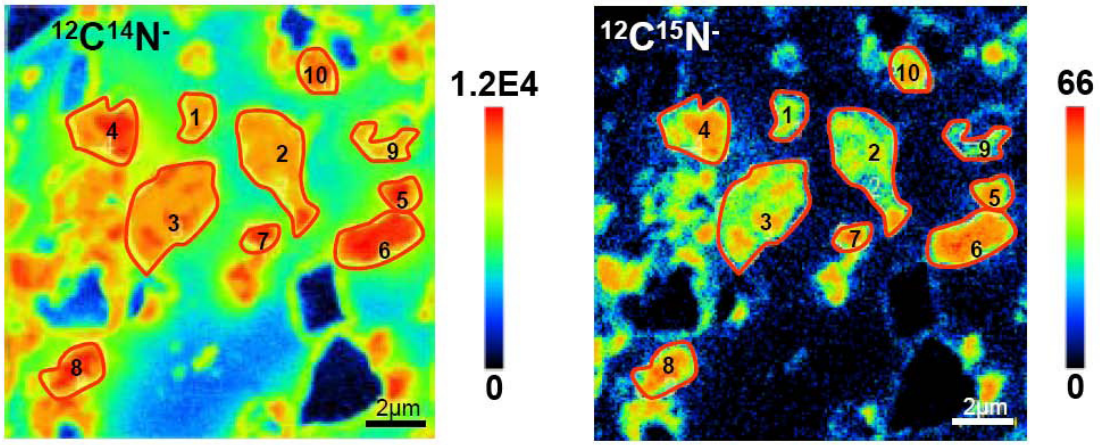

Figure 1. Spatial distribution of $^{12}C^{14}N^-$ and $^{12}C^{15}N^-$ at primary particles from the fine silt and clay fraction of the Ah horizon of the Albic Luvisol after 6 days of incubation. Investigated regions of interest are marked.

In Figure 2, it is clearly visible that a significant enrichment in both ^{13}C and $^{1}5N$ took place after addition of the labelled amino acid mixture. Over time, we detect a decrease in ^{13}C and ^{15}N, which is more pronounced for ^{15}N.

In the aggregates of the Haplic Chernozem, we detected that transport of the ^{13}C and ^{15}N labelled amino acids took place along a pore. Figure 3 shows a backscattered-electron image of the aggregate sampled after one day of incubation, in which the pore analysed by nanoSIMS is displayed. Moreover, the distribution of $^{12}C^{15}N^-$ in that particular pore is shown in the insert. The arrow indicates the direction of the line scan that was done; the small square indicates the width of it. The calculated isotopic ratios of the individual scan points along this transect demonstrate a decrease of ^{15}N towards the aggregate interior (Figure 4). Accordingly, we conclude that most likely diffusion of the labelled amino acids from the outside of the aggregate to its interior occurred along such pores.

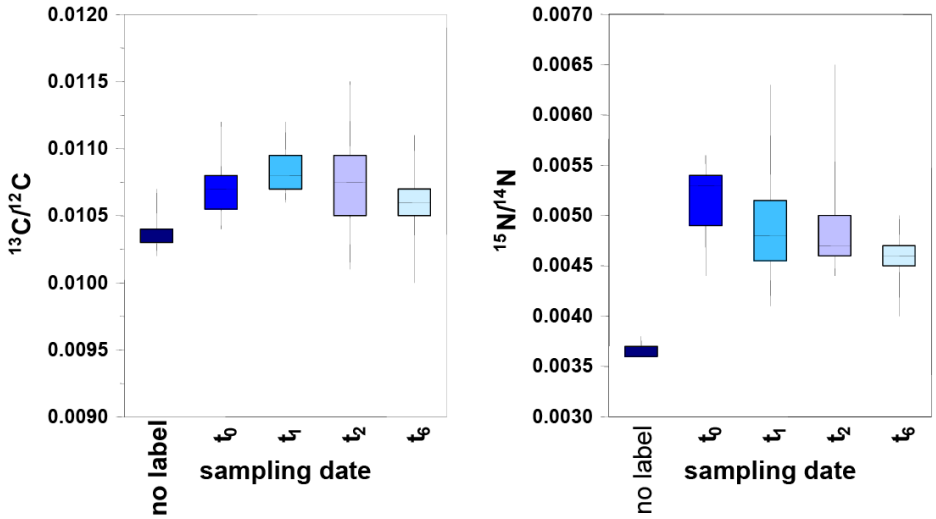

Figure 2. Development of $^{13}C/^{12}C$ and $^{15}N/^{14}N$ ratios calculated from measurements of selected regions of interest.

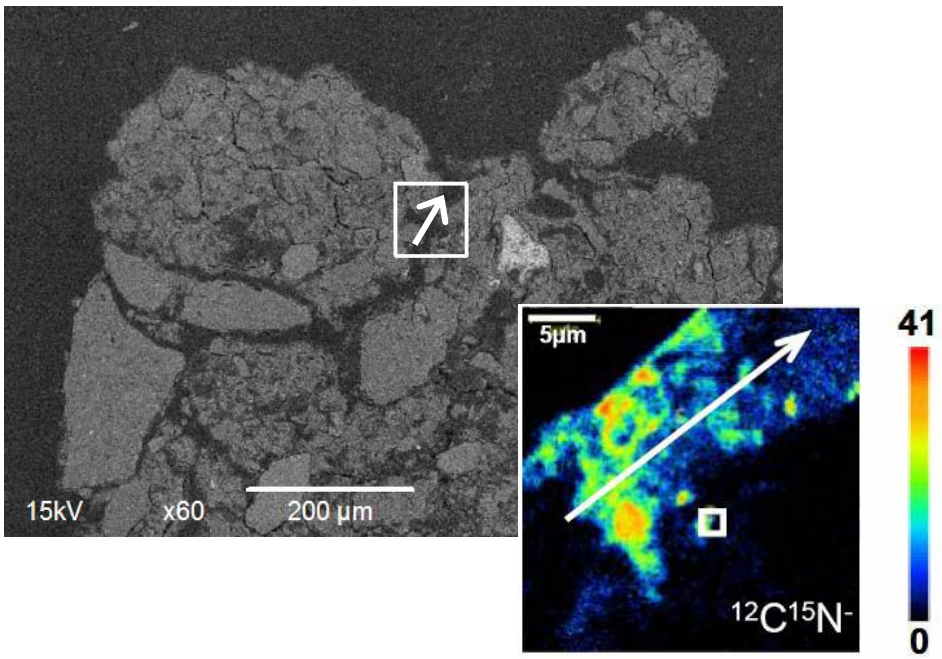

Figure 3. Backscattered-electron image of the aggregate of the Ap horizon of the Haplic Chernozem derived one day after incubation. The insert shows the spatial distribution of $^{12}C^{15}N^-$ along the investigated pore.

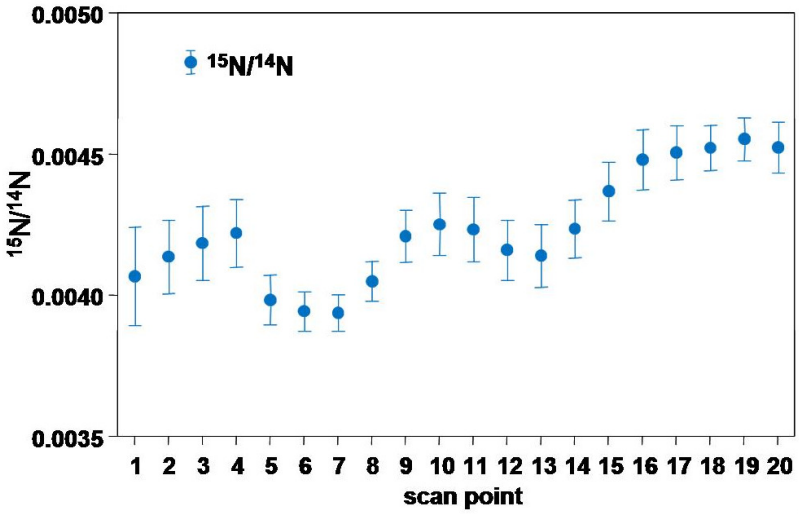

Figure 4. Variation of the $^{15}N/^{14}N$ ratio across the investigated pore of the aggregate.

Conclusions

The nanoSIMS technology enables us to explore the elemental and isotopic composition of soils at the submicron-scale. We developed sample preparation procedures to obtain samples that meet the enhanced requirements of the nanoSIMS for investigation of both primary soil particles as well as soil aggregates. An incubation experiment with primary particles of an Albic Luvisol and with soil aggregates of a Haplic Chernozem was conducted with a ^{13}C and ^{15}N labelled amino acid mixture. NanoSIMS analyses reveal that after label addition, primary soil particles high in carbon show enrichment in both ^{13}C and ^{15}N which decreases with time. In soil aggregates, nanoSIMS analyses illustrate the transport, which is most likely by diffusion, of the labelled amino acids from the outside to the interior of the aggregates along their pores. From these first results, it can be concluded that the nanoSIMS technology will boost our ability to locate the association of elements/isotopes in soil structural components at the submicron-scale and will thus allow a major step forward in the understanding of biogeochemical processes and properties of soil.

References

Lechene C, Hillion F, McMahon G, Benson D, Kleinfeld AM, Kampf JP, Distel D, Luyten Y, Bonventre J, Hentschel D, Park KM, Ito S, Schwartz M, Benichou G, Slodzian G (2006) High-resolution quantitative imaging of mammalian and bacterial cells using stable isotope mass spectrometry. *Journal of Biology* **5**, 20.

Herrmann AM, Clode PL, Fletcher IA, Nunan N, Stockdale EA, O'Donnell AG, Murphy DV (2007a) A novel method for the study of the biophysical interface in soils using nano-scale secondary ion mass spectrometry. *Rapid Communications in Mass Spectrometry* **21**, 29-34.

Herrmann AM, Ritz K, Nunan N, Clode PL, Pett-Ridge J, Kilburn MR, Murphy DV, O'Donnell AG, Stockdale EA (2007b) Nano-scale secondary ion mass spectrometry – a new analytical tool in biogeochemistry and soil ecology: a review article. *Soil Biology and Biochemistry* **39**, 1835-1850.

Totsche KU, Rennert T, Gerzabek MH, Kögel-Knabner I, Smalla K, Spiteller M, Vogel H-J (2010) Biogeochemical interfaces in soil: the interdisciplinary challenge for soil science. *Journal of Plant Nutrition and Soil Science* **173**, 88-99.

Estimating soil water retention in soil aggregates using an 'additivity' model for combining structural and textural pore spaces

Anatoly M. Zeiliguer[A], Reinder Feddes[B] and Olga S. Ermolaeva[C]

[A] Geo- and Hydroinformation Center, Moscow State University of Environmental Engineering Prjanishnikova Street, 19, Moscow 127550, Russia, e-mail: azeiliguer@mail.ru
[B] Wageningen University, Water Resource Department, Neuwe Kanaal 11, 6709 PA
[C] Geo- and Hydroinformation Center, Moscow State University of Environmental Engineering Prjanishnikova Street, 19, Moscow 127550, Russia, e-mail: o_ermolaeva@yahoo.com

Abstract
The 'additivity' model aiming to estimate water retention characteristic of aggregated soil layers is based on two main hypotheses: (1) subdivision of pore space into structural and textural pore spaces and their water retention characteristics; (2) estimation of water retention of both spaces as a linear combination of fractions of their main components. The adequacy of this model was tested with experimental data of measured water retention characteristics of soil cores consisting from aggregates of Halpic Chernozem, Podzoluvisol, and Halpic Kastanozem soils. Experimental cores were prepared from separated individual aggregate fractions with size ranges of 10-7, 7-5, 5-3, 3-2, 2-1, 1-0.5, 0.5-0.25, and <0.25 mm. The results demonstrated a good agreement with measured data as well as the sensitivity of the 'additivity' model to the size of aggregates, textural component distribution, and aggregate density.

Key Words
aggregated soil, soil structure, soil water retention, soil components, additivity model.

Introduction
Soil water retention measurements are relatively time-consuming and become impractical when hydrologic estimates are needed for large areas. In many applications, estimating water retention from basic soil data available from soil survey becomes an alternative to measurements. Statistical regressions are most often used to estimate the soil water retention characteristics from soil texture, bulk density, organic matter content, and other basic soil properties. For water retention, one approach consists in estimating soil water contents at several soil water potentials with a separate regression equation for each potential. Several studies tested the regression-based water retention estimates with different data used to develop the regressions. Results of such testing were put together consequently extrapolation of some regression equations beyond their development region was unsuccessful. Yet another approach to soil water retention estimation that is not based on regressions consists in composing soil water retention from water retention of its soil constituents (i. e., Zeiliguer and Voronin 1988, Zeiliguer 1992; 1997).

Methods
"Aggregated" Soil Medium model Description
Soil structure has a major effect on soil's ability to retain and to transport water. This is especially true for aggregated soils in which pore space consists of interconnected structural and textural pores with distinct hydraulic properties. When a proportion of the inter-aggregate pore space is significant, the conventional description of water flow with "one pore region – one continuum" models oversimplifies water retention and flow.
An 'addivity' model to estimate the aggregated soil water retention is based on the following assumptions:

- ✓ pore space of an aggregated porous medium can be subdivided into textural and structural quasi-homogeneous pore regions using the values of bulk density and aggregate density;
- ✓ water retention of both regions in the range of soil potentials between -1500 and 0 kPa can be estimated separately using the 'additivity' model;
- ✓ water retention associated with soil textural fractions is measured on samples consisting exclusively of those textural fractions;
- ✓ water retention of aggregate and textural fractions of the same size are assumed to have the same parameters;
- ✓ contributions of textural and structural fractions into the total water retention are proportional to the volumes of pore subspaces associated with the corresponding fractions.

Soil structural components, i.e., aggregates, or peds, create two own contiguous pore subspaces where soil

water is retained. First textural sub-space is created in interior part of these structural components that is build by textural components of these elements, i.e., soil elementary particles. Second structural sub-space is created in exterior part of the same structural components that build by them-self. There are not soil elementary particles in it. Subscripts "*T*" and "*S*" denote textural and structural pore subspaces, respectively. Soil water content for each soil water pressure head h is equal to sum of soil (gravimetric) water content of soil textural and structural sub-spaces

$$W(h) = W^T(h) + W^S(h). \quad (1)$$

Application of the additivity hypothesis for the capillary and residual water contents of both textural and structural components provides following equation:

$$W(h) = \varepsilon_C^S \frac{\sum_{j=1}^{N^S} f_j W_{j,0}^T S_j^T(h)}{\sum_{ji=1}^{N^S} f_j W_{j,0}^T} + \left(\varepsilon_C^T - \sum_{i=1}^{N^T} f_i W_{i,R}^T \right) \frac{\sum_{i=1}^{N^T} f_i W_{i,0}^T S_i^T(h)}{\sum_{i=1}^{N^T} f_i W_{i,0}^T} + \sum_{i=1}^{N^T} f_i W_{i,R}^T \quad (2)$$

here, ε_C^S, ε_C^T - respectively, pore volumes (averaged by dry mass of soil volume) of structural and textural subspaces, $W_{i,R}^T$- gravimetric residual water content of textural soil components (assuming that due to big dimension of soil aggregates structural residual content is $W_{i,R}^S = 0$), $W_{i,0}^T$ is the specific to *i*th fraction of soil components soil gravimetric water content at saturation, and $S_i^T(h)$ is the specific to *i*th fraction of soil components (aggregates and soil elementary particles) relative saturation, N^S, N^T is the total number of structural (aggregates) and textural (soil elementary particles) component fractions.

Figure 1 shows data on water retention of (textural) fractions of soil elementary particles (Michurin 1975; Stakman,1969) that has been used in this work. The Weibull equation was successfully used to fit steep experimental dependencies (Zeiliguer and Voronin 1988). Therefore it was found that a more accurate fit of some of data in Figure 1 could be obtained using a linear combination of two similar Weibull equations to fit water retention data. Use of a linear combination of two Weibull equations for *i*th textural fraction of soil component is given in the following form:

$$W_i^T(h) = W_{i,0}^T \left\{ q \exp\left[-\left(h/h_i^{'}\right)^{m_i^{'}} \right] + (1-q) \exp\left[-\left(\left(h/h_i^{''}\right) \right)^{m_i^{''}} \right] \right\} + W_{i,R}^T \quad (3)$$

where $h_i^{'}$, $h_i^{''}$ and $m_i^{'}$, $m_i^{''}$ were shape parameters, *q*- empirical parameter .

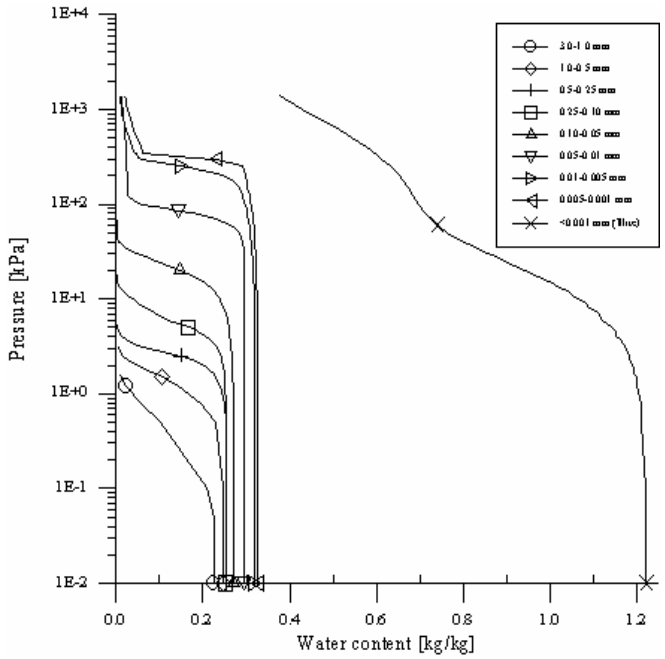

Figure 1. Water retention of samples (after [*Mitchurin 1975*], [Stackman 1968]) containing soil elementary particle fractions. Fraction d<0.001 mm is represented by the illite clay fraction.

Materials

To validate 'additivity' model we used the data on water retention and soil physical parameters of soil cores

consisting of fractions of aggregates obtained *in vitro* by T.N. Pochatkova (Pochatkova 1981). The following soil were used for model validation:

- ✓ five horizons horizons (A_d, A_1, B_1, B_2 and BC) of Ordinary Chernozem (Halpic Chernozem) from Kammenaya Steppe (Kursk, Russia) shown at Figure 2;
- ✓ two horizonts (B_1 and B_2) of Dernovo-Podzolic Soil (Podzoluvisol) from Chashnikovo (Moscow Region, Russia);
- ✓ one (A_1) of Kashatanovaya Soil (Halpic Kastanozem) from Volgograd Region (Russia);

From these samples the following individual aggregate fractions were used to fabricate soil cores: 10-7; 7-5; 5-3; 3-2; 2-1; 1-0.5; 0.5-0.25; <0.25mm).

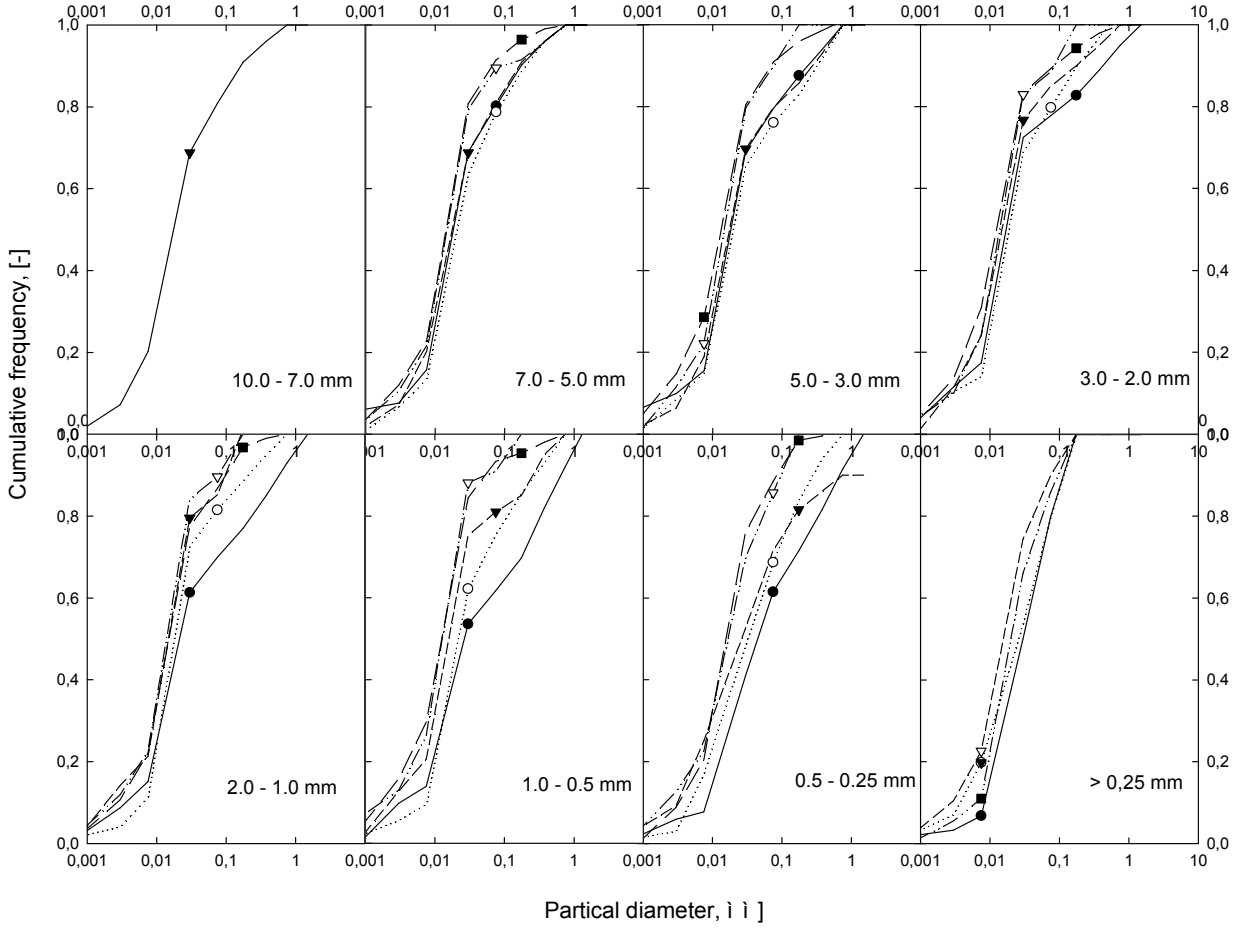

Figure 2. Elementary particle size-distribution of samples of soil cores with individual aggregate fractions of ordinary chernozem samples taken out from following horizons: Ад (○); A1 (▲); B1 (▼); B2 (+); BC (x).

After initial water saturation by capillary arising at these cores water retention characteristics were measured in drainage experimentation in porous plate equipment.

Results

The performance of the 'additivity' model can be judged from Figure 3 showing comparison of the measured ($W^m(h)/\varepsilon^m$) and calculated ($W^c(h)/\varepsilon^c$) soil relative saturation of samples of individual fractions of samples of ordinary chernozem. At this Figure at each soil core (fraction of aggregate diameter) two estimated curves are shown.

Conclusions

With the aim of some assumptions and hypotheses we developed 'additivity' model to estimate water retention of aggregated soil. Input parameters of the model are divided into two parts. First is done by physical soil parameters like bulk density, dry density of aggregate as well as structural and textural soil components (aggregate and soil elementary particle) size-distribution. Second set is done by empirical parameters fitted for Weibull equation parameters of water retention characteristics of fractions of textural components (soil elementary particles).

A validation of the model was done by comparison with measured water retention of soil cores fabricated from fraction of aggregates taken from some layers of three types of soil. Obtained by 'additivity' model results as well as measured soil water retention characteristics are quite sensitive to the dimension (diameter) of both soil components (aggregates and elementary particles) size-distributions.

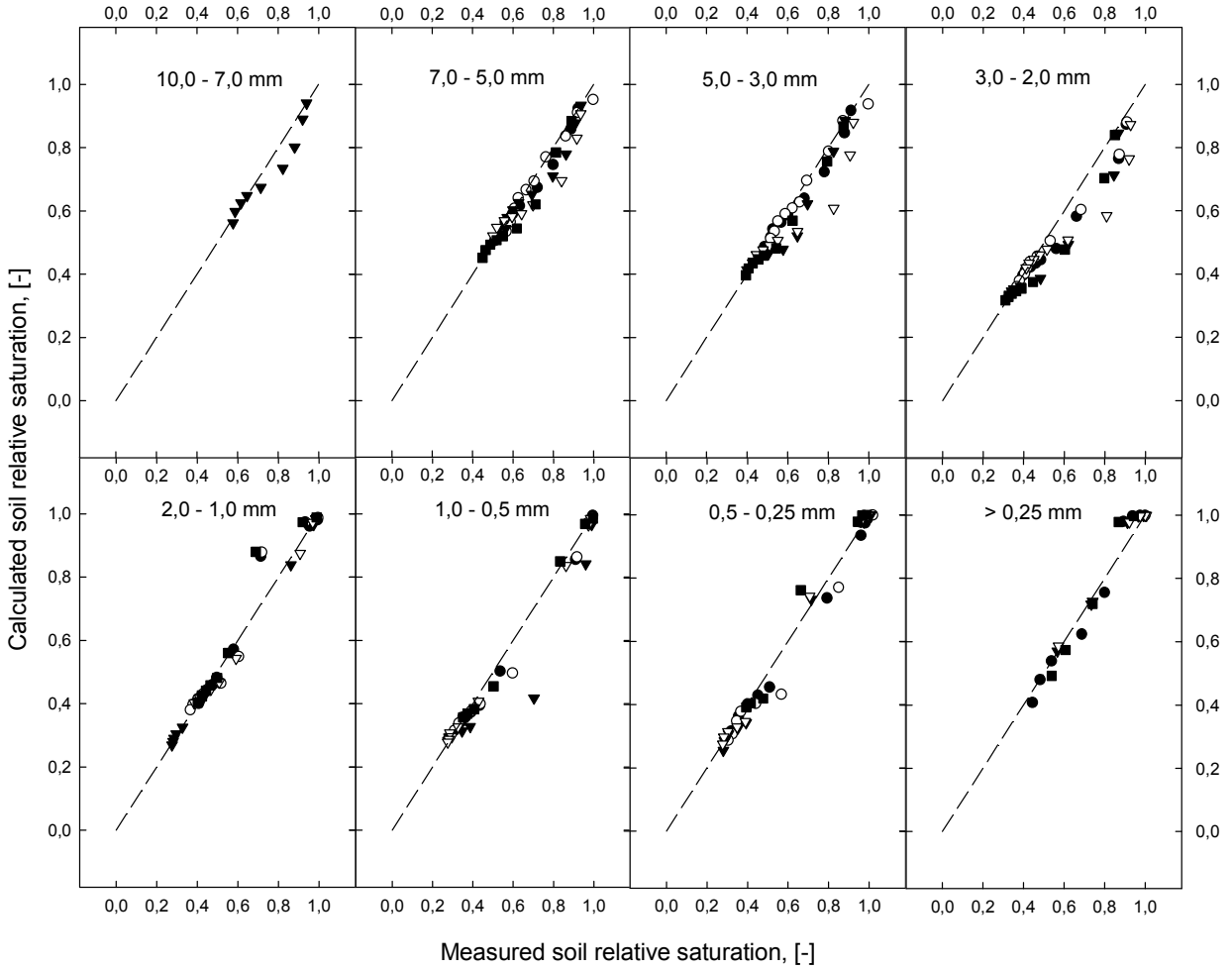

Figure 3. Measured and calculated by 'additivity' model soil relative saturation of samples of individual fractions of ordinary chernozem for samples taken out from following horizons: Ад (○); A1 (▲); B1 (▼); B2 (+); BC (x).

References

Michurin BN (1975) Energetics of soil water. Leningrad. *Gidrometeouizdat*. (In Rus.).

Pochatkova T (1981) The Structural Soil-Water properties. *Ph. D. Thesis*, Moscow.

Stakman WP (1969) The relation between particle size, pore size, and hydraulic conductivity of sand separates. In 'Water in unsaturated zone' V. 1, p. 373-382. (Wageningen).

Zeiliguer AM, Voronin AD (1988) Modeling the structure of the pore space of soils. 1. Calculation of the main hydrophysical characteristic of soil from particle-size and micro aggregate analysis. *Soviet Soil Science* **20**, 108-118.

Zeiliguer AM (1992) A hierarchical system to model the pore structure of soils. In 'Indirect Methods for Estimating the Hydraulic Properties of Unsaturated Soils'. (Eds M Th van Genuchten, FJ Leij, LJ Lund) pp. 499-514. (University of California, Riverside, CA).

Zeiliguer AM (1997) Estimating and Description of the Hydraulic Properties for Different Types of Soil Medium Models. In 'Proc. of the International Workshop "Characterisation and Measurement of the Hydraulic Properties of Unsaturated Porous Media'. pp. 1224-1229. Riverside October 22-24,

Estimating soil water retention of soil aggregate samples using the 'additivity' model for combination of intra- and into-aggregate pore spaces

Anatoly M. Zeiliguer[A], Olga S. Ermolaeva[B]

[A]Geo- and Hydroinformation Center, Moscow State University of Environmental Engineering Prjanishnikova Street, 19, Moscow 127550, Russia, Email azeiliguer@mail.ru
[B]Geo- and Hydroinformation Center, Moscow State University of Environmental Engineering Prjanishnikova Street, 19, Moscow 127550, Russia, Email o_ermolaeva@yahoo.com

Abstract
The developed 'additivity' model aiming to estimate water retention characteristic of aggregated soil layers is based on two main hypotheses: (1) of a subdividing of pore space to intra- and inter-aggregate pore subspaces as well as and their water retention characteristics; (2) estimating of water retention of both subspaces as a linear combination of fractions of their main components. The adequacy of this model was tested on experimental data of measured water retention characteristics of soil cores consisting from fractions of aggregate of Halpic Chernozem, Podzoluvisol, and Halpic Kastanozem, soils. Experimental cores were prepared from separated individual aggregate fractions with size ranges of 10-7, 7-5, 5-3, 3-2, 2-1, 1-0.5, 0.5-0.25, and <0.25mm. The obtained results demonstrated the good agreement with measured data and sensitivity of the 'additivity' model to respond to the size of aggregates, textural component distribution and aggregate density.

Key Words
Aggregated soil, soil structure, soil water retention, soil components, additivity model

Introduction

Soil water retention measurements are relatively time-consuming and become impractical when hydrologic estimates are needed for large areas. In many applications, estimating water retention from basic soil data available from soil survey becomes an alternative to measurements. Statistical regressions are most often used to estimate the soil water retention characteristics from soil texture, bulk density, organic matter content, and other basic soil properties. For water retention, one approach consists in estimating soil water contents at several soil water potentials with a separate regression equation for each potential. Several studies tested the regression-based water retention estimates with different data used to develop the regressions. Results of such testing were put together consequently extrapolation of some regression equations beyond their development region was unsuccessful. Yet another approach to soil water retention estimation that is not based on regressions consists of predicting soil water retention from water retention of its soil constituents (Zeiliguer and Voronin 1988; Zeiliguer 1992; 1998). The hypothesis is that soil water retention can be approximated by summing up water retention of pore subspaces related to the soil components is the base of the developed 'additivity' model.

Methods

"Aggregated" Soil Medium model Description

Soil structure has a major effect on soil's ability to retain and to transport water. This is especially true for aggregated soils in which pore space consists of interconnected intra- and inter-aggregate pores with distinct hydraulic properties. When a proportion of the inter-aggregate pore space is significant, the conventional description of water flow with "one pore region – one continuum" models oversimplifies water retention and flow.

An 'addivity' model to estimate the aggregated soil water retention is based on the following assumptions:
pore space of an aggregated porous medium can be subdivided into textural (into-aggregate) and structural (intra-aggregate) quasi-homogeneous pore regions using the values of bulk density and aggregate density;
water retention of both regions in the range of soil potentials between -1500 and 0 kPa can be estimated separately using the 'additivity' model;
water retention associated with soil textural fractions is measured on samples consisting exclusively of those textural fractions;
water retention of aggregate and textural fractions of the same size are assumed to have the same parameters;
contributions of textural and structural fractions into the total water retention are proportional to the volumes of pore subspaces associated with the corresponding fractions.

Soil structural components, i.e., aggregates, or peds, create two own contiguous pore subspaces where soil water is retained. First textural sub-space is created in interior part of these structural components that is build by textural components of these elements, i.e., soil elementary particles. Second structural sub-space is created in exterior part of the same structural components that build by them-self. There are not soil elementary particles in it. Subscripts "T" and "S" denote textural and structural pore subspaces, respectively. Soil water content (gravimetric) for each soil water pressure head h is equal to sum of soil water content of soil textural and structural sub-spaces

$$W(h) = W^T(h) + W^S(h) \quad (1)$$

Application of the additivity hypothesis for the capillary and residual water contents of both textural and structural components provides following equation:

$$W(h) = W_C^S \frac{\sum_{j=1}^{N^S} f_j W_{j,0}^T S_j^T(h)}{\sum_{j=1}^{N^S} f_j W_{j,0}^T} + \left(W_C^T - \sum_{i=1}^{N^T} f_i W_{i,R}^T \right) \frac{\sum_{i=1}^{N^T} f_i W_{i,0}^T S_i^T(h)}{\sum_{i=1}^{N^T} f_i W_{i,0}^T} + \sum_{i=1}^{N^T} f_i W_{i,R}^T \quad (2)$$

where W_C^S and W_C^S are gravimetric water content of both sub-spaces at saturation, f_j and f_i are fraction of jth structural and ith textural component, N^S and N^T are total number of components of both sub-spaces, $W_{j,0}^T$ and $W_{i,0}^T$ are gravimetric water content at saturation, $S_j^T(h)$ and $S_i^T(h)$ are relative saturation.

Figure 1 shows data on water retention of soil textural components (Michurin 1975; Stakman,1969) that has been used in this work. To use these data with various capillary pressure values, we needed to fit an equation to data. Water retention curves of monofractional samples are very steep (Figure 1). The Weibull equation was successfully used to fit steep experimental dependencies (Zeiliguer and Voronin 1988). Therefore we found that a more accurate fit of some of data in Figure 1 could be obtained using by applying a linear combination of two similar equations to fit water retention data. Use of a linear combination of two Weibull equations is given in the following form:

$$W_{i,T}(h) = W_{i,0}\left\{ q \exp\left[-\left(h/h_i'\right)^{m_i'} \right] + (1-q)\exp\left[-\left(\left(h/h_i''\right)\right)^{m_i''} \right] \right\} + W_{i,R} \quad (3)$$

where h_i', h_i'' and m_i', m_i'' shape parameters.

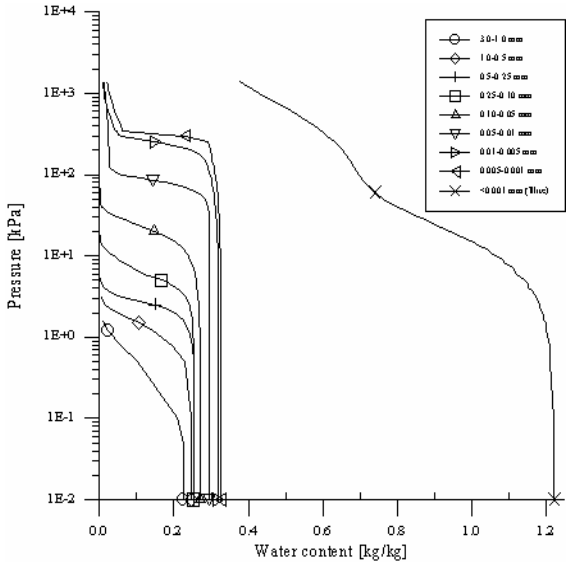

Figure 1. Water retention of samples after (Mitchurin 1975) and (Stackman 1968) containing soil textural fractions. Fraction d<0.001 mm is represented by the illite clay.

A code based on the modified Marquardt algorithm was used to find seven parameters h_i', h_i'', m_i', m_i'', q, $W_{i,0}$ and $W_{i,R}$.

Materials
In this work, we used the data on water retention and soil physical parameters obtained by T.N. Pochatkova (Pochatkova 1981). The following soil samples were used for model validation:
five horizons horizons (A_d, A_1, B_1, B_2 and BC) of Ordinary Chernozem (Black Soil) from Kammenaya Steppe (Kursk, Russia);
From these samples the following individual soil aggregate fractions were separated: 10.0-7.0mm; 7.0-5.0mm; 5.0-3.0mm; 3.0-2.0mm; 2.0-1.0mm; 1.0-0.5mm; 0.5-0.25mm; <0.25mm). The special soil cores were prepared from these separated individual fractions of aggregates. Initially the cores were saturated with water by capillary arising. The water retention characteristics of packed cores were measured in drainage experimentation in porous plate equipment.

Results
The overall performance of the model as well as its performance in various capillary pressure ranges can be judged from Figure 2.

Conclusion
The 'additivity' model was tested on estimation water retention of soil cores fabricated from individual fractions of aggregates taken from five horizonts of ordinary chernozem. The model is based on subdivisions of soil pore space into two sub-spaces of structural and textural soil components. Results of the testing shows a good agreement of obtained results with measured data.

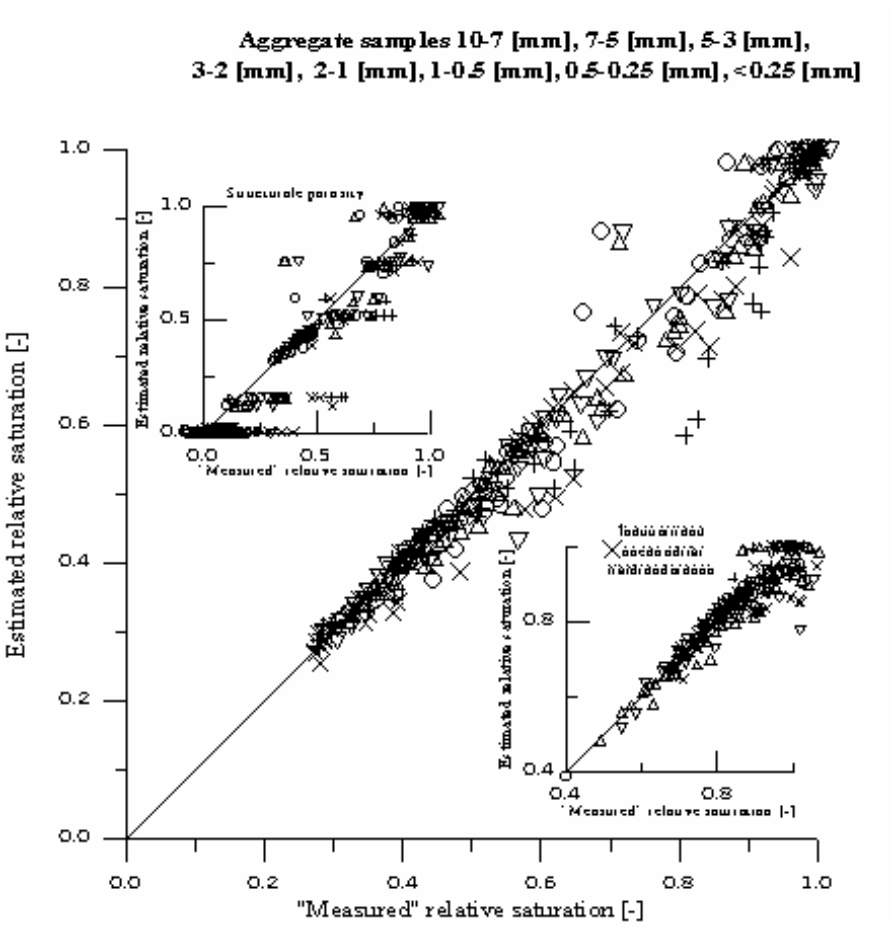

Figure 2. Comparison of the experimental and simulated water retention characteristics of samples of individual fractions of samples of ordinary chernozem: Ад - A1; B1; B2; BC.

References

Michurin BN (1975) Energetics of Soil Water. Leningrad, Gidrometeouizdat. (In Rus.).
Pochatkova TN (1981) The Structural Soil-Water Properties. PhD Thesis, Moscow.
Stakman WP (1969) The relation between particle size, pore size, and hydraulic conductivity of sand separates, pp. 373-382. *In* 'Water in unsaturated zone' Vol 1. Wageningen.

Zeiliguer AM, Voronin AD (1988) Modeling the structure of the pore space of soils. 1. Calculation of the main hydrophysical characteristic of soil from particle-size and micro aggregate analysis. *Soviet Soil Science* **20**, 108-118.

Zeiliguer AM (1992) A hierarchical system to model the pore structure of soils, *In* 'Indirect Methods for Estimating the Hydraulic Properties of Unsaturated Soils' (van Genuchten MTh, Leij FJ, Lund LJ Eds.), pp. 499-514. University of California, Riverside, CA.

Zeiliguer AM (1997) Estimating and description of the hydraulic properties for different types of soil medium models. *In* Proc. of the International Workshop "Characterisation and Measurement of the Hydraulic Properties of Unsaturated Porous Media", October 22-24, Riverside.

Functional characterization of soil structure field descriptions

J. Bouma[A]

[A]Wageningen University, The Netherlands.

Abstract
Databases all over the world contain soil structure descriptions, made in the context of soil surveys. They can be helpful in providing qualitative indications as to important soil properties such as rooting depth, permeability and biological activity. Modern applications of soil expertise, using modelling techniques, require more quantitative input. Continuous – and class pedotransferfunctions (pdf's) have been developed to relate soil characteristics from soil survey to physical and chemical parameters needed for quantitative applications. Most emphasis has been so far on the continuous pdf's and a case will be presented for class-pdf's using soil horizons and pedons as carriers of information. On the other hand, modelling of physical soil processes is hampered by implicit assumptions of homogeneity of the flow domain, following existing flow theory. Descriptions of soil structure can help to devise more representative sampling techniques and simulations of field conditions by defining preferential flow patterns. New monitoring techniques allow more precise measurements. Coupling soil survey expertise with process knowledge from soil physics allows more realistic representation of field conditions in simulation models than either discipline can achieve and is therefore a good example of hydropedology at work.

Key Words
Bypass flow, macropores, simulation.

Introduction
Soil databases all over the world contain soil profile descriptions of soil structure for each soil horizon in terms of type, grade and size of aggregates ("peds") and of soil consistencies as an estimate of soil stability. These qualitative characterizations allow reasonable indications as to rooting patterns, soil permeabilities , structural stability and occurrence of biological activity. Modern methods to quantify plant growth or to study effects of global climate change include use of simulation models that need specific parameters, also for the soil. Important parameters are hydraulic conductivity K(h) and moisture retention h(o) relations. Measurements of these physical characteristics are often cumbersome and costly so much attention has been paid to deriving methods that allow reliable estimates of such parameters using basic data from soil survey such as texture, organic matter content and bulk density by developing pedotransferfunctions (Bouma 1989; Pachepsky and Rawls 2004). Both continuous en class pedotransfunctions can be distinguished, the latter linking specific soil horizons or pedons to measured functional properties, such as K(h) and h(0). While pedology and soil survey move towards quantification, soil physics and hydrology increasingly suffer from limitations imposed by the underlying assumption of flow theory that soils are anisotropic and homogeneous, which- of course- they are not. Soil structure descriptions can be helpful to overcome these problems by:(i) improving physical measurements by e.g. defining representative sample sizes or subsampling procedures, and (ii) defining boundary conditions for the flow regime in terms of preferential flow in heterogeneous soil. Combining field descriptions of soil structure with process knowledge of soil physicists, as promoted by Hydropedology, can lead to much improved field characterization of soils in terms of their flow regimes and this, in turn, is important as a contribution by soil science to larger models now in use, covering the entire earth system.

Pedotransferfunctions
Bouma (1989) and Pachepsky and Rawls (2004) have discussed pdf's, distinguishing two types: continuous and class. The first type is most common and relates basic soil characteristics such as texture, organic matter content and bulk density to hydraulic characteristics such as hydraulic conductivity, K(h), and moisture retention , h(o). Often these characteristics are related to the parameters of the flow equations of van Genuchten. Pdf's allow rapid derivation of physical flow characteristics that are difficult to measure and can thus be quite helpful for hydrological studies. However, particularly in well structured soil, results can be poor because of bypass flow where water moves quickly downwards along the vertical faces of peds through an unsaturated matrix (Booltink and Bouma 2002). Also, hydrophobicity can result in uneven infiltration that is not predicted by models assuming homogeneity.

Class pdf's are presented for a given soil horizon a given soil type or as a characteristic for the soil type as such, which is used as a "carrier of information" as is common in soil survey interpretations (Bouma 1989). Indicating the variability among different hydraulic conductivity and moisture retention curves measured in different taxonomically identical horizons, allows calculations expressing internal and spatial variability of the particular soil type being studied. Systematic studies, exploring the feasibility of this approach for different soil horizons have not been made. They would be particularly valuable for structured soil horizons where the homogeneous flow model does not work.

Using structure descriptions to improve sampling for physical measurements

A standard soil core of 300 cm^3 may contain some 20,000 individual sand grains when a sandy soil is sampled. When sampling a strong, fine subangular blocky structure with peds of, say, 1 cm diameter, the number reduces to, perhaps 200 and the sample will probably still be representative for the horizon being sampled. When, however, a coarse prismatic structure is encountered, only part of the prisms will fit into such a core. A plea can therefore be made to use soil structure descriptions for defining representative volumes for sampling. Anderson and Bouma (1973) showed that any K-sat could be measured in a B horizon of a well structured silt loam soil by varying the height of the core. This could be explained quantitatively by defining pore-continuity patterns based on dye studies. This method was refined using thin sections and was used to predict K-sat of four clay soils in the Netherlands (Bouma *et al.* 1979). But why go to all this trouble to calculate K-sat while measurement is much easier? The most interesting result of the latter study was the observation that "Pore necks" with a width of 30 micron governed "saturated flow" occupying less than 0.1% of the soil volume. Such values were recently reported by Young (NRC 2009) using modern scanning techniques. This result implies that bulk density and porosity are too coarse a measure to predict K and are therefore unsuitable. Returning to the example of the prismatic soil, the recommendation has to be that large samples are needed, containing al least 20 peds (Bouma 1989). Sometimes, selective sampling is needed, for instance when bleached areas occur around prisms. Then, separate sampling of the peds and the bleached areas and determination of the relative surfaces they occupy is a feasible procedure. Just putting in soil cores at random in pedal soils results in an enormous variability that is not due to soil heterogeneity but to using the wrong sampling procedure. Occurrence of macropores, such as worm channels or vertical cracks, can offer special problems even when using large samples as advocated. Bouma (1991) showed that K-sat, defined as the flux at pressure head zero at gradient 1 cm/cm, varied between 80 m/day and 1 cm/day depending on the method of measurement. Observing macropores should therefore alert phycisists to improve measurement procedures.

Using structure description to provide boundary conditions for physical flow models.

Occurrence of macropores, as discussed here and as described in soil structure descriptions, can define boundary conditions for flow models when functional characterization using dyes is included. Bypass flow was measured in a dry clay soil and the processes could be well simulated by separating the flow model into two parts: one calculating vertical infiltration into the peds and one for lateral infiltration into the peds for bypass water moving down the walls of prisms. (Hoogmoed and Bouma 1980; Bouma 1991). Another example was presented for a silt loam soil with worm channels using the same approach (Bouma *et al.* 1983). These examples demonstrate that soil structure descriptions can form the basis for defining subsystems for flow in structured soils and, as such, demonstrate the hydropedology approach.

Conclusions

1. Pedotransferfunctions (pdf's) make soil data useful when deducing basic physical flow characteristics. They should, however, be used with care as they may yield irrelevant results in structured soils. Emphasis is now on continuous pdf's and more attention to class-pdf's may be profitable.
2. Soil structure descriptions made during soil survey and available in soil databases can be used to fine-tune soil physical sampling procedures, as demonstrated in this paper. Using standard sample sizes implicitly assumes that soils are homogeneous and isotropic. They are not and when using standard-size samples, irrelevant results may be obtained.
3. Soil structure descriptions combined with functional characterization with dyes, can improve simulations of water regimes in field soils as was demonstrated in this paper.
4. Hydropedology promotes combination of tacit knowledge of soil survey with process knowledge of soil physics/hydrology. Both disciplines will have more impact when cooperating.

References

Anderson JL, Bouma J (1973) Relationships between hydraulic conductivity and morphometric data of an argillic horizon. *Soil Sci. Soc. Amer. Proc.* **37,** 413-421.

Booltink HWG, Bouma J (2002) Bypass flow. In 'Methods of Soil Analysis. Part 4: Physical Methods'. pp. 930-933. (American Society of Agronomy Inc.: Madison, WI).

Bouma J (1989) Using soil survey data for quantitative land evaluation. *Advances in Soil Science* **9,** 177-213.

Bouma (1991) Influence of soil macroporosity on environmental quality. *Advances in Agronomy* **46,** 1- 37.

Bouma J, Jongerius A, Schoonderbeek D (1979) Calculation of saturated hydraulic conductivity of some pedal clay soils usinf micromorphomertic data. *Soil Sci. Soc. Am. J.* **43,** 261-264.

Bouma J, Belmans C, Dekker LW, Jeurissen WJM (1983) Assessing the suitability of soils with macropores for subsurface waste disposal. *J. Environ. Qual.* **12,** 305-311.

Hoogmoed WB, Bouma J (1980) A simulation model for predicting infiltration into cracked clay soil. Soil *Soil Sci. Soc. Am. J.* **44,** 458-461.

National Research Council (2009) 'Frontiers in Soil Science Research'. (National Academies: Washington DC, USA).

Pachepsky YA, Rawls WJ (2004) 'Development of Pedotransferfunctions in Soil Hydrology'. (Elsevier: Amsterdam).

Improved hydropedological identification of soil salinity types in upland South Australia using seasonal trends in soil electrical conductivity

Mark Thomas[AB], Rob Fitzpatrick[AB] and Graham Heinson[B]

[A] CSIRO Land and Water, PMB 2, Glen Osmond, Adelaide, SA 5064, Australia
[B] School of Earth and Environmental Sciences, University of Adelaide, North Terrace, Adelaide, SA 5001, Australia

Abstract
Our hydropedological methods explain variations in seasonal changes during late winter (September) and late summer (April) to electrical conductivity (i.e. solute concentrations) in 19 near-surface (< 0.7 m) soil profile layers from a range of topographic settings within a 120 ha study area in the Mount Lofty Ranges, South Australia. By combining down profile trends of clay per cent, 1:5 water extractable cations and ions, and soil-landscape and terrain analysis patterns, we establish existence of four salinity types consistent with a new process-based salinity classification; two were associated with upper slope positions featuring perched watertables while the other two were associated with deep saline watertables, though in upper and lower landscape positions. Conceptual toposequence models for each salinity type explain the interactions between groundwater, soil morphology and landscape position. The methodology provides a convenient, cost-effective adjunct to conventional groundwater approaches (e.g. nested piezometers) to determine patterns of water flow and solute transport in saline landscapes

Key Words
Salinity, electrical conductivity trends, 1:5 water extractable cations and anions, terrain analysis, hydropedology.

Introduction

Salt-affected soils fall into two categories: (i) saline soils, and (ii) sodic soils. In Australia, the latter have an exchangeable sodium percent (ESP) ≥ 6 (Isbell 1996). Saline soils are typically dominated by halite (NaCl), although carbonate (CO_3^-), sulfate (SO_4^{2+}) and salts of other anions may dominate locally. In sodic soils with low soluble salts, excessive Na^+ causes physical degradation of soil structure, creating problems such as hard setting, reduced hydraulic conductivity and dispersion (Sumner 1995). Soluble salts are dissolvable under field water conditions (Soil Survey Staff 1993). As such, prevailing landscape hydraulic conditions may be detected by measuring changes in saline groundwater wetting fronts, and formation and persistence of salt concentration zones within the soil profile (Shaw 1988). The integrated study of these soil-regolith conditions fall within the research discipline of hydropedology, which bridges the inter-related disciplines of pedology, geomorphology and hydrology (Lin *et al.* 2008).

Fitzpatrick (2008) presents a salinity classification based on soil-regolith-hydrology types, with indicative salinity ranges (electrical conductivity of saturated paste extract, EC_e) . In this scheme, groundwater associated salinity (GAS) corresponds to commonly referred "dryland salinity" in Australia, and is formed where saline watertables intersect at or near the soil surface. Solum-affected non-groundwater associated salinity (NAS) (Fitzpatrick 2008) occurs mostly in sodic soils, and is restricted to the soil solum (i.e. the A and B horizons, typically < 1.5 m). It is present in upper landscape positions with no hydraulic connection to deep saline watertables, and is restricted to semi-arid or arid winter rainfall zones where the annual evaporation rates exceed rainfall. The subsoil form of NAS (EC_e 2 - 8 dS/m) occurs typically in the depth range 0.3 - 1.0 m. Generally soils with solum-affected NAS feature loamy A horizons overlying clayey B horizons that are often sodic, and hence with low hydraulic conductivity. The poorly permeable B horizons contribute to formation of seasonally perched saline watertables in topographic sump-like landforms in the hillslopes, e.g. localised depressions. Salinity depth and concentration in these solum-affected NAS profiles therefore vary in response to seasonal conditions (i.e. rainfall, evaporation and transpiration rates).

The purpose of this paper is to apply the salinity classification that Fitzpatrick (2008) presents using multitemporal hydropedological approaches in a small (120 ha), rain fed catchment in the Mount Lofty Ranges (MLR) in South Australia to (i) diagnose salinity types, and (ii) develop conceptual models for the salinity types identified. The analytical methods apply repeat analysis of winter (2004) and summer (2005) salinity concentrations (i.e. EC_e and ionic) that are measured in fixed incremental-depth layers from 19 shallow (< 0.7 m) soil profiles. We augment salinity classifications and conceptual model development by

applying soil-landscape context (i.e. landform and hillslope position) supplied through field observation and digital terrain analysis.

Methods

Study area and soil sampling

The Herrmanns catchment is located in the Mount Lofty Ranges (MLR) 40 km east of Adelaide, South Australia. The climate is Mediterranean-like with rainfall occurring predominantly during winter (May to October). A typical toposequence (Fritsch and Fitzpatrick 1994) consists of the following: Typic Palexeralfs → Aquic Palexeralfs → Albic Glossic Natraqualfs → Typic Natraqualfs (Soil Survey Staff 1993). A digital elevation model (DEM) with two metre ground resolution was generated from a stereo pair of 1:40,000 aerial photographs. Using ArcMap GIS, terrain analysis was performed to create various GIS coverages of terrain attributes, including two metre elevation contours and topographic wetness index (TWI) showing near-surface soil water through-flow and accumulation patterns (Figure 1). Georeferenced year 2001 summer and winter aerial photographs were integrated in the GIS as interpretative backdrops.

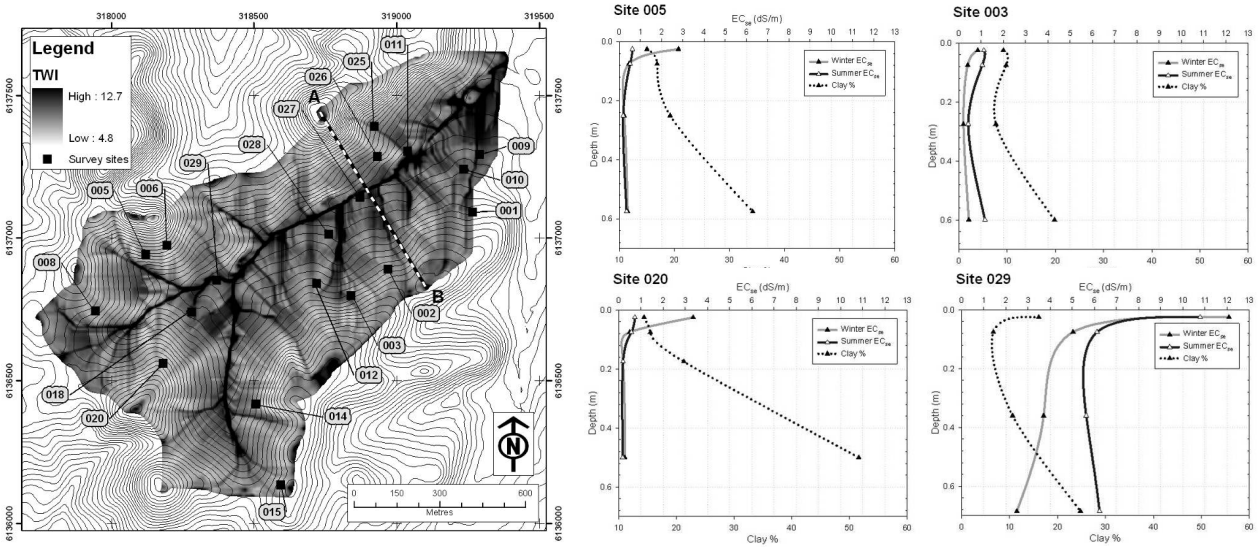

Figure 1. Left, Herrmanns catchment study area TWI coverage showing patterns of high (dark shades) and low (light shades) rates of near surface water through-flows. Also shown are soil survey site locations and 2 m elevation contours. Right, typic down profile salinity (EC_e) and texture (clay %) trends for Model 1(a) NAS (Site 005), Model 1(b) NAS (Site 003), Model 2(a) GAS, and Model 2(b) GAS

Nineteen soil profile locations were selected (Figure 1) based on prior field knowledge. Combinations of survey points were selected to form toposequences or paired sites from similar hillslope zones, but occupying positions in different local topographic features. Soil sampling was conducted during late winter (September) 2004 and then late summer (April) 2005. Each sampling site location was recorded using a differential GPS during the winter survey to assist site location during the subsequent survey. Sampling during the second survey was conducted one metre upslope of the first survey to negate altered soil profile hydrology. Four layers were sampled in each profile, comprising: L1 (0 – 0.05 m) and L2 (0.05 – 0.1 m), both dominating the A horizon; L3 (0.1 – upper B horizon), typically dominated by the E horizon and; L4 the upper B horizon to a maximum depth of 0.75 m.

Laboratory physicochemical analyses

Laboratory analyses were conducted on the ground (< 100 µm), dried < 2 mm soil fraction of samples. The analyses involved wet chemical analyses using 1:5 soil:water extractions (i.e. water extractable Ca, K Mg, Na, PO_4, Cl and SO_4) (Rayment and Higginson 1992). Mid-infrared (MIR) analysis was used to predict soil particle size analyses. The electrical conductivity of saturated paste extract (EC_e) was estimated using a conversion factor after Cass *et al*. (1996) from EC1:5 and soil texture. MIR was used to estimate the soil texture, which was incorporated to convert Shaw's (1988) soil texture classes used in the $EC1:5/EC_e$ conversion methodology.

Results

Physiochemical trends

Seasonal down profile solute trends are graphically displayed with clay per cent to assist interpretations of

near-surface hydrological processes and salinity types. Interpretations were assisted by knowledge of soil type and soil landscape patterns (e.g. TWI and elevation). Down-profile salinity trends for winter and summer plotted against clay per cent indicate the prevailing landscape hydraulic conditions according to: (i) changes in saline groundwater wetting fronts, and (ii) formation and persistence of salt concentration zones within the soil profile. Four salinity types were identified using the hydropedological methods (Figure 2). The salinity types identified are as follows:

i. Solum-affected NAS, topographically perched in upper hillslopes - Model 1(a);
ii. Solum-affected NAS, low lying areas of mid-upper hillslopes - Model 1(b);
iii. GAS, upper hillslopes - Model 2(a); and
iv. GAS, lower hillslopes - Model 2(b).

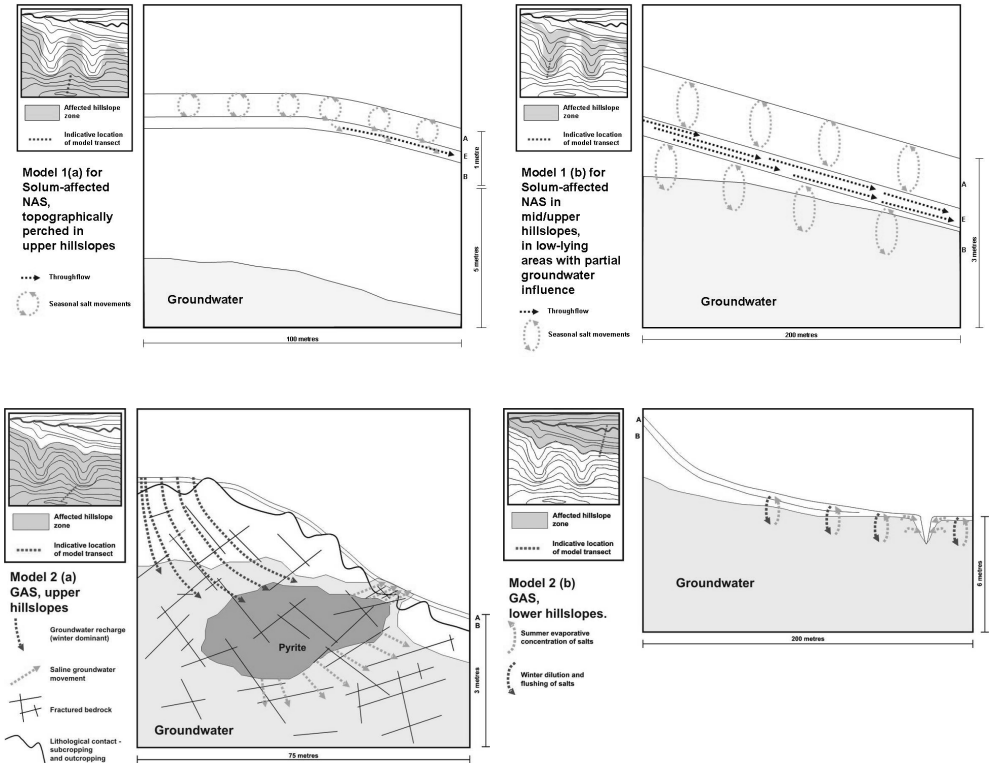

Figure 2. Conceptual models for Model 1(a) Model 2(b), Model 2(a) and Model 2(b) The conceptualised contour map that is inset identifies possible affected areas in the landscape, and the indicative location of the transect described in the model.

Conceptual models

Each salinity type showed distinct topographic setting and profile trends (Figure 2 and Table 1). Hydropedological conceptual models for each salinity type that summarise the key topographic, profile morphological and hydrological features of each are presented in Figure 2.

Conclusions

The hydropedological interpretation of combined site knowledge, soil layer texture (according to clay %), and seasonal soluble salt chemistry (inferred from EC_e and selected water extractable major cations and anions) at various near-surface profile depths (< 0.7 m) in a Mount Lofty Ranges catchment have given rise to four distinct hydropedological models for salinity types. These are presented as conceptual models in Figure 2. Two of the models are dominated by solum-affected non-groundwater-associated salinity (NAS) processes located at either topographically perched, upper hillslopes or from topographically non-perched, mid/upper hillslopes with groundwater influence. The remaining two models are dominated by groundwater-associated salinity (GAS) processes in either upper or lower hillslopes locations. The low-cost investigation methods described shows the importance of seasonal hydropedological changes in the near-surface (< 0.7) of soils in the study area. The multitemporal hydropedological method for identifying salinity types significantly augments the traditional approaches to interpret pedogenic and degradation processes in soil-landscapes, which include detailed layer morphological description and interpretation, and the installation of costly nested piezometers. The methodology will provide a convenient, cost-effective adjunct to

conventional groundwater approaches (e.g. nested piezometers) to help determine patterns of water flow and solute transport in saline landscapes.

Table 1. Summary of trends for salinity types presented in Figure 1.

Salinity type	Topographic position	Down profile morphology	Winter and summer down profile salinity trend (Figure 1)		Sites represented (Figure 1)	Description
			A horizon	B horizon		
Solum-affected NAS, Model 1(a)	topographically perched in upper hillslopes	Texture contrast	Seasonally variable, moderate to strong	Seasonally constant, low	001, 002, 005, 006, 008, 010, 012, 014, 015, 025, 026 and 028	Seasonal circulation of perched salts in A horizon. Saline groundwater beyond hydraulic influence of upper profile.
Solum-affected NAS, Model 1(b)	low lying areas of mid-upper hillslopes	Texture contrast, prominent E horizon	Seasonally variable, moderate	Seasonally changing, low	003 and 009	Seasonal circulation of perched salts in A horizon. Saline groundwater within seasonal hydraulic influence of upper profile. Prominent E horizon truncates hydraulic connectivity between upper A and B horizons.
GAS, Model 2(a)	upper hillslopes	Texture contrast	Seasonally variable, moderate	Seasonally constant, low	020	Upslope pyritic body flushed by groundwater supplies seasonal salts (featuring SO4-)to upper profile
GAS, Model 2(b)	lower hillslopes	Gradational	Seasonally constant, strong	Seasonally changing, strong	011, 018, 027 and 0029	Salts accumulate in A horizon while B horizon is influenced by seasonally changing watertable depth

References

Cass A, Walker RR, Fitzpatrick RW (1996) Vineyard soil degradation by salt accumulation and the effect on the performance of the vine. In 'Ninth Australian Wine Industry Technical Conference'. (Eds CS Stockley, RS Johnstone, TH Lee) pp. 153 - 160. (Adelaide, South Australia).

Fitzpatrick RW (2008) Soils and natural resource management. In 'Regolith Science'. (Eds KM Scott and CF Pain) pp. 307 - 340. (CSIRO Publishing: Melbourne).

Fritsch E, Fitzpatrick RW (1994) Interpretation of soil features produced by ancient and modern processes in degraded landscapes. I. A new method for constructing conceptual soil-water-landscape models. *Australian Journal of Soil Research* **32**, 889 - 907.

Isbell RF (1996) 'The Australian Soil Classification.' (CSIRO Publishing: Melbourne, Australia)

Lin H, Bouma J, Owens P, Vepraskas M (2008) Hydropedology: Fundamental issues and practical applications. *Catena* **73**, 151-152.

Rayment GE, Higginson FR (1992) 'Australian laboratory handbook of soil and water chemical methods.' (Inkata Press, Melbourne)

Shaw RJ (1988) Soil salinity and sodicity. In 'Understanding soils and soil data: invited lectures for refresher training course in soil science'. Brisbane. (Ed IF Fergus) pp. 109-134. (Brisbane Australian Society of Soil Science, Queensland Branch)

Soil Survey Staff (1993) 'Soil Survey Manual.' (U.S. Government Printing Office: Washington, USA)

Sumner ME (1995) Sodic soils: new perspectives. In 'Australian sodic soils: distribution, properties and management'. (Eds R Naidu, ME Sumner, P Rengasamy) pp. 1 - 34. (CSIRO Publications: Melbourne)

In-field visualisation of water infiltration and soluble salt transport

Andrei Rozanov[A] and Willem de Clercq[A]

[A]Department of Soil Science, University of Stellenbosch, 7600 South Africa, Email dar@sun.ac.za

Abstract
Visualisation of saline water infiltration pattern was done with digital photography. KI was added to water applied through double-ring infiltrometer. Fine layers of soil were excavated on completion of infiltration test and spray-treated with starch and pyroxide to develop blue colour shades from reaction with Iodine. Images of both vertical and sequential horizontal sections of the wetted profile were acquired. The images were rectified and post-processed to isolate and qualify the frontal and preferential flow.

Key Words
Preferential flow, flow visualisation, soil salinity.

Introduction

The study of salt transport in the lower catchment of the Berg River (Western Cape, South Africa) has raised questions whether it may be considerably affected by macropore water flow at the scale of soil profile. Field observations of cracks on the clayey soil surface in some parts of the catchment and multiple instances of termite activity suggested that preferential water flow may be present in the system. A quick test showed that flooding with small quantities of water may have substantial effect on the pattern of instant water infiltration in a cracking soil (Figure 1). The excavation of the flooded soil to the depth of some 5 cm demonstrated that only small fraction of the total soil volume around the cracks was wetted leaving most of the large blocky aggregates in dry state (Figure 1 c). This observation inspired detailed studies of infiltration patterns using a colour tracer to identify preferential flow pathways. Various in-situ (Gazis *et al.* 2004; Forrer *et al.* 2000) and ex-situ (Mooney 2006) methods of visualising the process were considered and slightly modified method based on iodine-starch staining (Hangena *et al.* 2003) was selected.

a) cracks on soil surface **b) flooding of cracked soil** **c) excavation of flooded soil**

Figure 1. Observations of instant preferential flow through cracked topsoil.

Methods

Field experiments

Soils of Glenrosa form (*Lithic Cambisol*) on Malmesbury shales were selected for the experiment, being some of the dominant soils according to the results of the soil survey. Standard double ring infiltrometer was used and pressure potential of 100 mm was maintained throughout the experiment. On completion of infiltration the water was allowed to drain for a short period of time (up to 2 hours) and both vertical and horizontal sections of the soil were exposed. One vertical and several horizontal sections were made per soil profile.

Summer infiltration

Three double ring infiltration sites were established as following.

a) Soil with few or no visible cracks on the surface next to one of the soil survey profiles.
b) Soil with visible termite activity.
c) Soil with visible sediment accumulation and extensive cracking above the contour bank.

The experiments included:

a) determination of infiltration rates

b) determination of soil bulk density and moisture content
c) visualization of water flow with KI-starch reaction.

Considering high variability of climate, it was decided to conduct the experiments twice – in summer and winter to compare infiltration rates for desiccated and pre-wetted soil.

Winter infiltration in wheat fields

Two sites were selected to repeat infiltration measurements with double ring infiltrometer for comparison with summer results. In addition two runs of rainfall simulation were conducted for observation on larger area in conditions of free run-off instead of a pressurized double ring infiltrometer system.

Visualisation

KI (potassium iodide) was selected as a tracer for several reasons.

a) reliable reaction with starch allowing high visibility in the soil.
b) high solubility and behaviour in soil, which would be similar to that of modelled salt fluxes and distributions.

Concentration of KI in water was 7% (half the amount used by Hangena *et al.* 2003), which was deemed to be sufficient considering the light background colour of the soil.

Soil sections were sprayed with (5%) pyroxide solution to facilitate release of I_2 from KI and further sprayed with household starch spray from a pressurized canister. The reaction of iodine with starch was considered completed after 10 mins and digital photographs in RAW format were taken with Canon G5 camera for image processing. The images were corner-stone projected and converted into the LAB colour space.

Results and discussion

The images were converted into the LAB colour space for enhancement (Figure 2). The processing of enhanced images is still under way and the exact methodology is in the development stage.

a) original image **b) image with contrasted "b" layer** **c) blue colour selection** **d) selection in greycolour**

Figure 2. Image enhancement by contrasting the the b layer in LAB colour space.

The current problems in image processing that have to be solved are

a) variations in illumination within the photograph.
b) influence of I_2 and starch concentrations on the colour characteristics.
c) the influence of background colour variations on colour characteristics of the stained area.

The observed infiltration rates were extremely slow, though large unrecorded volumes of water were required to fill up the infiltrometers. Over 24 hours of infiltration resulted in very shallow water penetration as wetting front progressed (Figure 3a), however deep water channeling was observed in some macropores of the lithocutanic B horizon (Figure 3b). One of the important points was that the observed pattern of iodine distribution in the soil was not corresponding well with the measured bulked values of soil moisture content noted by Weiler and Flühler (2003) for various dyes. Increase in moisture content was observed deeper than the visible penetration of the wetting front. The most reasonable explanation for that is the attenuation of KI for clay and participation in exchange reactions in soil. The soil was performing as a chromatographic column leaving most of the KI at the top of the profile. This was somewhat aggravated by relatively low concentrations of KI, and possibly some patchiness in distribution of pyroxide and starch over the sprayed surface, though every effort was made to ensure a dense mist spraying.

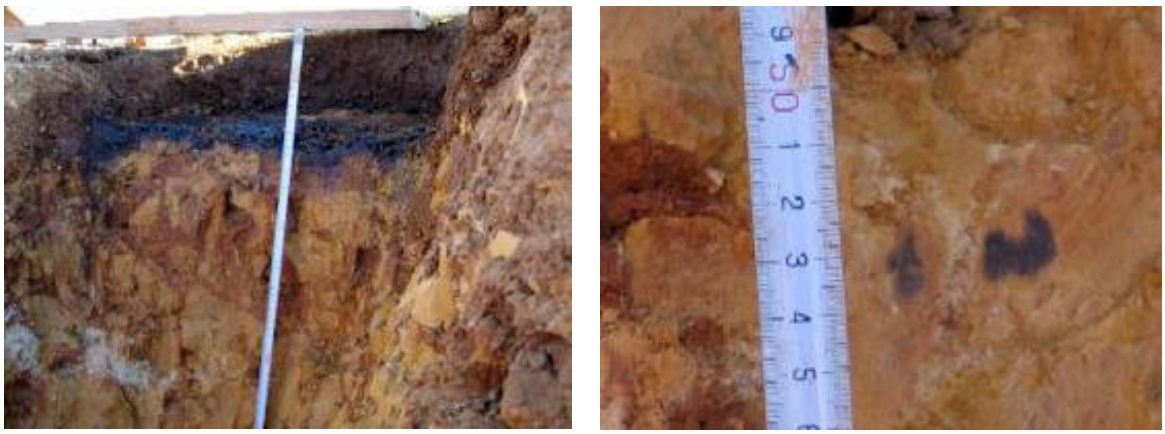

a) Frontal infiltration observed in the lithocutanic (cambic) B horizon **b) spot of iodine-starch complex channelled to the depth of 53 cm**

Figure 3. Infiltration into the lithocutanic B horizon of the Glonrosa soil at Goudertrou.

During the winter run of the infiltration experiments the infiltration rates were higher, seemingly due to higher initial moisture content of the soil and recent land preparation. It was also observed that presence of plants in the field improves infiltration by channelling water along the stalk towards the rooting zone and, ultimately into the prepared row of wheat. This phenomenon was observed both in the ring infiltrometer and under rainfall simulator (Figures 4 and 5).

In case of rainfall simulation sub-samples of wheat were taken from irrigated and non-irrigated parts of the field, showing water interception by wheat averaging at 85% of total dry mass. Interception by the canopy of the crop leads to shading of the soil and channeling of water. However, since the same phenomenon was observed in the flooded double ring infiltrometer experiment, one can say that two mechanisms are at play here:

a) interception by the canopy and channelling of rain water along the stalks of wheat;
b) channelling of water through the soil along the root canals.

a) rainfall simulator **b) ring infiltrometer**

Figure 4. Effect of furrows with wheat on water infiltration at the depth of 6 cm.

Image enhancement considerably improves the identification of wetted pores through the oriole effected formed on the boundary of the pore and adjacent surface treated with pyroxide and starch (Figure 5). It allows to semi-automate the process of image classification and provides sharp boundaries.

Conclusion

It was shown that KI may be successfully used as a tracer for visualizing water infiltration and soluble salt movement against the contrasting background of light-coloured soil. The method is also inexpensive, but requires further calibration and image interpretation studies. Quantification of water infiltration using the suggested visualisation technique is problematic due to partial dye retention and may be further complicated by iodine volatilisation and transport through air-filled pores. The errors introduced by the above effects require further study and quantification. The main advantage of this method is the possibility of in-field visualisation as opposed to core sample analysis, and imposes practically no restrictions either the size of the

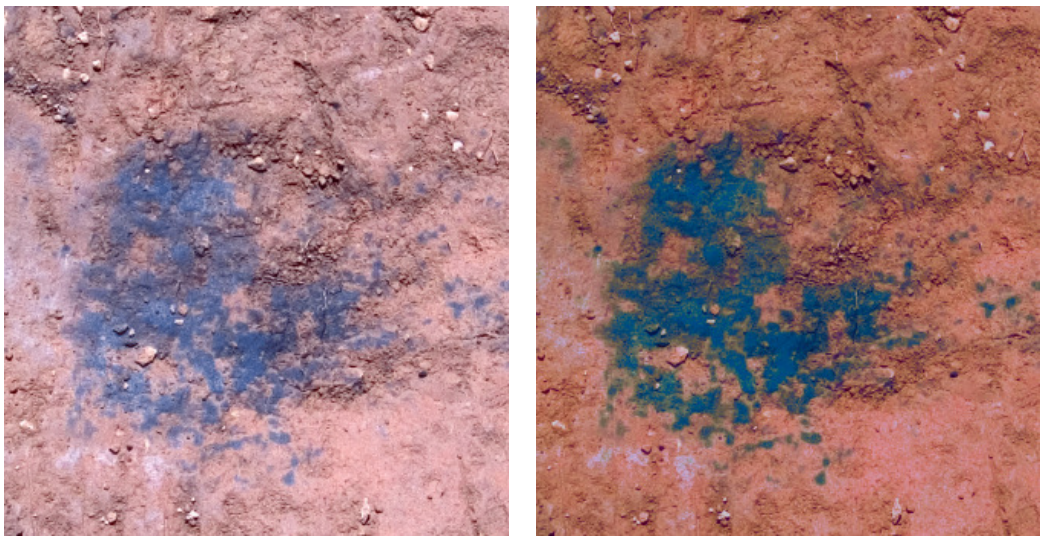

a) raw image **b) enhanced image showing distinct boundary oriole effect around the wetted zone**

Figure 5. Effect of wheat roots on water infiltration at the depth of 30 cm.

studied macropopores or that of the experimental plot itself if KI solution is applied through rainfall simulator or irrigation system. The method allowed to distinguish between the effect of land preparation practices and biological macropores on preferential flow patterns in the bulk volume of soil under wheat fields and may be applied as a useful tool in the study of cultivation systems and implements.

References

Forrer J, Papritz I, Kasteel A, Flühler R, Luca HD (2000) Quantifying dye tracers in soil profiles by image processing. *European Journal of Soil Science* **51**, 313–322

Gazis C, Feng X (2004) A stable isotope study of soil water: evidence for mixing and preferential flow paths. *Geoderma* **119**, 97– 111

Hangena E, Gerke HH, Schaaf W, Hüttl RF (2003) Flow path visualization in a lignitic mine soil using iodine–starch staining. *Geoderma* **120**,121–135

Mooney SJ (2006) Three-dimensional visualization and quantification of soil macroporosity and water flow patterns using computed tomography. *Soil Use and Management* **18**, 142-151.

Weiler M, Flühler H (2003) Inferring flow types from dye patterns in macroporous soils. *Geoderma* **120**,137–153

Integrating physical and chemical techniques to characterise soil microsites.

Wilfred Otten[A], Dmitri Grinev[A], Philippe Baveye[A], Zi Wang[C], Simona Hapca[A] and Clare Wilson[B]

[A]SIMBIOS Centre, University of Abertay, Dundee, UK, Email w.otten@abertay.ac.uk
[B]Sbes, University of Stirling, Stirling, UK Email c.wilson@stirling.ac.uk
[C]ENSTA, Paris tech, France

Abstract
Many problems in environmental and soil research require techniques that quantify the soil micro-environment. It has become increasingly apparent that we need novel micro-analytical techniques to compliment well established methods that study soils at macro-spatial scales. Despite tremendous progress in this field over the last decade, quantitative methods have developed within separate disciplines and operate at different spatial scales hampering their integration. Moreover, it means that opportunities to integrate these methods may be overlooked. In this paper we develop methods that enable integration of a 3-D non-invasive technique to characterise soil structure (X-ray CT) with a 2-D spectroscopic method that characterises the spatial distribution of chemical elements on surfaces (SEM-EDX). First we developed statistical software to locate the 2-D plane in which SEM-EDX analyses were performed within the 3-D volume. Then we demonstrate that selected compounds, including particulate sources of C and $CaCO_3$, can be quantified with SEM-EDX and subsequently visualized within the 3-D soil environment. Finally, we demonstrated that when we characterized sequential slices with SEM-EDX we could use co-kriging methods to predict the 3-D spatial distribution of chemical elements. We discuss the possibilities and problems that need to be resolved to combine these methods.

Key Words
X-ray tomography, soil-micro habitat, scanning electron microscope, co-kriging. modelling.

Introduction
Increasingly, over the last few years, it has become clear that our measurements in soils are made at scales too coarse to allow for precise prediction of ecosystem processes. Fortunately, recent technological advances allow us to unravel the physical, chemical, and biological heterogeneity of soils, which, when combined with modelling techniques, allow us to make sense of the complexity of soil systems. However, separation of disciplines still hampers progress. Soil physics and soil chemistry are highly interdependent, with the heterogeneous spatial distribution of chemical species intertwined with soil structure. Examples include the role of metal complexes and clay minerals in the formation and stabilization of aggregates (Tisdall and Oades 1982), gleyic features in poorly drained soils, or soils contaminated with metals. Correlations between soil structure and chemical properties also have significant impact on macro-pore flow of solutes (Ellerbrock *et al*. 2009).

To date, our understanding of soil structure has relied heavily on the concept of soil aggregates. Advances in the use of X-ray CT, however, enable quantification of the internal structure of soils at microscopic scales without physical disruption. Similarly, microscopic and micro-spectroscopic analyses (soft tissue X-ray microscopy and near edge X-ray absorption fine structure) are beginning to increase the spatial resolution of chemical analysis. However, these chemical techniques to date are restricted to small samples (a few mm in diameter) and often require access to synchrotron facilities, even though the development of tabletop X-ray CT/ micro XRF scanners is making rapid progress (Sasov *et al*. 2008). Combining non-invasive and invasive techniques that operate at microscopic scales may offer a way beyond what can be achieved with current techniques.

Despite the overwhelming evidence of close links between chemical composition and soil structure, techniques for quantification are often separate, and it may be a few years before 3-D mapping of the physical, chemical and biological properties in soils is possible at a range of spatial scales. In this paper we investigate if we can combine 3-D X-ray CT with semi-quantitative element maps obtained with 2-D spectroscopic methods (SEM-EDX) to unravel the interactions between soil physical and chemical characteristics. The voxel greyscale value in a 3-D X-ray CT reconstruction represents the linear attenuation coefficient, which is a function of the atomic number detected by SEM-EDX, hence the potential for

integration of these techniques. The overarching aim is to explore and develop methods to combine 2-D chemical analyses with 3-D physical data. We aim to achieve this through the following specific objectives: **1.** to use X-ray tomography and identify organic and mineral compounds that differ sufficiently in attenuation to be visualized in 3-D. **2.** to produce parallel 2-D slices through soil and analyze these with SEM-EDX. **3.** to apply and test statistical methods to interpolate between the parallel slices and produce a 3D map that visualises the distribution of the 3-D soil structure.

Methods

Sample preparation and procedure

A sandy loam soil was air-dried, sieved to 1-2 mm and repacked at a bulk-density of 1.2 Mg/m^3. Blocks were resin impregnated and precision-sliced to produce a 1 cm^3 soil cube. The physical structure was quantified using X-ray CT (see below). After that, the cube was sliced to produce parallel slices of about 500 μm thick, and the slices that were scanned on both sides with SEM-EDX to identify both mineral and organic components.

SEM-EDX

We used the SEM-EDX system (Jeol 6460LV and Oxford Instruments InCA X-Sight) to quantify and map elemental spatial distributions on the surfaces of slices from a resin-impregnated 1 cm^3 of soil. Element maps were acquired at 15 kV with a spatial resolution of 8 μm. External elemental and mineral standards were used to ensure data quality control during data acquisition. Phase analysis was used to identify distinctive chemical compounds based on their chemistry. Phase analysis, was also used to isolate the impregnating resin's chemistry from the soil data.

X-ray micro-tomography

The 3-dimensional pore space was visualised with a METRIS HMX micro-tomography system at 8 μm resolution. High resolution CT data sets were reconstructed in 3-D using floating point grey scale to enhance contrast between the phases. We used in-house developed software for a quantitative analysis, segmentation, and visualization of the 3-D pore structure and solid phases.

Analytical methods: Combining X-ray CT and SEM-EDX

We explored two ways of combining the techniques: (1) use SEM-EDX to characterise compounds that differ in attenuation in X-ray CT, so that they subsequently can be visualized in 3-D and (2) use co-kriging to predict the 3-D distribution having located the sequential slices within a 3-D volume. In the first method we identified compounds in the X-ray CT data with an attenuation coefficient significantly different from the surrounding soil matrix (Young *et al*. 2009). Typically these include particulate sources of organic matter (e.g. black carbon), horneblends, or $CaCO_3$.We segmented out these identifiable objects using in-house developed thresholding software and algorithms, and then obtained a thin section in which the chemical composition is quantified using SEM-EDX. In the second method, we first aligned the spatial resolution, and then used spatial cross-variograms to locate the 2-D SEM-EDX plane within the 3-D physical structure. A close (μm's) alignment is essential due to the huge microscopic heterogeneity. Based on the spatial correlation between the physical and chemical data we then applied ordinary co-kriging to predict the 3-D distribution of chemical elements.

Results

Using SEM-EDX it was possible to obtain detailed information on the spatial distribution of chemical elements for a relatively large sample area (1 cm^2). We produced spatial maps of several elements including C, O, K, Ca, and Si, which demonstrated the high spatial variability of those elements at small scales (Figure 1). The data showed a good spatial correlation between the physical structure and the concentration of some elements such as carbon which was mainly occupying the pore space as it is associated with the resin used to impregnate the soil sample, silicon that was present mostly on the solid phases, and calcium-carbonate that was associated with very large greyscale values in the X-ray CT images.

Some chemical elements had attenuation coefficients in the X-ray CT data sufficiently different from the background to allow for segmentation (Figure 2). For example, the light 'kidney-shaped' object in the X-ray CT data set (Figure 2a) was quantified by SEM-EDX as $CaCO_3$ (Figure 2b), evidenced by a quantitative analysis of the composition of this object as C = 22.73%, O = 39.5%, Ca = 37.1%, and Si, Al, and Mg <0.5 % on a weight basis. Further analysis of the X-ray CT data enabled us to visualize this compound, now identified as $CaCO_3$, in 3-D within the soil volume (Figure 2c).

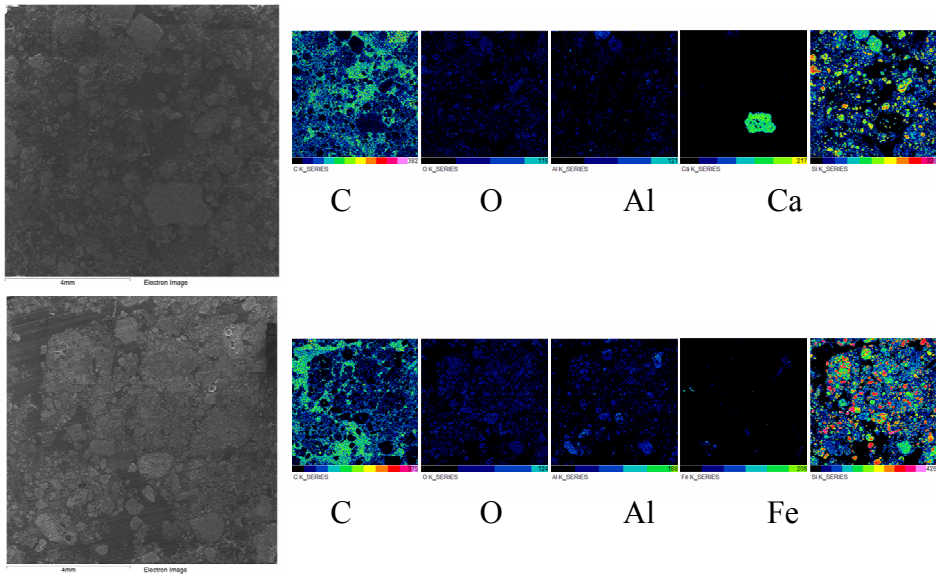

Figure 1. SEM image of the two 1 cm^2 faces of a 500 µm thick soil slice, and the spatial distribution of C, O, K, Ca, Fe, and Si within these slices quantified at an 8 µm resolution.

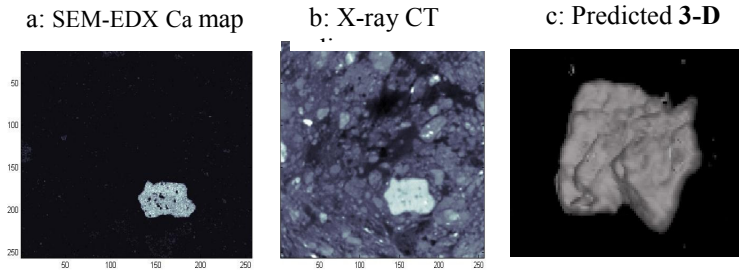

Figure 2. A spatial map obtained with SEM-EDX for (a) Ca, the same slice within the 3-D data obtained with X-ray CT (b), and segmentation of $CaCO_3$ from the X-ray CT data (c).

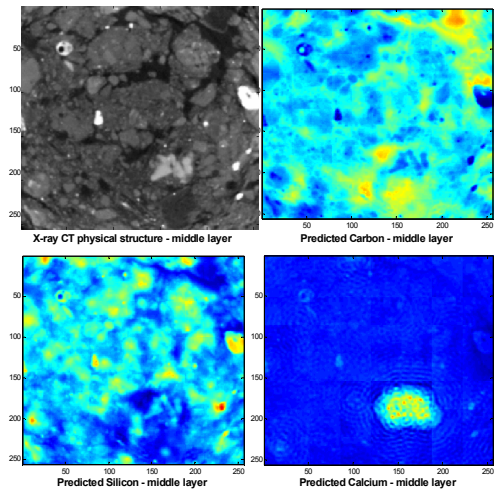

Figure 3. An example of the use of co-kriging to predict the spatial distribution of C (top right), Silicon (left bottom) and Ca (right bottom) in the plane half-way between the two layers that were analysed with SEM-EDX. The figure top left is the X-ray CT slice of the same layer. The figure shows that even with only 2 layers in which chemical data are available a reasonable prediction in 3-D can be made.

Based on the spatial correlation between the physical and chemical variables, we applied an interpolation method using ordinary co-kriging, to predict the internal 3D chemical structure. The predicted chemistry showed a good agreement with the physical structure as indicated by the co-dispersion coefficient between the two variables. In particular, the predicted carbon concentration remained consistent with the pore space,

(Figure 3), while silicon was present in soil aggregates. In this initial stage the statistical results look promising and further investigation including method development and data acquisition for model validation will be undertaken to improve the prediction of 3D chemical structure.

Conclusion

To forward our understanding of soil ecosystems it is imperative that we advance our current techniques to obtain a characterization of the soil micro-environment. Major advances have been made recently for the physical characterization of soil, but 3-D insight into the distribution of chemicals and microbes remains challenging. In this paper we demonstrated that by combining techniques and using statistical models it is possible to obtain a 3-D quantification and visualization of the chemical heterogeneity at microscopic scales. We tested two methods to combine X-ray CT and SEM-EDX. In the first method we identified objects that can be distinguished with X-ray CT and subsequently quantified and chemically characterized them with SEM-EDX. We demonstrated how this can be applied to CaCO3 in our soil sample. This method is however restricted to a limited number of compounds but promising compounds include hornblends and particulate organic matter, including black carbon. This does enable to isolate fractions and visualize them within a 3-D environment, though the full range of options requires further investigation in particular if the material is more heterogeneous by nature.

The SEM-EDX application is restricted to 2-D surfaces of soils. However, by taking sequential slices a 3-D visualization of the chemical heterogeneity can be obtained. It is however useful to be able to reduce the number of slices that is required for extrapolation to 3-D, as characterization of 2-D surfaces with SEM-EDX is time consuming, and because some material gets lost when preparing sequential slices through a soil sample. The agreement between X-ray CT and SEM-EDX did allow us to test if co-kriging methods can be used to interpolate chemical data between two sequential 2-D layers. Co-kriging by combining X-ray Ct and SEM-EDX significantly reduced the number of slices that is required to predict the 3-D chemical heterogeneity. The predicted chemicals were in good agreement with the physical structure as indicated by the co-dispersion coefficient between the two variable. This was in particular the case for carbon and silicon, with carbon predominantly associated with the pore space (resin of the impregnated blocks) and silicon with the solid phase. Further investigation is however required to improve the statistical techniques and to optimize the sampling strategy to obtain the best possible prediction.

Acknowledgement

The authors wish to acknowledge the Scottish Alliance for geosciences, Environment and Society (SAGES) for financial support.

References

Ellerbrock RH, Gerke HH, Bohm C (2009) In Situ DRIFT Characterization of Organic Matter Composition on Soil Structural Surfaces. *Soil science Society of America Journal* **73**, 531-540.

Sasov A, Liu X, Rushmer D (2008) EMC 2008 volume 1: *Instrumentation and methods*, pp. 705-706. DOI: 10.1007/978-3-540-85156-1_353.

Tisdall JM, Oades JM (1982) Organic matter and water-stable aggregates in soils. *Journal of Soil Science* **33**, 141-163.

Young IM, Crawford JW, Nunan N, Otten W, Spiers A (2009) Microbial distribution in soils: physics and scaling. *Advances in Agronomy* **100**, 81-121.

Linking Principles of Soil Formation and Flow Regimes

Henry Lin

Dept. of Crop and Soil Sciences, The Pennsylvania State Univ., University Park, PA 16802, USA, Email henrylin@psu.edu

Abstract
Preferential flow (PF) is a fundamentally important soil hydrologic process that controls a variety of soil physical, chemical, and biological functions. However, the lack of theory in this field and the existence of conceptual and technological bottlenecks continue to hinder the advancement in understanding and predicting PF. This paper explores three theories that link pedogenesis to flow regimes, including 1) non-equilibrium thermodynamics as applied to the open dissipative system of field soils with continuous energy and mass inputs that results in the dual-partitioning of pedogenesis into organizing and dissipating processes; 2) constructal theory that explains the tendency for dual-flow regimes in soils, one with high resistivity (Darcy flow) and the other with low resistivity (PF), together they form natural PF configuration that provides the least global flow resistance; and 3) theory of evolving networks that sheds light on diverse PF networks for increasing the efficiency or effectiveness of energy and mass transfer in the subsurface. All three theories support the notion that PF is likely universal in natural soils. However, some controversies associated with these theories require more concerted efforts to systematically test their applicability and to formulate quantitative relationships between PF occurrence and its macroscopic controls.

Key Words
Preferential flow; pedogenesis; non-equilibrium thermodynamics; constructal theory; network theory.

Introduction

Preferential flow (PF) is a generic term that refers to the process whereby water (and materials carried by water) moves by preferred pathways in an accelerated speed through a fraction of a porous medium, thus bypassing a portion of the matrix. Numerous studies over the past four decades or so have demonstrated that PF can occur in practically all natural soils and landscapes. Mechanism-wise, all PFs are essentially heterogeneity-related, including macropore flow, finger flow, funnel flow, and hydrophobicity-induced flow that are more frequently reported in the soil science literature (at the pore and pedon scales), and pipe flow, return flow, throughflow, depression-focused flow, and flow at the soil-bedrock interface that are more commonly reported in the hydrology literature (at the hillslope and catchment scales).

In a new vision for watershed hydrology, McDonnell *et al.* (2007) raised a number of fundamental questions: "*Why heterogeneity exists? Why there is preferential, network-like flow at all scales?*" In light of these concerns and the need to develop PF theory, the objective of this paper is to discuss some physics-based theoretical understanding of PF occurrence and its links to soil formation and evolution.

Non-Equilibrium Thermodynamics and Dual-Partitioning of Pedogenesis

Real-world systems are not isolated from their environment and therefore are continuously exchanging energy and matter with their surroundings (including being driven by external energy sources as well as dissipating internal energy to the surroundings). It is such energy and mass flow across various gradients and boundaries that have driven the evolution and functioning of soils and ecosystems. Non-equilibrium thermodynamics can describe how soil systems interact with their surroundings and their evolution.

The second law of thermodynamics states that the entropy (S) of an isolated system not in equilibrium will tend to increase over time, approaching a maximum at equilibrium. Thermodynamic entropy can be interpreted as a measure of a system's disorder or randomness: the higher the S, the greater the mixedupness or homogeneity (Boltzmann 1896). Interestingly, S is the *only* quantity in physical sciences that seems to imply a particular direction for time (so it is also called an arrow of time) (Prigogine 1961; Tiezzi 2003). Prigogine (1961) distinguishes two terms in the total change of entropy, dS, in an open system: the first, d_iS, is the S produced inside the system; the second, d_eS, is the transfer of S across the system boundaries. According to the second law of thermodynamics, the first term is always positive:

$$dS = d_iS + d_eS, \qquad d_iS \geq 0. \qquad [1]$$

It is in this formulation that the distinction between *reversible* and *irreversible* processes is essential (Prigogine 1961). Only irreversible processes (such as convection, diffusion, and chemical reactions)

contribute to *S* production, leading to one-sidedness of time. This irreversibility results from a certain heat energy dissipation due to intermolecular friction and collisions—energy that can not be recovered if the process is reversed. From a thermodynamics perspective, all complex natural processes are essentially irreversible (Prigogine 1980), including pedogenesis and PF. Often, a threshold behaviour is involved in the time evolution of complex systems and their responses to external forcing.

In an open dissipative system like field soils, while d_iS is always positive, d_eS can be positive or negative depending on *S* exchange between the soil system and its environment (Smeck *et al*. 1983). A dissipative system is a thermodynamically open system that is operating far from equilibrium in an environment with which it exchanges energy and matter (Prigogine 1961). A dissipative system is characterized by the spontaneous appearance of *symmetry breaking* (leading to *anisotropy*) and the *formation of complex structures* (leading to *heterogeneity*) (Prigogine 1980). Heterogeneity here differs from randomness: the former is associated with order while the later is linked to disorder.

Ordering vs. Dissipative Processes in Pedogenesis

Pedogenesis is an energy-consuming process. Smeck *et al*. (1983) explained that soil systems experience outfluxes as well as influxes of energy and matter, but the net balance must favor energy influxes in order to drive soil-forming processes for soil development to proceed. Soil systems with aggregates, horizons, and profiles formed (from parent materials) over time represent more and more ordered states than their precursors (Smeck *et al.* 1983), suggesting an overall reduction in a soil system's thermodynamic *S* and an increased likelihood for PF.

Energy (*E*) inputs and *S* production result in two categories of processes during pedogenesis (Lin, 2010): (1) *Ordering processes* that lead to the formation of soil profile and soil structure, which generally involve *S* reduction, such as aggregation, humus accumulation, horizonation, flocculation, and others; and (2) *Dissipative processes* that lead to destruction of soil structure and the formation of soil matrix, which generally involve *S* increase, such as aggregate degradation, humus decomposition, erosion, dispersion, and others. Such dual-partitioning of pedogenesis results in a variety of soil architecture (which is equivalent to soil structure + soil matrix) that leads to the likelihood for PF occurrence. Similar to Prigogine's (1961) formulation, ΔS_{soil} may be partitioned as (here we use Δ instead of *d* to present longer time interval):

$$\Delta S_{soil} = \Delta S_{matrix} + \Delta S_{structure}. \quad [2]$$

where S_{matrix} is the *S* related to dissipative processes (including *S* generated internally in the soil), while $S_{structure}$ is the *S* related to organizing processes (notably *S* exported from the soil to the surrounding). Smeck *et al*. (1983) have suggested that ΔS_{soil} for most soils are negative after grouping soil-forming processes into positive and negative ΔS: positive ΔS assigned to processes that result in disorder of soil (e.g., physical mixing and primary mineral weathering) and negative ΔS assigned to processes that sort soil constituents (e.g., leaching and accumulation of organic matter).

Near-equilibrium, Far-from-equilibrium, and Models of Soil Development

Because of the irreversible nature of pedogenesis, the second law of thermodynamics essentially dictates that all field soils will evolve towards structured heterogeneity and thus non-uniform flow. Non-equilibrium conditions may be approximated using assumptions of local equilibrium and local *S* production, which can be determined the conjugate force-flux relation.

Near-equilibrium systems tend towards a unique steady-state condition bounded by the force-flux relations. Near-equilibrium fluxes exhibit linear relations to their conjugate forces, as exemplified by the laws of Darcy, Fourier, Fick, and Ohm for water, heat, gas, and electrical transfer processes, respectively. As the forces or gradients become steeper, the linear postulates become unreliable, and systems transition through threshold and bifurcation phenomena to the nonlinear realm of far-from-equilibrium thermodynamics (Nicolis and Prigogine 1989). Open, far-from-equilibrium systems exhibit organization that is dependent on the force-flux relation and the continuous flux of energy and mass across the system boundaries. Interestingly, far-from-equilibrium systems evolve to a state of organization that most efficiently dissipates the flux of available energy, resulting in a state that maximizes the flow of energy, mass, and entropy through the system (Nicolis and Prigogine 1989; Bejan 2000).

Constructal Theory and Preferential Flow Configuration Generation and Evolution

Flow Configuration Generation and Evolution

Emerging constructal theory explains and predicts the occurrence of flow patterns in nature under a principle

summarized below: *"For a finite-size flow system to persist in time (to survive), it must evolve in such a way that it provides easier and easier access to the currents that flow through it"* (Bejan 2000; 2007). This flow tendency calls for at least two flow regimes—one with high resistivity (Darcy flow) that fills the greater part of the available space and the other with low resistivity that provides fast access through various preferred pathways (such as channels and macropores). Together, the fast flowpaths and slow interstitial space constitute natural PF architecture—the configuration that offers the least global flow resistance.

While constructal theory is largely a statement without rigorous mathematical formulae at the present time and its application in the real world soils and hydrologic systems remains to be seen, this somewhat controversial theory offers an interesting perspective regarding the possible generation and evolution of PF in soils. This is because the dual-flow regime anticipated by this theory is in line with the dual-porosity system commonly reported for soils and geological materials (e.g., van Genuchten and Wierenga 1976; Flury *et al*. 1994), and it is also consistent with the pedogenic dual-partitioning discussed above.

Soil Development and Soil Hydraulic Properties Change over Time

Bejan (2000; 2007) suggested three principles to explain how flow configuration evolves over time: (1) survival by increasing flow performance; (2) survival by increasing svelteness; and (3) survival by increasing flow territory. The three constructal principles can be used to explain soil development and associated flow path generation and evolution employing. We can view flow channel openings during weathering to result from either physical breakdown of rocks or cracking, or from chemical or biological processes. Following the constructal principles, we may expect the following sequence to occur as weathering proceeds: (1) At first, as time increases, more pore space would gradually become available for flow within the weathering zone. This results in a reduced flow resistance in the weathering zone; (2) Once the above process reaches a limit (e.g., set by a maximum pore space in the material being weathered), then the weathering would expand into new parent material underneath, which will start the above 1st step again; and (3) As the overall weathering profile thickness reaches a possible limit (e.g., set by environmental constraints, such as climate), then the weathering profile would start to increase its svelteness. This would lead to the formation of a possible compacted layer in the soil profile (e.g., a degraded argillic horizon or a fragipan).

Translating the above general understanding into soil properties change over time, we may expect the following general trend of soil development (without other complicating factors): soil thickness would increase as weathering increases, but soil saturated hydraulic conductivity would first increase and then decrease in the subsoil. Furthermore, as more organization and structural heterogeneity developed through pedogenesis, more PF paths would likely to occur (either vertically or laterally or both).

Network Theory and Preferential Flow Networks in Soils

Networks Theory

A network is nothing more than a set of discrete nodes, and a set of links (representing interactions) that connect the nodes together. The nodes and their links can be anything—such as individuals (nodes) and their social interactions (links), web pages (nodes) and WWW (links), species (nodes) and food webs (links), or individual soil pores (nodes) and their connectivity (links).

In the past decade, a burst of interest in complex networks has sparked rapid growth in their theoretical studies and diverse applications, largely due to a drastic increase in the availability of network datasets coming from the Internet and electronic databases (Barabási 2009). The evolution of network theory has gone through the stages of random graph theory, small-world networks, and scale-free networks.

Network modeling has shifted from the reproduction of network's *structure* (topology) to the modeling of its *evolution* (dynamics), leading to the emerging theory of evolving networks (Albert and Barabási 2002). Another turning point in the modern view of complex networks is *preferential attachment* (Barabási and Albert 1999), meaning that new edges are not placed at random but tend to connect to vertices that already have a large degree of connectivity. Another feature in the theory of evolving networks is that processes operating at the local level both constrain and are constrained by the network structure. The inseparability of the topology and dynamics of evolving networks is increasingly recognized—though far from being fully understood. This is similar to the inseparability of soil architecture and flow dynamics in soils.

Flow Networks in Soils

Despite the difficulty of direct observations, networks are abundant in soils, such as root branching networks, mycorrhizal mycelial networks, animal borrowing networks, crack and fissure networks, and others. Energy

inputs cause flow networks to form in soils, and networks provide a means of minimizing energy dissipation. Like the energy of water flowing over the land surface that creates dendritic stream networks, water flowing through soils also creates network-like flow paths in the subsurface. As water moves through soils, changes in soil texture, structure, organic content, mineral species, biological activities, and other features will modify the resistance to the flow, causing change in flow path to allow water to follow the least resistant path, thus resulting in a PF network that has the least global flow resistance. Some evidence has suggested that a similarity may exist between river dendritic structure and subsurface PF networks.

Depending on the governing physical processes, flow networks may exhibit different topologies. Overall, flow and transport networks in soils are formed by the forcing of soil formation, mainly climate and organisms. Cycles of wetting and drying, freezing and thawing, shrinking and swelling, coupled with organic matter accumulation and decomposition, biological activities, and chemical reactions have led to the formation of diverse soil aggregates and pore networks in the subsurface. In particular, plant roots, burrowing animals, and mycorrhizal mycelia are active in creating networks in soils. Common PF networks in soils include crack and interpedal networks, root networks, mycorrhizal mycelial networks, animal borrowing networks, and man-made subsurface drainage networks.

Various vertical and lateral PFs in soils constitute subsurface flow networks that dictate how water percolates through the soil, runs down the hillslope, and moves across the watershed. The origin, dynamics, and recurrent patterns of self-organization of such flow networks in the subsurface have become the subjects of recent research and model development. For instance, during storms with wet soil conditions, a subsurface network often provides preferred pathways for water to flow down gradient with high velocities. Thresholds may occur when significant changes happen rapidly. A number of studies have suggested that precipitation thresholds for subsurface stormwater generation may be widespread phenomena. Even individual short PF pathways can be linked via a series of nodes in a network, which may be switched on or off and expand or shrink depending on local soil moisture conditions, rainfall inputs, or landscape positions.

Conclusion

The lack of PF theory in field soils requires concerted efforts to synthesize concepts and to advance techniques for measuring and modeling PF across space and time. The theories of non-equilibrium thermodynamics, constructal theory, and evolving networks provide some encouraging perspectives towards a physics-based understanding and prediction of PF that is closely linked to soil formation and evolution.

References

Albert R, Barabási AL (2002) Statistical mechanics of complex networks. *Reviews of Modern Physics* **74**, 47-97

Barabási AL (2009) Scale-free networks: A decade and beyond. *Science* **325**, 412-413..

Barabási AL, Albert R (1999) Emergence of Scaling in Random Networks. *Science* **286**, 509-512.

Bejan A (2000) Shape and Structure, from Engineering to Nature. Cambridge Univ. Press, Cambridge, UK.

Bejan A (2007) Constructal theory of pattern formation. *Hydrology and Earth System Sciences* **11**, 753-768.

Boltzmann L (1896) Lectures on Gas Theory. Dover Publications (March 27, 1995).

Flury M, Flühler H, Jury WA, Leuenberger J (1994) Susceptibility of soils to preferential flow of water: a field study. *Water Resources Research* **30**, 1945–1954.

Lin, H.S. 2010. Comments on Energy-based Pedogenic Models by Field and Minasny (2008) and Rasmussen (2008). *Soil Science Society of America Journal* **74**, 1-3.

McDonnell JJ, Sivapalan M, Vache´ K, Dunn S, Grant G, Haggerty R, Hinz C, Hooper R, Kirchner J, Roderick ML, Selker J, Weiler M (2007) Moving beyond heterogeneity and process complexity: A new vision for watershed hydrology, *Water Resources Research* **43**, W07301.

Nicolis G, Prigogine I (1989) Exploring Complexity. W. H. Freeman, New York.

Prigogine I (1961) Introduction to thermodynamics of irreversible processes. John Wiley, New York, NY.

Prigogine I (1980) From being to becoming : time and complexity in the physical sciences. W. H. Freeman.

Smeck NE, Runge ECA, Mackintosh EE (1983) Dynamics and genetic modeling of soil systems. In 'Pedogenesis and Soil Taxonomy'. (Eds LP Wilding *et al.*) pp. 51–81. (Elsevier, New York).

Tiezzi E (2003) The essence of time. WIT Press.

van Genuchten MT, Wierenga PJ (1976) Mass transfer studies in sorbing porous media Part 1 analytical solutions. *Soil Science Society of America Journal* **40**, 473-480.

Resilience of soil to biological invasion: analysis of spread on networks.

Wilfred Otten[A] , Dmitri Grinev[A], Francisco Perez-Reche[B], Franco Neri[C], Luciano da Costa[D], Marcel Biana[D], Chris Gilligan[C], and Sergei Taraskin[B]

[A]SIMBIOS Centre, University of Abertay Dundee, UK, Email w.otten@abertay.ac.uk
[B]Department of Chemistry, University of Cambridge, UK
[C]Department of Plant Sciences, University of Cambridge, UK
[D]Instituto de Fisica de Sao Carlos, Universidade de Sao Paulo, Sao Carlos, SP, Brazil

Abstract
A network model for soil pore volume is presented and applied to the analysis of biological invasion of microorganisms. The pore geometry of two soils with a relatively high or low bulk density were quantified with the use of X-ray tomography and networks were constructed to present the pore space by channels connecting intersecting points. This network was subsequently quantified by the measurement of biologically relevant parameters, such as the distribution of lengths of the links between two nodes, the coordination number of the nodes, and the distribution of the sizes of the links between two nodes. Spread of microorganisms was subsequently considered as a function of these characteristics and embedded into a simple epidemiological model for spread that can be mapped onto percolation theory. We found that the networks display critical behaviour for biological invasions with a greater resilience to invasion for the more densely packed soil. We also found that inherent heterogeneity of soil systems further contributes to resilience to invasion.

Key Words
X-ray tomography, percolation, micro-organisms, epidemiological models, soil structure, modelling.

Introduction

Soil structure is of significant importance for various dynamical processes in soil, including the movement of water, gasses and microorganisms. Several techniques have been used to quantify soil structure and microscopic heterogeneity including serial thin sectioning, but with the rapid advances in the use of X-ray tomography quantification of real structures is becoming increasingly routine. Whereas various transport models have been developed over recent years to cope with transport and the distribution of water and air in heterogeneous soil environments, there is less theoretical understanding of the impact of microscopic heterogeneity on biological invasion. A problem here is that inclusion of biological complexity to capture the growth dynamics in real 3-D structures is computational demanding.

The use of network representations of real soil pore geometries may however offer a way forward. The use of network descriptions of soil has increased over recent years, but this analysis has only recently been extended to consider biological invasions (Perez-Reche *et al.* 2009). The analysis of biological invasions has been studied extensively in human, animal and plant epidemiology (Otten and Gilligan 2006), and this theory can be readily extended to consider the spread of microorganisms on a 3-D complex network.

In this paper we demonstrate how networks can be derived from real 3-D data, and how epidemiological models can be mapped onto these networks to quantify the probability of invasion. We test if thresholds can be found for biological invasions, which would indicate that only small changes to either the soil structure or the ability of microorganisms to move can result in rapid different ecological outcomes. We do the analysis for a soil with a low and a soil with a relatively high bulk density to test the effect of soil structure on the reliance to invasion.

Methods

Sample preparation and X-ray micro-tomography
Soil aggregates (1 − 2 mm) of an arable sandy loam were packed to attain bulk densities of 1.2 or 1.4 Mg/m^3, representing two characteristic examples of a loosely and densely packed field soil, respectively for this soil type. Previously we experimentally quantified the spread of fungi into these soil samples, and full details can be found in Harris *et al*. (2004). We refer to these two soil samples as loosely (1.2 Mg/m3) and densely (1.4 Mg/m3) packed soils hereafter. We scanned these samples with a Metris X-TEK Benchtop micro-tomography system (Johnson *et al*. 2009), using a molybdenum target, X-ray source settings of 155 kV and

25 μA, and an aluminum filter (0.25 mm) to reduce beam-hardening artefacts. 2-D radiographs were collected at 1169 angular positions and then reconstructed using a filtered back projection algorithm with a resolution of 74 μm. Both 3-D volumes were then imported into VGStudioMax v.1.2.1 (Volume Graphics) and converted into 260×525 8-bit TIFF image stacks with voxel-thick slices. Binary data sets were created by thresholding the grey-scale image stacks in ImageJ. The choice of the threshold parameter was based on the 3-D statistical analysis of the histogram region corresponding to the pore-solid interface.

Derivation of the network from X-ray CT data sets
The procedure to derive a network from the soil data is described by Perez-Reche *et al*. 2009. In short, all the pores were processed by a thinning algorithm (Costa and Cesar 2002; Viana *et al*. 2009), required to reduce each object (pore) to a respective 1-voxel skeleton. The skeleton is a thin structure located at the most central parts of the respective original shape. The skeleton retains all the topological features of the original shape (e.g. branching structure and cycles). The skeletonized pores were then mapped onto a network as follows. The skeleton is a set of intersecting curves with some dead ends (where the skeleton terminates). Each intersection point and all dead ends were associated with the nodes of the network (Viana *et al*. 2009). The pore space around the skeleton between two nodes is called a channel or link (edge) between two nodes. The axis of the channel thus coincides with the skeleton. Various network characteristics were calculated that can be important for biological invasion including (1) fraction included in the largest connected cluster, (2) the number of links attached to each node, (3) the arc-length of the channels and (4) the bottleneck diameter of each channel.

Biological invasion on networks
We considered the spread of micro-organisms through soil represented by a network. Specifically we analysed invasive spread through the network from a single site. We start from an arbitrary selected node in the network, and consider the spread to a neighbouring node as a stochastic process with a specified probability, and from then on the same rules are followed with the exception that the microorganisms do not move back. Under these rules we can derive models that are identical to those used in epidemiology and fall under a SIR (susceptible-infected-removed) class of models. These models can subsequently be mapped onto percolation by associating the probability to spread along a channel with the bond probability.

The biological invasion was assumed to be a Poisson process with a rate of spread along a link dependent on a typical velocity of motion and the length of the link. As this would lead to the entire networks to be invaded with infinite time, something which is unlikely to happen with limited resources, we introduced an available time for invasion. In our approach we assume a local clock for colonization of each successive pore (link). Under these assumptions, the probability of invasion of a neighbouring node, transmissibility, depends on the channel characteristics and varies from channel to channel throughout the network. We consider two situations: the first one takes an average transmissibility (T) over the entire network; the second one takes the value calculated for each link and therefore better reflects the soil heterogeneity. For further analysis we assume that the values for the velocity and the finite time are the same for each channel which leads to the concept of a local invasion scale (k). The local invasion scale has the meaning of a typical channel length such that channels which are longer than the local invasion scale are likely to be closed and those that are shorter are likely to be open for invasion.

Results
An example of visualization of loosely packed soil samples is provided in Figure 1, together with an example of a derived network. In constructing the network and to enhance visibility, isolated pores with volume smaller than 104 voxels were discarded. This has negligible impact on the topology of the resulting network on which we perform our analysis. In the loosely packed soil, the largest connected cluster percolated through the sample comprising 10183 nodes connected by 11369 channels, but the more dense packed soil did not have a cluster spanning the entire soil sample and the largest cluster contained only 2613 nodes connected by 2823 channels. We restricted our analysis of biological invasion to this largest connected cluster.

We characterised our networks according to properties that are likely to affect the spread of microorganisms, such as the node degree distribution. The networks were rather sparsely connected with mean degrees of 2.23 and 2.13 for the loosely and densely packed soil, respectively. The arc-lengths of the links differed for both soils with the more densely packed soil having fewer short as well as fewer very long pores. Further analysis

of the lengths revealed that the majority of the links did not deviate much in length from the shortest possible path between two nodes. A final property that is relevant for biological invasion is the bottleneck diameter of each link, with the more densely packed soil having smaller bottle neck diameters, hence more links that could become restrictive for spread.

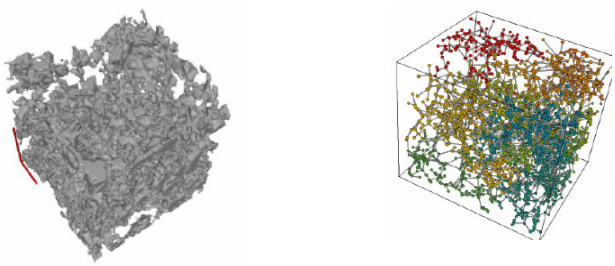

Figure 1. An example of a pore volume visualized with X-ray tomography (left) and its representation as a network (right).

Biological invasion

The probability to invade the largest cluster shows a threshold like behaviour with increasing local invasion scale (k) and with increasing transmissibility (T) (Figure 2). The probability to invade the soil sample (P_{inv}) increases non-linearly with increasing local invasion scale, with a critical value (the absence of a sharp threshold is due to finite-size of the sample) of approximately 15 and 35 for densely and loosely packed soil, respectively. This indicates that the densely packed soil is more resilient to biological invasion due to the fact that pore sizes are smaller, which means that the local invasion scale must be larger in order to 'activate' more channels to achieve the same level of invasion.

The probability of invasion also changes with the transmissibility T, which is analogous to the bond probability for percolation. For small transmissibility the probability of invasion is close to 0, and the value where it increases significantly from zero is the invasion threshold. The values for this probability are relatively high: approximately 0.81 and 0.96 for the dense and loosely packed soil, as compared with for example 0.25 on a simple cubic lattice. This is a consequence of the low node coordination number of these networks. Variability in transmissibility made the networks more resilient to invasion. This indicates that correlations in transmissibility play a significant role in the spread as for random variables the two probabilities should have coincided. Correlations reduce the transmissibility for a given value and thus make real soil networks more resilient to invasion.

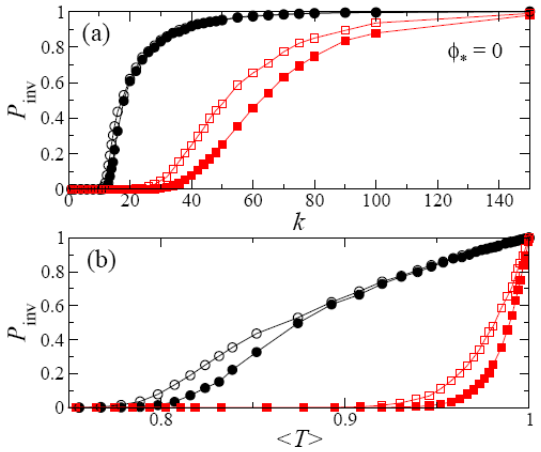

Figure 2. The probability of invasion versus a local invasion length-scale (k) and versus the transmissibility (T) in networks representing loosely packed (circles) or densiely packed (squares) soil on homogeneous (closed) and heterogeneous (open) networks (from Perez-Reche *et al.* 2009).

Conclusion

We have presented a network based on real data for soil structure and used this to analyse biological invasion in soil. The main idea is to reduce the complex geometry of the porous network to a network which is topologically equivalent to the original pore space. We demonstrated how epidemiological models can be

used to analyse the ability of organisms to invade the soil volume. With this approach biological spread became a critical phenomenon which either can or cannot invade the soil sample depending on the values of the control parameter. This will enable a quick assessment of the ability of organisms to invade a soil sample based upon simple biological parameters such as the critical pore diameter for spread. We have also demonstrated that soil networks are significantly heterogeneous in topology and that this makes them more resilient to invasion. Finally we demonstrated that increase in bulk density has a considerable impact on pore networks and makes a soil more resilient to biological invasion.

References:

Costa LF, Cesar RM (2001) Shape analysis and classification: theory and practice. CRC Press Boca Raton.

Harris K, Young IM, Gilligan CA, Otten W, Ritz K (2003) Effect of bulk-density on the spatial organization of the fungus Rhizoctonia solani in soil. *FEMS Microbiological Ecology* **44**, 45-56.

Johnson SN, Crawford JW, Gregory PJ, Grinev DV, Mankin RW, Masters GJ, Murray PJ, Zhang X (2007) Non-invasaive techniques for investigation and modelling root-feeding insects in managed and natural systems. *Agricultural and Forest Entomology* **9**, 39-46.

Otten W, Gilligan CA (2006) Soil structure and soil-borne diseases: using epidemiological concepts to scale from fungal spread to plant epidemics. *European Journal of Soil Science* **42**, 131-134.

Perez-Reche P, Taraskin SN, Neri FM, Gilligan CA, da Costa F, Vianna MP, Otten W, Grinev D (2009) Biological invasion in soil: complex network analysis. **IEEE Xplore**: Special issue Digital Signal Processing, 1-7. [doi:10.1109/ICDSP.2009.5201098].

Viana MP, Tanck E, Beletti ME, Costa LF (2009) Modularity and robustness of bone networks. *Molecular Biosystems*, submitted.

Soil pore architecture and irrigation practices in vineyards: evaluation by X-ray micro-tomography

Giacomo Mele[A], Marcella Matrecano[A], José Moràbito[B] and Santa Salatino[B]

[A]Istituto per i Sistemi Agricoli e Forestali del Mediterraneo (ISAFOM), Consiglio Nazionale delle Ricerche (CNR), Ercolano, NA, Italy, Email giacomo.mele@cnr.it
[B]Centro Regional Andino (CRA), Instituto Nacional del Agua (INA), Mendoza, Argentina, Email cra_riego@lanet.com.ar

Abstract
Surface soil samples from three experimental plots subject to three different irrigation practices have been scanned by x-ray micro-tomography and 3D images have been reconstructed and analysed. Pore size distribution and connectivity analysis of the samples showed that drip irrigation with no tillage practice produced the most heterogeneous size range with the highest vertical connectivity of the pore network.

Key Words
X-ray micro-tomography, soil porosity, irrigation, soil image analysis.

Introduction

Soil structure at the pore scale is a key to understanding soil physical, chemical and biological processes (Kutilek and Nielsen 2007; Aochi and Farmer 1995; Young and Ritz 2000). Since the seventies quantification of pore geometry has been achieved by means of image analysis techniques (Jongerius *et al.* 1972, Ismail 1975) on 2D sections of soil blocks impregnated with resin. Walker and Trudgil (1983) have been among the first to point out the need of a three-dimensional representation of the pore space. Such a need has also been demonstrated comparing 2D and 3D images of both natural soil (Moreau *et al*. 1999) and different inhomogeneous virtual pore media (Sevostianov *et al.* 2004). Recent advances in non-destructive 3D imaging systems allow to overcome most of the limitations in image resolution, sample size and time consumption (Cousin *et al.* 1996, Vogel 1997, Mele *et al*. 1999) which for a fairly long time have braked proliferation of 3D soil pore visualisation and quantification. X-ray micro-tomography based on synchrotron radiation or micro-focus cone beam source has become the most applied technique to represent the soil pore architecture at few micron scale, actually enhancing the potential to address soil processes related to real applicative problems (Appoloni *et al.* 2007, Peth *et al.* 2008, Kribaa *et al.* 2001). Pagliai *et al.* 1983, Shiptalo and Protz 1987, Mermut *et al.* 1992, Pagliai *et al.* 2004, Kribaa *et al.* 2001, are examples of studies in which the link between soil pore geometry and agricultural practices has been investigated. In this work we focus on the changes of soil surface structure due to three different irrigation practices under study in a vineyard area in the basin of the Mendoza river (Argentina). 3D image analysis procedures have been used in order to calculate size distribution and connectivity of the pore network of three samples reconstructed by micro focus cone beam X-ray micro-tomography.

Methods

Study site, experimental plots and material

Undisturbed soil samples were collected at the experimental farm of the Instituto National de Tecnologìa Agropecuaria located in Chacras de Coria, department of Luján de Cuyo, Mendoza, Argentina (32º 59’ S, 68º 52’ W, 920.82m a.s.l.). It is an alluvial area in the basin of the Mendoza river where furrow irrigation is largely used in vineyards. Soil shows a silty-loamy texture, a very low organic matter content and is rich in potassium and phosphorus (Romanella 1957). In the experimental vineyard (cv Syrah) three irrigation practices were used: furrow irrigation (LT=labranza traditional), drip irrigation with no tillage (LC=labranza cero) and irrigation by submersion with grass covered surface (CV=cobertura vegetal). Soil samples were collected by aluminium cylinders; in this study three subsurface sample volumes (about 30 cm^3), taken between rows, were examined.

Image reconstruction

The SKYSCAN 1172 desktop micro-tomograph (www.skyscan.be) has been used for the reconstruction of the images. The system is based on a cone microfocus beam source with a tungsten X-ray tube having focal spot of 5 microns (at 4W). Voltage can be set from 20 to 100 kV with current which meets 250 A. The detector is an high resolution CCD camera (4000x2624 pixels) coupled with a FOS (Fiber Optic plate with

X-ray Scintillator) which allows high X-ray sensitivity and wide acquisition area. System has copper and aluminium filter plates which can be used if needed in order to increase the tungsten energy spectrum. Image reconstruction software NRecon (www.skyscan.be) is based on last generation algorithms which apply both "convolution" and "back-projection" procedures. Filtering and correction procedures for "ring artifact" and "beam hardening" (due to the polychromatic source) are included in order to enhance accuracy of the reconstructed images. Rotation of the sample is variously programmable and can be set specifically to avoid artifact due to metal materials in the sample. Resolution of the reconstructed images has been set at 10 microns per voxel; this means that in the following only porosity larger than 10 microns has been considered.

Image analysis
Images have been visualized using the Image ProPlus package (www.mediacy.com). Pore size distribution quantification has been performed using the successive "Opening" algorithm based on procedures of mathematical morphology (Serra 1982, Soille 2003) whose application to the soil porosity have been pointed out by Horgan (1998). Pore connectivity has been measured by propagation methods on the pore network between two opposite edges of an image after steps of opening using the approach described by Lantuejoul and Maisonneuve (1984). These operations allow to draw the "percolation curve" which indicates the percent of the pore space connected, at a given pore diameter, with two opposite sides of a ROI (region of interest) till reaching the throat threshold values for the pore network. Such algorithms have been implemented by the authors in Matlab environment (www.matlab.com).

Results
Solid and pore phase of the three soil samples are shown in Figure 1. Cubic regions of interests (ROIs) having side of 3.5 mm have been visualised and analysed. The results of the pore size distribution and connectivity are shown in Figure. 2 and Figure 3, respectively.

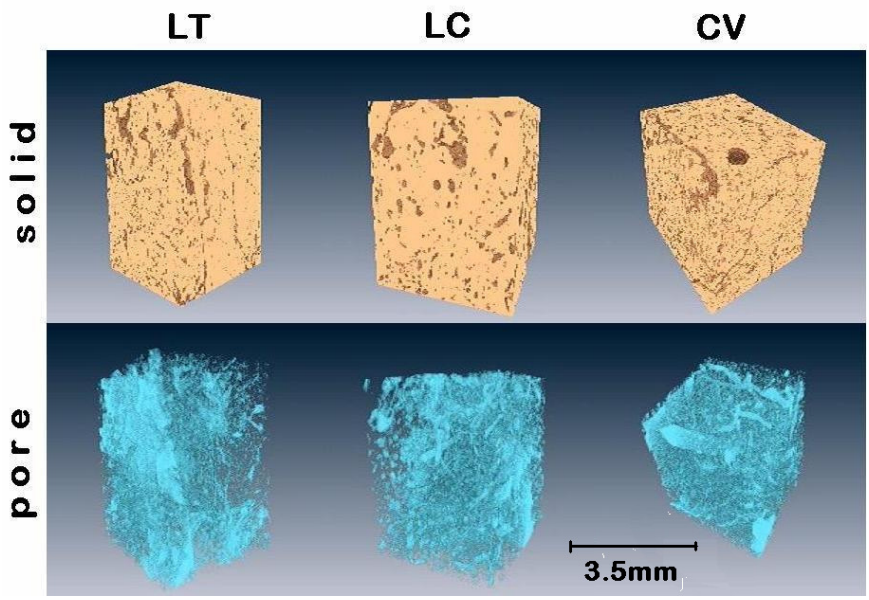

Figure 1. Visualisation of the solid and pore phase of the three samples at 10 micron image resolution. Volumes are cubes with side of 3.5mm.

Differences in porosity values (see the box in Figure 2) highlighted the compactness of the sample from the furrow irrigated plot (LT). This showed also a narrow pore size distribution (Figure 2) around the modal value of 90 microns and a porosity peak around 550 microns due to presence of not continuous cracks (see Figure 1); no continuous paths (larger than image voxel resolution) resulted in the pore network (see LT line in Figure 3). The CV sample (water submersion with grass covered surface) showed an higher and slightly wider pore size distribution around the modal value of 110 microns; porosity peaks around 550 microns and in the range between 1000 and 1300 micron were due to the presence of large tubular pores left by the roots of the grass cover. In the LC case a multi-modal pore size distribution resulted in the range 0-500 microns, indicating the highest heterogeneity of pores in this size range. Complexity of the pore space organisation can be generally considered as a good indicator of soil physical quality due to, for example, the plurality of habitats available for microbiological activity and the better effectiveness of water and air flow for the functioning of the roots.

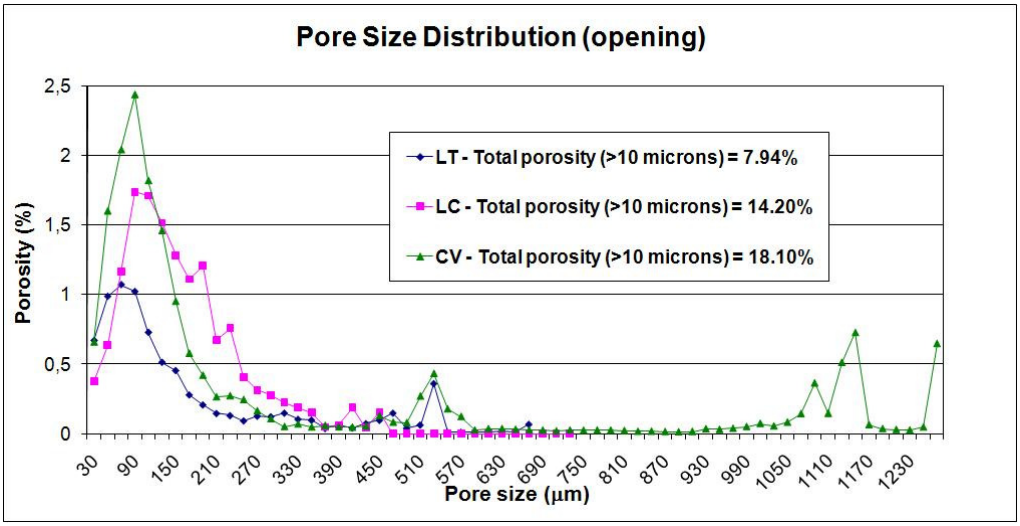

Figure 2. Pore size distribution of the three samples calculated using the "opening" algorithm (Serra 1982, Soille 2003). Porosity having size lower than the image voxel resolution has not been taken into account.

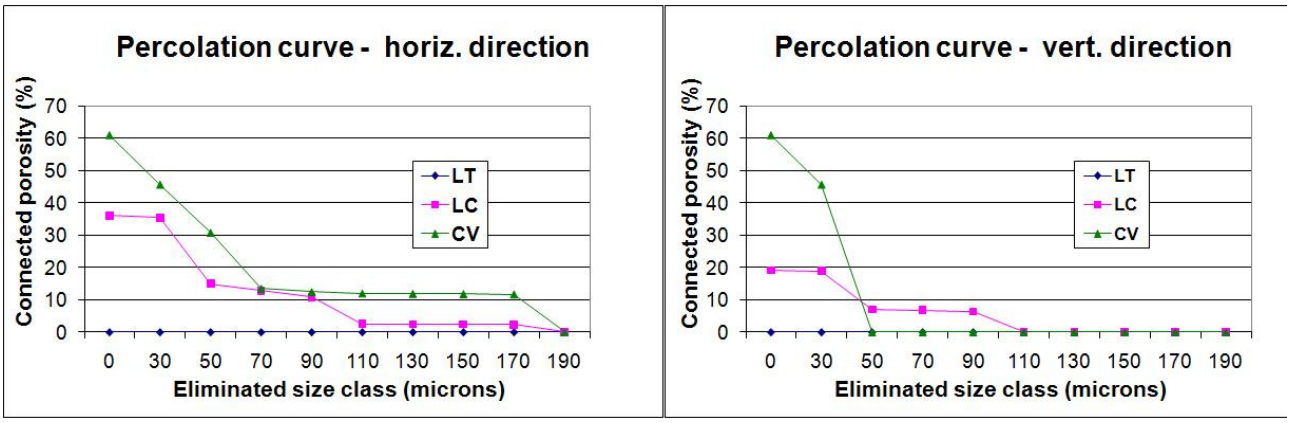

Figure 3. Horizontal and vertical pore connectivity (>10 microns) evaluated by the "percolation curve" procedure (Lantuejoul and Maisonneuve 1984).

Percolation curves (Figure 3) indicated that the pore network of both LC and CV samples were more connected in horizontal than vertical direction. In the LC case 35% and 20% of total porosity resulted to be connected in horizontal and vertical direction, respectively while percolation thresholds were of 190 and 110 microns, respectively. In the CV case 60% of porosity resulted to be connected in both vertical and horizontal direction, but the vertical percolation threshold showed a lower value of 50 microns. Therefore the CV sample, notwithstanding its highest porosity, exhibited narrower necks in vertical direction than in the case of the LC sample, allowing to presume a worse fluid flow in the pore network.

Conclusions

The pore size distribution of the sample of the furrow irrigated plot (LT) showed the lowest presence of pores in the whole size range and allowed to quantify the extreme compactness in soil induced by such irrigation practice. The CV irrigation practice produced the highest value of soil porosity, however the resulting pore size distribution and connectivity analysis indicated a lower soil structure quality than that of the LC case, where total porosity was better distributed in the 0-500 microns pore size range and the highest vertical percolation threshold value was measured.

Results shown in this paper are part of a multi-approach more general investigation to evaluate convenience in changing the traditional irrigation practice in the area of the Mendoza river (Argentina), in order to enhance water use efficiency and crop quality. They overall demonstrate the useful contribution of the 3D pore image analysis in understanding the consequences of the three alternative practices under study on the subsurface soil pore architecture.

Acknowledgements
This work has been carried out in the framework of the scientific cooperation between CNR (Italy) and CONICET (Argentina) "Ecophysiology of irrigated fruit crops: analysis of processes and its application to productivity improvement" (2003-2008).

References

Aochi YO, Farmer WJ (2005) Impact of soil microstructure on the molecular transport dynamics of 1,2-dichloroethane. *Geoderma* **127**, 137-153.

Appoloni CR, Fernandes CP, Rodrigues CRO (2007) X-ray microtomography study of a sandstone reservoir rock. *Nuclear Instruments & Methods in Physics Research*, **80**, 629-632.

Cousin I, Levitz P, Bruand A, (1996) Three-dimensional analysis of a loamy-clay soil using pore and solid chord distributions. *European Journal of Soil Science* **47**, 439–452.

Horgan GW (1998) Mathematical morphology for analysing soil structure from images. *European Journal of Soil Science* **49**, 161-173.

Ismail SNA (1975) Micromorphometric soil porosity characteristics by means of electro-optical image analysis_Quantimet 720., Soil Survey Papers, No. 9. Netherlands Soil Survey Institute, Wageningen

Sevostianov I, Agnihotri G, Garay JF (2004) On connections between 3D microstructures and their 2D images. *International Journal of Fracture* **126**, 65-72.

Jongerius A, Schoonderbeek D, Jager A, Kowalalinski T (1972). Electro-optical soil porosity investigation by means of Quantimet-B equipment *Geoderma* **7**, 177–198

Kribaa M, Hallaire V, Curmi P, Lahmar R (2001) Effect of various cultivation methods on the structure and hydraulic properties of a soil in a semi-arid climate. *Soil and Tillage Research* **60**, 43-53

Kutilek M, Nielsen DR (2007) Interdisciplinarity of hydropedology. *Geoderma* **138**, 252–260.

Lantuejoul C, Maisonneuve F (1984). Geodesic methods in quantitative image analysis. *Pattern Recognit.* **17**, 177–187.

Mele G, Basile A, Leone AP, Moreau E, Terribile F, Velde B (1999) The study of soil structure by coupling serial sections and 3D image analysis. In 'Modelling of transport processes in soils. Int. Workshop of EurAgEng's Field of interest on Soil and Water'. (Eds Feyen, K.Wiyo. Leuven) pp.103-117.

Mermut AR, Grevers MCJ, de Jong E (1992) Evaluation of pores under different management systems by image analysis of clay soils in Saskatchewan, Canada. *Geoderma* **53**, 357–372.

Moreau E, Velde B, Terribile F (1999) Comparison of 2D and 3D images of fractures in a Vertisol *Geoderma* **92**, 55–72.

Pagliai M, La Marca M, Lucamante G (1983) Micromorphometric and micromorphological investigations of a clay soil in viticulture under zero and conventional tillage. *J. Soil Sci*. 391-403

Pagliai M, Vignozzi N, Pellegrini S (2004) Soil structure and the effect of management practices. *Soil Tillage Res.* **79**, 131–143.

Peth S, Horn R, Beckmann F, Donath T, Fischer J, Smucker AJM (2008) Three-Dimensional Quantification of Intra-Aggregate Pore-Space Features using Synchrotron-Radiation-Based Microtomography. *Soil Science Society of America Journal,* **72,** 897-907.

Romanella C (1957) Los suelos de la región del río Mendoza". In 'Boletín de studios geográficos. Volumen IV. Instituto de Geografía. Facultad de Filosofía y Letras'. (Universidad Nacional de Cuyo. Mendoza. Argentina).

Serra J (1982) 'Image analysis and mathematical morphology'. (Academic Press, London).

Shipitalo MJ, Protz R (1987) Comparison of morphology and porosity of a soil under conventional and zero tillage. *Canadian Journal of Soil Science* **67**, 445-456.

Soille P (2003) 'Morphological image analysis—Principles and applications'. (Springer, Berlin, Germany).

Vogel HJ, Weller U, Babel U (1993) Estimating orientation and width of channels and cracks in polished soil blocks, a stereological approach. *Geoderma* **56**, 301–316.

Walker PJC, Trudgil ST (1983) Quantimet image analysis of soil pore geometry: comparison with tracer breakthrough curves. *Earth Processes and Landforms* **8**, 465–472.

Young IM, Ritz K (2000) Tillage, habitat space and function of soil microbes. *Soil & Tillage Research* **53**, 201-213.

The gas-diffusivity-based Buckingham tortuosity factor from pF 1 to 6.91 as a soil structure fingerprint

T. K. K Chamindu Deepagoda[A], Per Moldrup[B], Seiko Yoshikawa[C], Ken Kawamoto[D] , Toshiko Komatsu[E] , and Dennis E. Rolston[F]

[A]Dept. of Biotechnology, Chemistry and Environmental Engineering, Aalborg University, Email dc@bio.aau.dk
[B]Dept. of Biotechnology, Chemistry and Environmental Engineering, Aalborg University, Email pm@bio.aau.dk
[C]National Agricultural Research Center for Western Region, Japan, E-mail seikoyo@affrc.go.jp
[D] Graduate School of Science and Engineering, and Institute for Environmental Science and Technology,Saitama University, Email kawamoto@mail.saitama-u.ac.jp
[E]Graduate School of Science and Engineering, and Institute for Environmental Science and Technology,Saitama University, Email komatstu@mail.saitama-u.ac.jp
[F]Dept. of Land,, Air, and Water Resources, University of California, Davis, USA, Email derolston@ucdavis.edu

Abstract
Subsurface migration of greenhouse gases and other gaseous phase contaminants is predominantly controlled by soil gas diffusion coefficient (D_p) and its variations with soil-air content (ε) and soil moisture (or potential) status. Buckingham (1904) stated that D_p is proportional to ε^X with X characterizing the tortuosity and connectivity of air-filled pore space. In the Buckingham model, as well as many subsequent power-law models, the tortuosity factor, X, is assumed to be constant for a given soil irrespective of its soil potential status. This study shows a marked variation of X with soil matric potential (ψ) given by pF [= log (-ψ, cm H_2O)] ranging from 1 to 6.91 for a range of structureless and, in particular, aggregated/structured soils. The X-pF function for aggregated soils showed a monotonic decrease with increasing pF up to pF 3 near which inter-aggregate pores are completely drained, and an increase from pF 3 to pF 6.91 with the draining of intraaggregate pores. Two X(pF) expressions are proposed in order to independently describe the inter-aggregate tortuosity viz X, (for pF ≤ 3) and intra-aggregate tortuosity, X*, (for 3 ≤ pF ≤ 6.91), These expressions not only yielded better predictions of D_p but also provided useful soil structure fingerprints across a wide range of soil types.

Key Words
Power-law model, pore tortuosity factor, soil matric potential and pF, aggregated soils.

Introduction
Growing concerns over the global, regional and local environmental problems such as global warming, climate shifts and indoor/outdoor air pollution emphasize the need of accurate prediction of gas transport parameters in soils. Gas diffusion coefficient in soil (D_p) is a key parameter controlling emission of greenhouse gases (Smith *et al.* 2003) and migration of volatile organic compounds from contaminated sites (Jury *et al.* 1990). Soil gas diffusivity (D_p/D_o, where D_o is the gas diffusion coefficient in free air), and its variation with air-filled porosity at differing soil moisture conditions, has been studied for more than a century after the pioneering work of Buckingham (1904). The aim is a universal expression for $D_p(\varepsilon)/D_o$. Buckingham (1904) suggested a power-law model to describe the relation between gas diffusivity (D_p/D_o) and air-filled porosity (ε) as follows:

$$D_p/D_o = \varepsilon^X \quad (1)$$

where X is the power-law exponent which can be calculated from measured $D_p(\varepsilon)/D_o$ values by

$$X = \frac{\log(D_p/D_o)}{\log(\varepsilon)} \quad (2)$$

Buckingham's model, as well as many similar power-law models subsequently developed for dry porous media, assumed X as a constant value, for example, X = 2 (Buckingham, 1904), X = 1.5 (Marshall 1959) , and X = 1.33 (Millington 1959). The idea of non constant X also emerged later, for example Currie (1960) interpreted X as a particle shape factor and material-dependent whereas Shimamura (1992) found X for repacked dry soils to vary with percentage of finer particles. Further, Moldrup *et al.* (1999; 2000) observed X to be soil water characteristic-dependant and proposed $X(b)$ functions in terms of a pore size distribution index ,b. In wet porous media, additional water-induced discontinuity due to water blockage effects further enhances tortuosity. Thorbjørn *et al.* (2008) considered solids-induced tortuosity and water-induced discontinuity separately to yield

$$X = X_{dry} + f(\theta) \quad (3)$$

where X_{dry} is solid-induced tortuosity and $f(\theta)$ is a function of volumetric water content (θ) to account for water-induced discontinuity.

Only few studies, however, have considered the variation of X with soil matric potential (ψ) or pF [= log (-ψ, cm H_2O)]. For example, for well-aggregated volcanic ash soils (Andisols), Resurreccion *et al.* (2008) proposed the following X –pF relationship:

$$X = B + A_1 \left| pF - pF^* \right|^{A2} \quad (4)$$

where A_1, A_2, B, and pF* are curve-fitting constants.

Our main objectives of this study were to (i) examine the variation of gas diffusivity-based Buckingham tortuosity factor, X, with soil water matric potential (given by pF) ranging from wet (pF 1) to completely dry (pF 6.91) conditions, particularly for aggregated soils, in order to derive simple and working expressions for X(pF) and (ii) observe the applicability of X-pF characteristics as soil functional structure fingerprints.

Methods

We used soil gas diffusivity data from Ozosawa (1998) for ten repacked soils, with varying bulk densities/total porosities: three Andisols, four lysimeter soils, and three Gray-Lowland soils. With the exception of one lysimeter soil (Lysimeter 4), all have aggregated soil structures. Gas diffusivity measurements were carried out at different matric potentials ranging from pF 1 to pF 6.91 (oven dry). 100-cm^3 repacked samples were first saturated and drained stepwise to desired matric potentials. For gas diffusivity measurements, the experimental set-up and procedure outlined by Schjønning (1985) was used. For sampling, preparation and soil characteristics, we refer to Ozosawa (1998).

Results

Figure 1a shows the variation of tortuosity factor (X), Eq. (2), as a function of pF for the selected soils. The X values initially showed monotonic decrease with increasing pF due to draining of inter-aggregate pores reaching a minimum value at around pF 3.0 (shown by dotted line) near which inter-aggregate pores were assumed to have completely drained (Resurreccion *et al.* 2008). During subsequent draining from pF 3 to 6.91, when the aggregates themselves were draining, all soils (except for lysimeter 4 soil) showed an increase in X because the diffusion now also occurred in more tortuous air-filled pores within the aggregates which were remote and separate from main diffusion pathways. These observations are in good agreement with the results of previous studies (eg., Resurreccion *et al.* 2008; Currie 1961) and further support the concept that the transition from inter- to intra-aggregate pores occur around -1000 cm H_2O (pF 3) for aggregated porous media. Lysimeter 4 soil, on the other hand, consisted mainly of non-aggregated dune sand with uniform coarse sand particles which probably explain its different behaviour compared to the other aggregated soils.

Note here that for pF > 3, the tortuosity factor (X) shown in Figure 1a is a lump factor representing both inter- and intra-aggregate tortuosity. For the purpose of analysis, we separated the inter-aggregate tortuosity, X, as described by Eq.(2), from intra-aggregate tortuosity, denoted by X^*, which can be written as,

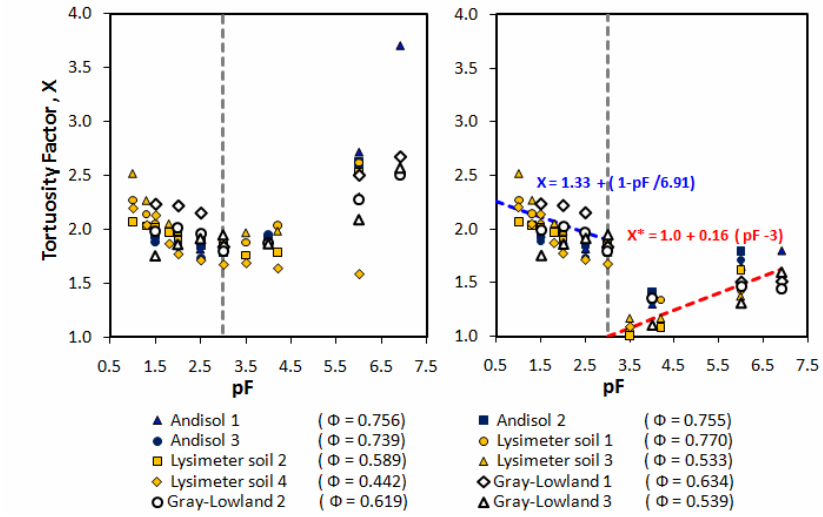

Figure 1. *X*-pF variations for aggregated soils. The proposed X(pF) expressions are shown in dotted line in (b).

$$X^* = \frac{\log\left(D_p/D_o - D_p/D_o\big|_{pF=3}\right)}{\log\left(\varepsilon - \varepsilon\big|_{pF=3}\right)} \quad (5)$$

Figure 1b illustrates the variation of X (pF ≤ 3) and X^* (pF ≥ 3) as a function of pF. We observed that an X-pF expression, previously proposed for structureless soils for the entire range of pF values (1≤ pF ≤ 6.91), is also applicable for aggregated soils in the range of pF ≤ 3:

$X = 1.33 + (1\text{-pF}/6.91)$ (6)

Note that at completely dry conditions (i.e., pF = 6.91), X reduced to 1.33, a constant suggested by Millington (1959) for dry porous media.

On the other hand, the intraaggregate tortuosity factor, X^*, showed a linear increase with increasing pF which can be expressed by,

$X^* = 1.0 + 0.16(\text{pF-3})$ (7)

Figure 2 illustrates the observed gas diffusivities (D_p/D_o) as a function of air-filled porosity (ε) for some selected soils.

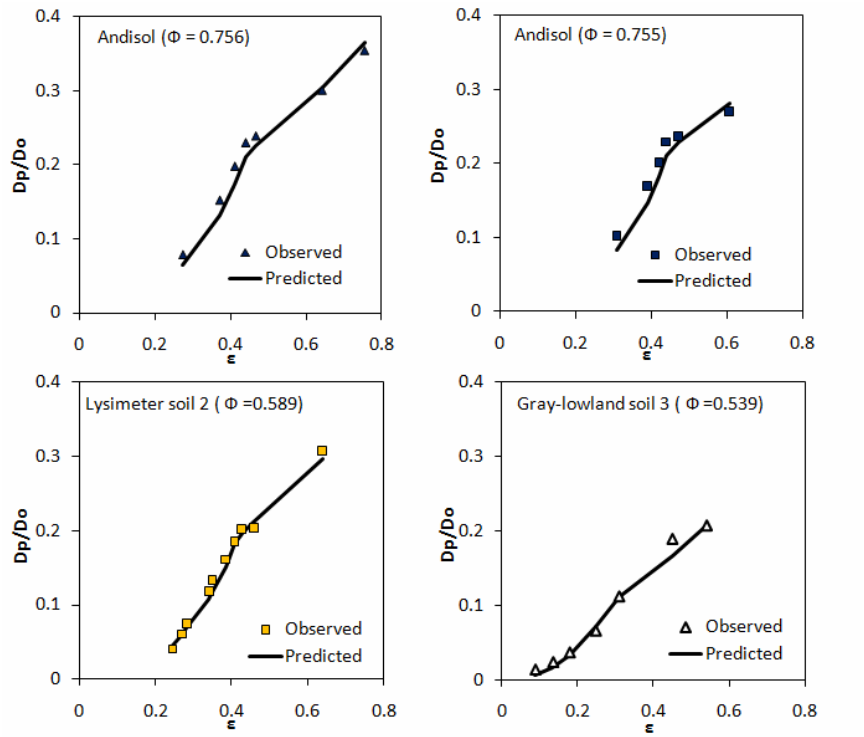

Figure 2. Observed and predicted gas diffusivities (D_p/D_o) as a function of air-filled porosity (ε) for selected soils.

The model predictions using Eq. (6) and Eq. (7) in combination with Eq. (1) are also illustrated. The predictions are in good agreement with the measured data suggesting that the two proposed X-pF expressions can be successfully used to describe gas diffusivity in aggregated soils throughout the entire range of matric potentials. Similarly, the X-pF relationship (Eq. (6)) was tested for structureless and weakly-structured soils with promising results (not shown) hence proved its usefulness across wide range of soil types. Moreover, the X-pF function exhibited unique behaviour for differently-structured soils thereby giving a valuable insight into the soil inner space. These unique X-pF relations are a promising tool for fingerprinting soil functional architecture (Moldrup *et al.* 2009).

Conclusions

The classical Buckingham-based power-law exponent, tortuosity factor X, was reintroduced as a function of soil matric potential (ψ), expressed by pF (= log [-ψ, cm H_2O]) ranging from 1 to 6.91, for both structureless as well as structured/aggregated porous media. For aggregated soils, X monotonically decreased with increasing pF reaching a minimum at pF 3 and increased again at higher pF values. The proposed linear X-pF expression for structureless soils for the entire range of pF values was also applicable for aggregated soils to describe inter-aggregate tortuosity in the range of pF ≤ 3. A different X (pF) expression was proposed for pF ≥ 3 to account for intra-aggregate tortuosity. X-pF behaviour has a unique relationship to soil functional structure and hence provides useful soil architecture fingerprints.

Acknowledgements
This study was supported by the projects Gas Diffusivity in Intact Unsaturated Soil ("GADIUS") and Soil Infrastructure, Interfaces, and Translocation Processes in Inner Space ("Soil-it-is") from the Danish Research Council for Technology and Production Sciences.

References

Buckingham E (1904) 'Contributions to our knowledge of the aeration of soils'. *Bur. Soil Bull*. **25**. (U.S. Gov. Print. Office: Washington, DC).

Currie JA (1960) Gaseous diff usion in porous media: Part 2. Dry granular materials. *Br. J. Appl. Phys.* **11**, 318–324.

Currie JA (1961) Gaseous diff usion in porous media: Part 3. Wet granular materials. *Br. J. Appl. Phys*. **12**, 275–281.

Jury WA, Russo D, Streile G, El Abd H (1990) Evaluation of volatilization by organic chemicals residing below the soil surface. *Water Resour. Res*. **26**, 13–20.

Marshall TJ 1959. The diffusion of gases through porous media. *J. Soil Sci*. **10**, 79-82.

Millington RJ 1959. Gas diffusion in porous media. *Science* **130**, 100-102.

Moldrup P, Hamamoto S, Kawamoto K, Komatsu T, Yoshikawa S, Rolston DE (2010) Taking soil-air measurements towards soil-architectural fingerprints. In '19th World Congress of Soil Science, Soil Solutions for a Changing World 1 – 6 August 2010, Brisbane, Australia'. Published on CDROM.

Moldrup P, Olesen T, Schjønning P, Yamaguchi T, Rolston DE (2000) Predicting the gas diffusion coefficient in undisturbed soil from soil water characteristics. *Soil Sci. Soc. Am. J*. **64**, 94-100.

Moldrup P, Olesen T, Yamaguchi T, Schjønning P, Rolston DE (1999) Modeling diffusion and reaction in soils: IX. The Buckingham-Burdine-Campbell equation for gas diffusivity in undisturbed soil. *Soil Sci*. **164**, 542-551.

Osozawa S (1998) A simple method for determining the gas diffusion coefficient in soil and its application to soil diagnosis and analysis of gas movement in soil. PhD diss. Bull. **15**, (Natl. Inst. Agro-Environ. Sci.: Ibaraki, Japan). (in Japanese with English summary)

Resurreccion AC, Moldrup P, Kawamoto K, Yoshikawa S, Rolston DE, Komatsu T (2008) Variable pore connectivity factor model for gas diffusivity in unsaturated, aggregated soil. *Vadose Zone J*. **7**, 397–405.

Schjønning P (1985) A laboratory method for determination of gas diffusion in soil. Rep. S1773. *Danish Inst. of Plant and Soil Sci*., Tjele. (in Danish with English summary)

Shimamura K (1992) Gas diffusion through compacted sands. *Soil Sci*. **153**, 274-279.

Smith KA, Ball T, Conen F, Dobbie KE, Massheder J, Ray A (2003) Exchange of greenhouse gases between soil and atmosphere: Interactions of soil physical factors and biological processes. *Eur. J. Soil Sci*. **54**, 779-791.

Thorbjøern A, Moldrup P, Blendstrup H, Komatsu T, Rolston DE (2008) A gas diffusivity model based on air-, solid, and water-phase resistance in variably saturated soil. *Vadose Zone J*. **7**, 1-11.

The Through Porosity of Soils as the Control of Hydraulic Conductivity

Andrey Guber[1], Markus Tuller[2], Fernando San Jose Martinez[3], Pavel Iassonov[2], Miguel Angel Martin[3],

[1] USDA-BARC-EMFSL, Beltsville MD, USA, Andrey.Guber@ars.usda.gov;
[2] Dept. of Soil, Water and Environmental Science, University of Arizona, Tucson, AZ, USA;
[3] E.T.S.I. Agrónomos, Technical University of Madrid (UPM), Madrid, Spain.

Abstract
The prominent contribution of macropores to water flow and solute transport points to the need for thorough characterization of soil void structure. Undisturbed soil columns need to be studied to infer topological properties of macropores. Three undisturbed soil columns (7.5 cm ID, 16 cm length) of the Taylor soil were taken at a grassed floodplain in Franklin County, PA. The FlashCT - 420 kV system and supplied software (HYTEC Inc.) were used for X-ray CT scanning and image reconstruction in the columns. A MatLab® software was developed for the 3D reconstruction and analysis of pores larger than 110 μm in diameter. The saturated hydraulic conductivity was measured on the 16 cm long columns and then on 8, 4, and 2 cm-thick columns obtained by consecutive slicing of the original columns. The macropore network was reconstructed from the imagery and the through pores were identified in each section as voids open to top and bottom of columns and column sections. Saturated hydraulic conductivity was affected by the column length and the minimum size of through pores. The increase in overall macroporosity did not necessarily translate into large hydraulic conductivity of columns. Introducing a novel parameter - the through macroporosity - was useful to quantify the effect of differences in pore space structure on the differences in hydraulic conductivity.

Key words
Macropore structure, computed tomography, water conductivity, sample size.

Introduction

Soil hydraulic properties are essential inputs of water flow and chemical transport models. Typical measurement scale for soil hydraulic characterization is in order of 10 cm. Soil parameters obtained from a decimeter-scale measurements are often used in numerical models with a grid ten times as large, with the numerical results extrapolated to the field scale. It has been shown in numerous publications that saturated hydraulic conductivity (K_s) can vary with sample size. Shouse *et al.* (1994) and Haws *et al.* (2004) have observed an increase in average K_s values with increase in area of measurement. Other researchers have shown that K_s values decreased as the sample length increased (Anderson and Bouma 1973; Mallants *et al.* 1997; Fuentes and Flury 2004). The changes in K_s with the sample size were attributed to soil spatial heterogeneity and to the effect of macroporosity on saturated flow at larger scales.

The concept of effective porosity (φ_e) as the pore volume fraction that dominates the flow of water when the soil is saturated has been introduced by Brooks and Corey (1964). Ahuja *et al.* (1984) used this concept to derive a power law relationship between K_s and φ_e by generalizing the Kozeny-Carman equation (Carman 1956). Replacing the effective porosity (φ_e) with the macroporosity (φ_{ma}) Messing and Jarvis (1995) developed the equation:

$$K_s = B\varphi_{ma}^n \qquad (1)$$

where B and n are empirical parameters. The values of parameter n were 7.17 and 4.24 for different soil layers in their study. Although the authors did not study soil pore structure, the difference in n was attributed to difference in tortuosity, pore size distribution, pore continuity and presence of "necks" in flow pathways between these layers.

The X-ray computed tomography (CT) has recently become available for the noninvasive study and the 3-D quantification of macropore structure in soils (Perret *et al.* 1999; Luo 2008) and made it possible to relate soil hydraulic properties to the pore structure. Objectives of our study were: (a) to use CT to search for parameters of soil pore space affecting saturated hydraulic conductivity, and (b) to evaluate the core length effects on saturated soil hydraulic conductivity as related to macropore structure.

Materials and methods

Three undisturbed columns (7.5 cm ID, 16 cm length) of the Taylor soil were taken at a grassed floodplain in Franklin County, Pennsylvania from A horizon. Soil texture was loam. The cores were carved out with acrylic rings using a core sampling device. Some soil cores had visible macrospores, which presumably

served as water conduits. The columns were X-ray CT scanned using the FlashCT - 420 kV system (HYTEC Inc.) and images were reconstructed using the FlashCT-DAQ, the FlashCT-DPS, and the FlashCT-VIZ software. About 1500 cross-section images with resolution of about 110 microns were obtained for the columns. The images were binarized, and 3D pore structure was reconstructed using a software written in MatLab® (The MathWorks, Inc.).

The soil cores were saturated from the base during a period of 24 hours and the saturated hydraulic conductivity was measured using the constant pressure method (Reynolds *et al.* 2002). Then soil cores were drained overnight and sliced into two 8-cm sections with a band saw. The sliced core sections were saturated and K_s measurements were repeated as described above. The 8-cm core sections were cut into 4-cm and later on into 2-cm sections for measurements at smaller scales.

The porosity value was calculated as a ratio of number of pore voxels to total number of voxels in core sections. The through pores were identified in each section as the voids which are open to both sides of the core sections. Total and minimal volumetric contents were calculated for each through pore individually. Parameters B and n were estimated by fitting Eq. (1) to the experimental data.

Results and Discussion

The visual inspection showed that circular pores dominated in pore structure of column 1, planar pores dominated in column 3, and circular and planar pores were equally presented in column 2. In general, the total measured porosity and complexity of the pore network increased with the depth in all columns. The number of through pores also increased with depth and with the decrease of core height indicating discontinuity of large pores (Figure 1). The through porosity was zero in 16-cm long columns, and the maximum porosity was found in the bottom 2-cm cores. Both an increase and a decrease in core porosity were observed with a decrease in core height (Figure 2a), so that the standard deviation of porosity tripled while core height decreased from 16 to 8 cm.

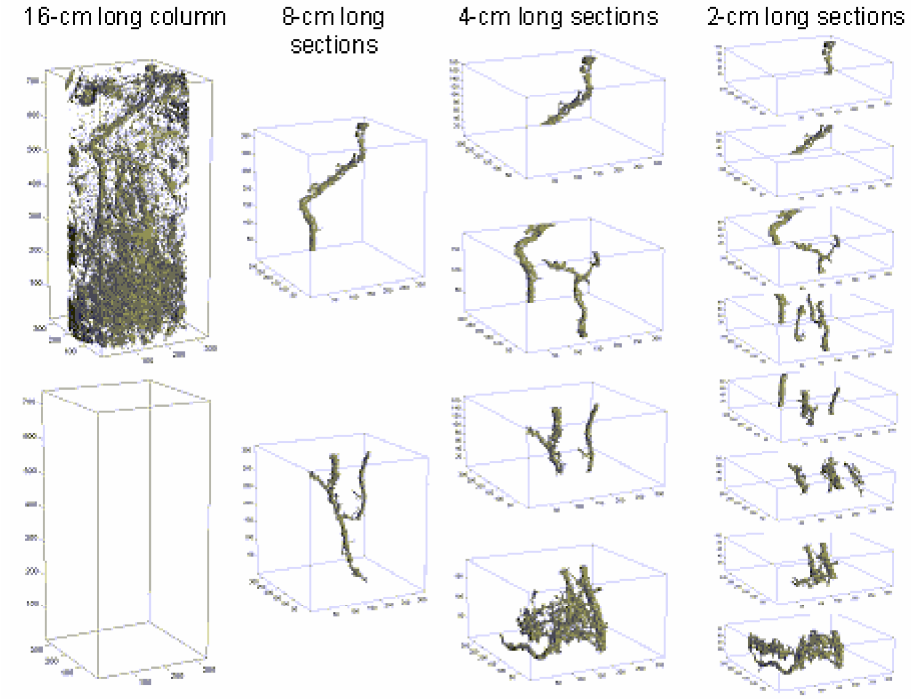

Figure 1. A three-dimensional visualization of the total porosity (top left) and trough pores large than 110 µm in soil sections of column 1.

The through porosity averaged among each core height group decreased with the increase in the height, while the standard deviation remained about the same and was in the range from 0.016 cm^3 cm^{-3} to 0.018 cm^3 cm^{-3} (Figure 2b). Changes in the core height affected soil saturated hydraulic conductivity (Figure 2c). Smaller values of K_s corresponding to $\log(K_s)=0.32\pm0.40$ were observed in 16-cm columns as compared to 2-8 cm high cores where $\log(K_s)$ varied from 0.75 ± 0.82 to 1.00 ± 1.20 (mean ± standard deviation). Equation (1) was fitted to the values of different porosities paired with K_s in each column (Figure 3). High R^2 values

were obtained only for the relationship between K_s and minimal through porosity in the soil cores (Figure 3c). Values of the parameter n were 0.72, 0.55 and 2.02 in columns 1, 2 and 3, respectively, and reflected the differences in pore shape. Smaller n values were observed in columns with circular pores, and with both circular and planar pores; maximum n was in column with dominated planar pores in pore network. These results are consistent with the experimental results and theoretical model developed by Anderson and Bouma (1973), and imply sharp changes in K_s for planar pore systems caused by changes in size of pore necks that restrict water flow.

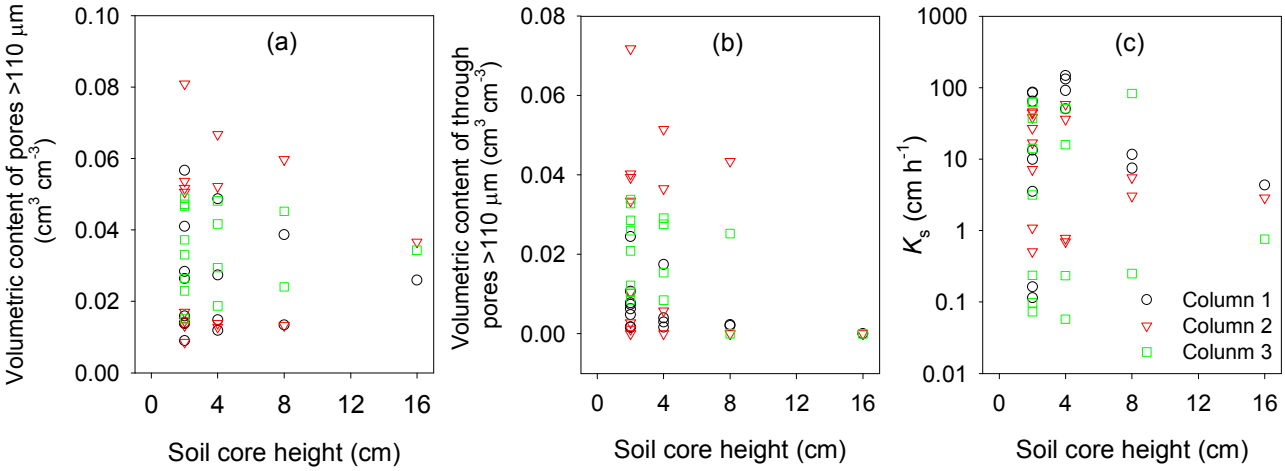

Figure 2. Changes in the volumetric content of all pores larger than 110 µm (a), the volumetric content of through pores larger than 110 µm (b), and the saturated hydraulic conductivity K_s (c) with the soil core height.

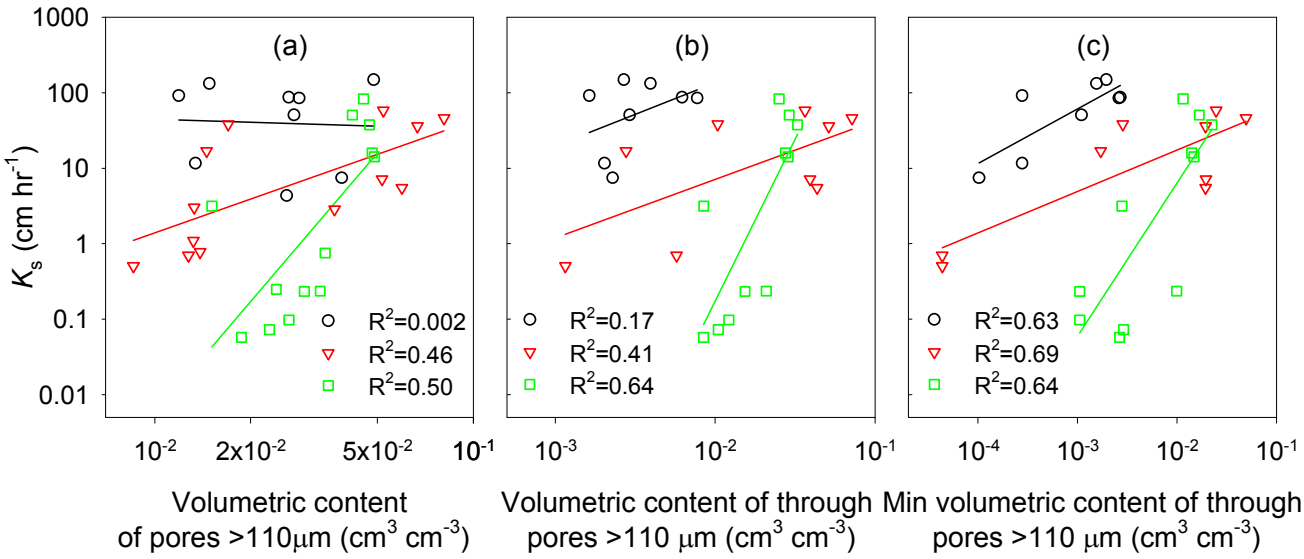

Figure 3. Relationships between saturated hydraulic conductivity (K_s) and volumetric content of different pores for columns: (○) – 1, (▽) – 2, and (□) – 3.

Conclusions

This study showed that, due to discontinuity of soil macropores, larger macroporosity did not necessarily translate into the larger hydraulic conductivity. The CT provided the quantification of the soil through macroporosity and the insight into observed differences in slopes of the log-linear regressions "minimal through porosity vs. saturated hydraulic conductivity". Changes in K_s with scale could be attributed to the differences in macropore continuity and to changes in minimial through porosity with the core thickness.

References

Ahuja LR, Naney JW, Green RE, Nielsen DR (1984) Macroporosity to characterize spatial variability of hydraulic conductivity and effects of land management. *Soil Science Society of America Journal* **48**, 699-702.

Anderson JL, Bouma J (1973) Relationships between saturated hydraulic conductivity and morphometric data of an argillic horizon. *Soil Science Society of America Proceedings* **37**, 408-413.
Brooks RH, Corey AT (1964) Hydraulic properties of porous media. Hydrology Paper 3, Colorado State University, Fort Collins.
Carman PC (1956) Flow of gases through porous media. (Academic Press Publishing: New York).
Messing I, Jarvis NJ (1995) A comparison of near-saturated hydraulic properties measured in small cores and large monoliths in a clay soil. *Soil Technology* **7**, 291-302.
Shouse PJ, Ellsworth TR, Jobes JA (1994) Steady-state infiltration as a function of measurement scale. *Soil Science* **157,**129–136.
Reynolds WD, Elrick DE, Youngs EG, Amoozegar A (2002) Saturated and field saturated water flow parameters. In 'Methods of soil analysis. Part 4. Physical Methods'. (Eds JH Dane, GC Topp) pp. 797-878. (SSSA Inc. Publishing: Madison, Wisconsin, USA).
Mallants D, Mohanty BP, Vervoort A, Feyen J (1997) Spatial analysis of saturated hydraulic conductivity in a soil with macropores. *Soil Technology* **10**, 115-131.
Haws NW, Liu B, Boast CW, Rao PSC, Kladivko EJ, Franzmeier DP (2004) Spatial variability and measurement scale of infiltration rate on an agricultural landscape. *Soil Science Society of America Journal* **68,** 1818-1826.
Luo LF, Lin HS, Halleck P (2008) Quantifying soil structure and preferential flow in intact soil using X-ray computed tomography. *Soil Science Society of America Journal* **72**, 1058–1069.
Perret J, Prasher SO, Kantzas A, Langford C (1999) Three-dimensional quantification of macropore networks in undisturbed soil cores. *Soil Science Society of America Journal* **63**, 1530–1543.